

# Offshore Wind Farm Layout Optimisation

To provide insight in what can be expected from offshore wind farm layout optimisation

M.R.Thomson

Delft University of Technology

# Offshore Wind Farm Layout Optimisation

To provide insight in what can be expected  
from offshore wind farm layout optimisation

by

M.R.Thomson

to obtain the degree of Master of Science in Sustainable Energy Technology at Delft University of  
Technology

Thesis committee:	Dr. DA von Terzi	Chairman
	Dr.ir. MB Zaayer	Daily supervisor
	Dr.ir. G. la Rocca	External committee member

Wind Energy Group, Faculty of Aerospace Engineering, Delft University of Technology

An electronic version of this thesis is available at <http://repository.tudelft.nl/>.

# Acknowledgements

First and foremost, I would like to express my most profound appreciation to Michiel Zaaijer, who gave me the opportunity to work on such an interesting topic. The completion of this thesis would not have been possible without him. The patience, guidance and critical notes at our meetings every two weeks were very helpful for my understanding and work on this thesis. Our meetings often took longer, and he always seemed to have extra time. The clear examples he gave to illustrate his points were enlightening and definitely will come in handy for other applications. I always looked forward to our meetings to discuss the thesis and share our enthusiasm for wind energy.

Thanks to Michiel, I contacted Sebastian Sanchez Perez-Moreno, who helped me get started in Python with different types of optimisers. He shared his insights on the topic and provided me with additional tips.

I would like to extend my sincere gratitude to Dominic von Terzi and Gianfranco La Rocca for taking their time to review my work and for completing my thesis committee.

On a personal note, I am thankful to my friends and roommates: Robert de Nie, Robin Terstappen, Thijs Jonkman, Skip de Mets and Martijn de Jong. They made working at home during the Covid-19 pandemic a lot more durable and fun. Last but certainly not least, I would like to thank my family for their love and encouragement.

*M.R. Thomson*  
*Delft, November 2021*

# Abstract

The potential gain in energy production and profit by improving the placements of turbines within a wind farm is driving interest. However, finding the optimal placements provides a complex problem. A large number of inter-dependent design variables create a design space that is difficult to solve. Therefore there is much attention for offshore wind farm layout optimisation (OWFLO) in practice and literature. Most of the research is done in selecting and creating the best optimisation algorithms, wake models and cost models.

This is not yet another study into better modelling or optimiser selection for OWFLO. Instead, this study aims to provide insight into what performance can be expected from OWFLO and to know when further optimising is not justifiable anymore. The study consists of three parts. All three parts make use of a referent. A referent can be considered a close representation of reality, obtained by a best-practice implementation of the optimisation problem and its associated models. It is assumed that the referent has the same characteristics as reality and that deviations of other implementations of OWFLO from the referent are representative of their deviations from the true optimisation problem.

In this study, the referent is defined by, amongst others, the use of the Bastankhah and Porté-Agel Gaussian wake model, a 12 sector wind rose with a Weibull distribution per sector and the gradient-free covariance matrix adaptation evolution strategy. The referent is used to maximise annual energy production (AEP).

The first part uses the referent to find and understand the characteristics of the OWFLO problem. Wind farms with 9, 25 and 64 turbines have been optimised 100 times with the referent. The results show a small spread in the performance of the found optimised layouts, indicating that many local optima exist with similar performances in an OWFLO problem. The spread between the highest and lowest found performance decreases with increasing numbers of turbines. A special form of the response surface is used to visualise the response surface. The visualised response surfaces, with only two design variables, showed that the wakes of the turbines created multiple local optima.

The second part compares performances from optimised layouts with 25 turbines resulting from optimisations with alternative implementation choices, evaluated by the referent model. The performances are represented in boxplots for 100 optima each. The boxplots show that the influence of alternative implementation choices depends on the slightly different locations of the local optima in the design space and the roughness of the response surface they create. The influence of the shifts in locations of the local optima on the performance turned out to be minimal. An increase in the roughness of the response surface meant an increase in the spread of the performances. The difference in performance resulting from the alternative optimisers indicates that improvement of a state-of-the-art optimiser is not expected to lead to much better results.

The third part explores the need for improvement of the analysis by adding a phenomena currently not considered in OWFLO. The influence of neighbouring wind farms on layout optimisation without including atmospheric stability is explored. Three cases have been defined to show the influence of neighbouring wind farms on layout optimisation. It is concluded that adding neighbouring wind farms for accurate energy yield assessments is necessary. However, for layout optimisation, the benefit of including neighbouring wind farms is not evident.

# Contents

<b>Acknowledgements</b>	<b>i</b>
<b>Abstract</b>	<b>ii</b>
<b>1 Introduction</b>	<b>1</b>
1.1 Overview . . . . .	1
1.2 Problem analysis . . . . .	2
1.3 Scope . . . . .	2
1.4 Objective . . . . .	2
1.5 Thesis outline . . . . .	2
<b>2 Methodology</b>	<b>3</b>
2.1 Goal & Activities . . . . .	3
2.2 Referent. . . . .	4
2.3 PyWake . . . . .	5
<b>3 Reality</b>	<b>6</b>
3.1 OWFLO . . . . .	6
3.1.1 Reality. . . . .	6
3.1.2 Practical implementations . . . . .	7
3.2 Elements of the numerical optimisation . . . . .	7
3.2.1 Problem formulation . . . . .	7
3.2.2 Analysis . . . . .	9
3.2.3 Optimiser . . . . .	12
3.3 Known phenomenons that are not implemented . . . . .	12
<b>4 Description and analysis of the referent</b>	<b>16</b>
4.1 Description of the referent . . . . .	16
4.1.1 Overview and purpose . . . . .	16
4.1.2 Problem formulation . . . . .	16
4.1.3 Analysis . . . . .	17
4.1.4 Optimiser . . . . .	18
4.2 The three cases . . . . .	18
4.3 Identifying the characteristics of the OWFLO problem . . . . .	20
4.4 Response surfaces . . . . .	27
4.4.1 Optimised layouts . . . . .	27
4.4.2 Second row . . . . .	33
4.5 Insights obtained from the referent cases . . . . .	35
<b>5 The effect of key influencers on optimality</b>	<b>37</b>
5.1 Selected key influencers . . . . .	37
5.2 Alternative practical implementation choices . . . . .	38
5.3 Comparative analysis . . . . .	42
5.4 Results from the comparative analysis . . . . .	44
5.4.1 Influence from the alternative implementation choices . . . . .	44
5.4.2 Correspondence between the performance of the alternative implementation choices and the referent. . . . .	51
5.5 Response surface . . . . .	53
5.5.1 Optimised layouts . . . . .	53
5.5.2 second row . . . . .	56
5.6 Insights obtained from the alternative implementation choices . . . . .	60

---

<b>6</b>	<b>Future improvements: an example</b>	<b>61</b>
6.1	Future improvements . . . . .	61
6.2	Neighbouring wind farms . . . . .	61
6.3	Three cases and a reference . . . . .	62
6.4	Results from optimising with neighbouring wind farms . . . . .	64
<b>7</b>	<b>Conclusion and Recommendations</b>	<b>69</b>
7.1	Conclusion . . . . .	69
7.2	Recommendations . . . . .	70
	<b>References</b>	<b>74</b>
	<b>Appendices</b>	<b>75</b>

# Introduction

## 1.1. Overview

The past decade has seen a rise in offshore wind farm developments. The prices of development are dropping, and subsidy is no longer needed. With this increasing development in offshore wind farms, there is a quest from wind farm developers to optimise the placement of wind turbines. The combined locations of the wind turbines are called the layout of a wind farm. Often, the goal of optimising the layout is to obtain the lowest possible wake losses. In large wind farms, a 0.1% energy gain can result in several million euros in revenue over their lifetime. There is much attention for wind farm layout optimisation (WFLO) in practice and literature. Most of the research is done in selecting and creating the best optimisation algorithms [1] [2] [3] [4] [5] [6], wake models [7] [8], [9] [10] [11], and cost models [12] [13].

The research in different optimisation algorithms is done to find a better optimum without increasing computational costs. A WFLO problem can be categorized as an NP(non-deterministic polynomial time)-hard optimisation problem, which contains many local optima. Exact optimisation methods have severe difficulties to solve the WFLO problem. Therefore, optimisers with a heuristic search method are dominant within WFLO [14]. The list of optimisation algorithms that have been used in WFLO is extensive and is given here: Genetic Algorithms, Simulated Annealing, Differential Evolution, Simulated Evolution, Ant Colony optimisation, Particle Swarm optimisation, Stochastic Evolution, Definite Point Selection, Bionic optimisation, Gradient-based optimisation, Numerical added simulation, and Monte Carlo optimisation technique [15]. Although heuristic optimisation algorithms try to alleviate the problem of exact algorithms finding local optima, they are also known to find local optima. That heuristic optimisation algorithms find local optima can be identified by the different resulting layouts that almost have the same performance [16].

One of the dominant factors for WFLO is the effect of wakes, which wake model is selected therefore influences the optimised layout. The research in wake models is done to develop models that come closer to the effect of real wakes. Low computational costs is required in WFLO, which prohibits the use of high fidelity models. Therefore, simplified engineering wake models are used based on fundamental fluids principles or empirical data. These wake models generally show good results but have limitations. Some wake models are more accurate for near wakes, and others are more accurate for far wakes [15]. Also, wake interactions can be modeled in different ways [17]. A common method used is the root mean squared method. The choices for modelling the wakes, which are used by the wind farm developer, influence the final optimal layout.

Different objective functions can be used in WFLO. The three dominant ones are the annual energy production(AEP), the levelized cost of energy(LCoE), and optimising for profit. The latter two objective functions need a cost model. Depending on the extensiveness of the cost models, these can include the electrical collection system, the support structures, installation cost, and more. For these calculations, assumptions need to be made for costs and revenue. As wind turbine development is still happening at

a fast pace, the assumptions come with high uncertainties. With fluctuating energy prices, calculating revenues is also uncertain.

Besides the selected optimiser, wake models, and cost models, more choices from the wind farm developer influence the found optimal layout. To name a few: wind rose sector size, wind direction simulation sample size, turbulence model, and wind turbine type.

## 1.2. Problem analysis

The state-of-the-art technologies seem to be tunnel-visioned in pushing WFLO to find better optimisers, better wake models, and better cost models. Project leaders want to squeeze out the last millipercentages of increasing AEP to improve funding for their project. However, previous work on WFLO shows that results are imperfect. These results however, don't provide an outlook of what is realistically achievable with WFLO nor give a clear justification for the amount of work that is necessary for further improvement of the analysis.

Therefore, this thesis will look at the fundamental expectations for layout optimisation and how wind farm layout optimisation is influenced by the choices of the wind farm developer. The results obtained within this thesis will provide insights into when there is no more use in further pushing and developing a wind farm layout optimisation. Currently insight into when further gain can still be expected is missing.

## 1.3. Scope

As large wind farms are placed more and more offshore, this thesis only focuses on Offshore Wind Farm Layout Optimisation (OWFLO). Within this thesis wake models are used which have been validated. The validation of the wake models with measurements from wind farm data is therefore outside the scope of this project.

With the complexity and added computational time the cost models are left out of this research. Consequentially the objective of the optimisation becomes maximizing AEP.

## 1.4. Objective

The goal of this project is to provide insight into what performance can be expected from OWFLO and to know if further optimising and further improvement of the analysis is justifiable.

The driving questions that this work aims at answering are given below:

- What are the characteristics of the OWFLO problem?
- With maximizing AEP as objective, what are the influences and uncertainties from the selected key influencers?
- Is there a need to improve the analysis by adding phenomena currently not considered in OWFLO?

## 1.5. Thesis outline

This thesis has the following structure:

- *Chapter 2* explains the proposed methodology and introduces the use of a 'referent'
- *Chapter 3* is about the reality surrounding OWFLO, how it is best described in practical implementations and what parts of reality have not yet been implemented.
- *Chapter 4* gives a description of the referent, analysis the characteristics of the OWFLO problem and explores a special form of the response surface.
- *Chapter 5* presents an overview of the key influencers, shows the alternative practical implementation choices and their influence on optimality.
- *Chapter 6* explores the need for improvement of the analysis by adding a phenomena currently not considered in OWFLO.
- *Chapter 7* gives the conclusion and recommendations.

# 2

## Methodology

This chapter presents the methodologies and software which are used for this research. First, the goal and the activities are presented. Secondly, the methods of the activities are briefly described. Thirdly, the use of a referent is further elaborated on, following the idea proposed by Roza [18]. Finally, the software tool in which the optimisations are performed is introduced.

### 2.1. Goal & Activities

As mentioned in section 1.4, the goal of this project is to provide insight into what performance can be expected from OWFLO and to know if further optimising and further improvement of the analysis is justifiable. To achieve this, the following activities are undertaken:

#### *Chapter 3*

1. Describe the OWFLO problem.
2. Outline the real physics and nature of the OWFLO problem and how this is captured in practical implementations.

#### *Chapter 4*

3. Decide upon a model that describes reality and can be used as a referent.
4. Find and understand the characteristics of the OWFLO problem.

#### *Chapter 5*

5. Identify different possible implementation choices of OWFLO.
6. Assess the influence of practical implementation choices by optimising the layouts with other settings, other wake models, and other optimisers.

#### *Chapter 6*

7. Implement a future improvement of the analysis.
8. Assess the influence of a neighbouring wind farm on OWFLO.

1.

To describe the OWFLO problem, a diagram is presented with the fundamental elements found in reality and its correspondence with practical implementations.

2.

To outline the real physics and nature of the OWFLO problem and how this is captured in practical implementations of OWFLO, a literature review on the physics, economics, and OWFLO problem is conducted. Software tools like AWS OpenWind[19], and DTU's PyWake[20] are looked at for their practical implementation possibilities.

3.

To decide upon a model for the referent, a literature review is conducted. A selection is made with considerations for the purpose of the referent and its computational time. Section 2.2 will explain what is meant by the term referent.

4.

To find and understand the characteristics of the OWFLO problem, the response surface of the objective function and the layouts of different local optima are assessed with the referent. This is done for wind farms of 3, 9, 25, and 64 wind turbines.

5.

To identify different possible implementation choices of OWFLO, an overview is made. Secondly, a logic-based selection is made of the implementation choices that are found to have a significant impact on the final found layout. The term for this selection that is used in this paper is *key influencers*.

6.

To assess the influence of practical implementation choices by optimising the layouts, a comparative analysis is conducted with other settings, other wake models, and other optimisers for a wind farm of 25 turbines. For each optimised layout, the performance is recalculated with the referent for a fair comparison.

7.

To implement a future improvement to the analysis three new cases are introduced which all have a neighbouring wind farms

8.

To assess the influence of a neighbouring wind farm on OWFLO the cases are optimised both with and without the future improvement and than compared.

## 2.2. Referent

For both finding the OWFLO problem's characteristics and assessing the influence of practical implementation choices, the use of a referent was found appropriate. The idea is proposed by Roza [18] and helps to solve the problem of having no real-world data to compare against. Ideally, to specify and measure the influence from different choices within OWFLO, simulation results would be compared with real-world data, and the found optima would be compared with known optimum layouts. However, for OWFLO, the real-world data of all layouts in the optimisation iterations don't exist, and the true optimum is unknown. Therefore, a computable proxy of reality is used. The idea is illustrated in Figure 2.1, in which this proxy of reality is called the referent.

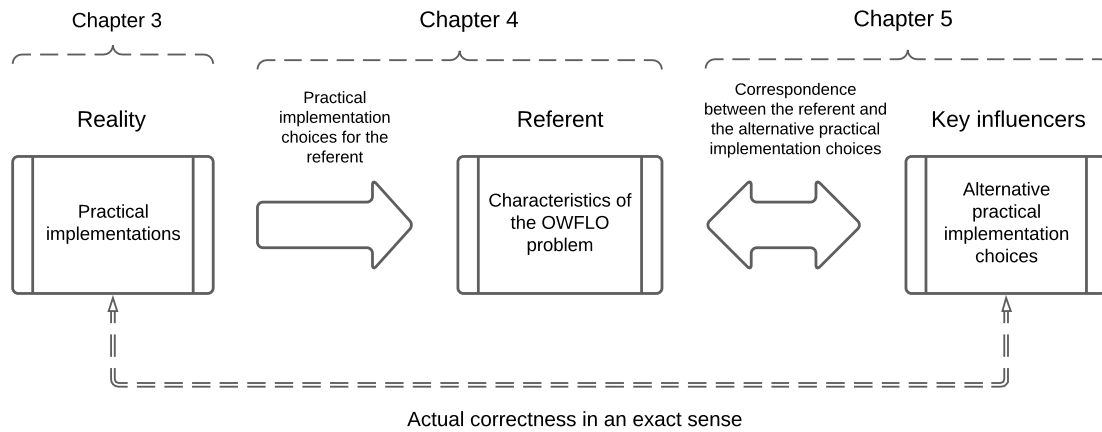


**Figure 2.1:** Reality, referent and models diagram

A referent can be considered a close representation of reality, obtained by a best-practice implementation of the optimisation problem and its associated models. For some practical implementation choices a best-practice model would be computational too heavy, therefore the referent that is used here contains models and settings that are considered to have a general consensus within the OWFLO community. It is assumed that the referent has the same characteristics as reality and therefore it can be used to find and understand what those characteristics are. The deviations between alternative practical implementations of OWFLO and the referent indicate the range of the deviations amongst practical implementations. The influence from practical implementation choices can now be assessed with the deviations between the referent and the models.

## 2.3. PyWake

PyWake is an open-source wind farm simulation tool build in Python. Despite Python being a “fast to code, slow to run” programming language, PyWake is made to be also very fast to run, therefore being suitable for layout optimisation. This is accomplished by taking advantage of the numerical libraries and heavy vectorization, making it just as fast as other programming languages. PyWake is capable of calculating wind farm flow fields, wind turbine power production, and AEP. It includes different engineering models that can be selected and have been validated against measurements, LES, and RANS simulations [20]. PyWake is primarily developed by DTU Wind Energy.

# 3

## Reality

This chapter first describes OWFLO with a high level perspective both in reality and in practical implementations terms. Secondly, three practical implementation elements of the OWFLO problem are discussed in more detail together with what they resemble in reality. Thirdly, other parts of reality that are not implemented in OWFLO will be discussed.

### 3.1. OWFLO

The high level perspective of OWFLO is first described in reality terms, and secondly in practical implementation terms. This is done to show a clear distinction between the OWFLO problem in reality and the approaches which are commonly used to model this problem.

#### 3.1.1. Reality

Offshore wind farm layout optimisation is done to better satisfy the wishes of the wind farm developer. The placements of the turbines determine to what extent certain aspects of the desirability from the wind farm developer are met. They influence, among other things, the energy yield, costs, and environmental impact. Knowing to what extent and how this influences the desirability requires knowledge of various 'disciplines.' These disciplines evaluate the expected performance of the layout with respect to the wishes of the developer. Being able to evaluate the wind farm's performances accurately is essential for improving the wind farm in reality. It is the designer's job to search for the layout that best meets these wishes within the limitations of the project. In reality the possibilities of the designer include other design choices like the hub height, number of wind turbines, type of cable, or type of wind turbine which are also important design choices that influence the wind farm. Within this thesis and also frequently found in modelling tools, these design choices are set before performing OWFLO. Three distinctions can be found in the reality of OWFLO and are illustrated in Figure 3.1, the search, the wishes, possibilities and limitations, and the evaluation. The wishes, possibilities and limitations are presented in red and surround the search and evaluation. This illustrates that the wishes, possibilities and limitations confine what the search and evaluation contain.

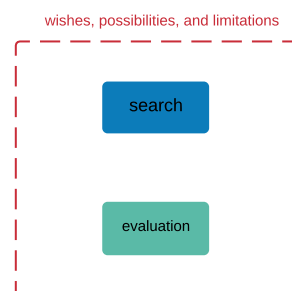


Figure 3.1: Overview of the three distinctions found in reality

### 3.1.2. Practical implementations

In practical implementations, the OWFLO problem is often converted to a numerical optimisation. Within this numerical optimisation, a distinction can be made between the problem formulation, analysis and optimiser, which is illustrated in Figure 3.2. They represent the wishes, possibilities and the limitations, the evaluation and the search, respectively. The problem formulation captures the objective function, constraints and design variables. Within Figure 3.2 the design variables, objective function and constraints between the arrows represent the data flow between the optimiser and analysis. Within the constraints and by variation of the design variables, the objective function is either maximized or minimized by the optimiser. The optimiser represents a 'search engine', which changes the design variables to search for the optimal solution. As offshore wind farms usually consist of many wind turbines, there are endless possibilities for placing them. Therefore, an optimiser that can search in an efficient way is required. The optimisation algorithm determines the way in which the search is conducted. Numerous optimisation algorithms exist. The optimiser provides the analysis with design variables representing a layout. The analysis evaluates the layout, and the performance is coupled back to the optimiser. Depending on the objective function, the analysis contains physics models and/or cost models.

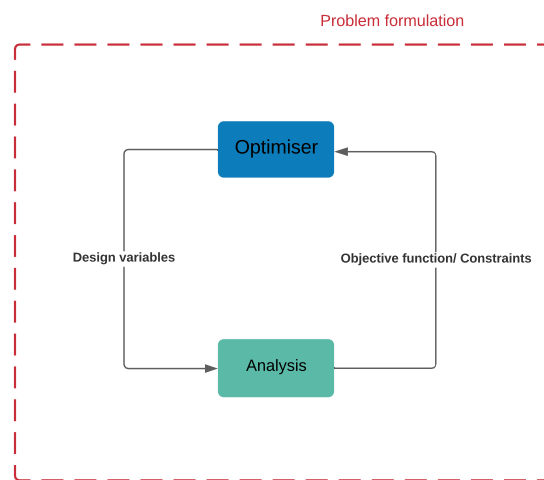


Figure 3.2: Overview of the numerical optimisation

## 3.2. Elements of the numerical optimisation

In this section the three elements of the numerical optimisation are discussed. The parts of reality that are converted to practical implementations by means of models, functions, or parameters will be further elaborated below.

### 3.2.1. Problem formulation

#### *Reality*

The wind farm developer's wishes, possibilities and limitations represent the problem formulation in reality. As discussed in section 3.1.1 the possibilities for design choices are limited to the placements of the turbines.

The wind farms developer's wishes can be an extended list which can also have conflicting interests, like quality versus costs. The main wishes of a wind farm developer can be captured by the list below:

- low cost
- high revenue
- high annual energy production

- low maintenance
- good sustainability

Other wishes that are hard to take into account are given in the list below:

- low environmental impact
- appealing aesthetics

The wind farm designer may make manual adjustments to the found optimal layout to avoid constraints or to improve aspects of the wishes that were not formalized.

The limitations within OWFLO come from the regulations of the local government, the design codes from the wind turbine manufacturer, the site conditions and the choices of the wind farm developer. The government sets area restrictions, to have space for military training, fishing, and ferry routes. The wind turbine manufacturer provides design codes to ensure safe operation, which include a maximum allowable loading both for extreme loads and for the fatigue life of the turbines. The site conditions can give unforeseen area restrictions due to shipwrecks, boulders, and even unexploded bombs. The wind farm developer can set additional area restrictions, because of the water depth or the type of soil.

#### *Practical implementation*

The practical implementation of the wind farm developers wishes, the regulations and the design choices are formalised in practice by the objective function, constraints and design variables within OWFLO.

The main objective functions found in practice within OWFLO are maximizing annual energy production (AEP), maximizing profit and minimizing the levelized cost of energy (LCoE). By maximizing the annual energy production, the modeled wind farm generates the most energy, and thereby the wind farm generates the most revenue. The annual energy production can be represented with equation 3.1.

$$AEP_{net,t} = (AEP_{gross,t} - E_{Loss,wake,t} - E_{Loss,elec,t} - E_{Loss,downtime,t}) \quad (3.1)$$

The  $AEP_{net,t}$ , represents the net AEP, which is the gross AEP ( $AEP_{gross,t}$ ) minus the energy loss from wakes ( $E_{Loss,wake,t}$ ), electrical components ( $E_{Loss,elec,t}$ ) and downtime ( $E_{Loss,downtime,t}$ ).

An alternative to this objective function is minimizing the levelized cost of energy (LCoE). The LCoE calculates the cost per energy unit produced ( $\text{€}/MWh$ ). By minimizing the LCoE, the developer is said to have the best business case. The aim is to minimize the costs of the wind farm while also having high energy production. The LCoE can be defined in different ways. Equation 3.2 gives an example.

$$LCoE = \frac{CAPEX + \sum_{t=1}^T \frac{OPEX_t}{(1+r)^t} + DEC_T}{\frac{AEP_t}{(1+r)^t}} \quad (3.2)$$

The capital expenditures(CAPEX) consist of the cost for development, installation, electrical infrastructure, wind turbines, and support structures. All of them are considered to be made at  $t = 0$ . The operational expenditures(OPEX) includes maintenance costs and insurance premiums. The AEP and OPEX are discounted over the year and the decommissioning costs(DEC) are made in year T.

Another economic objective function, which is growing in interest, is optimising for profit. The objective is to maximize the profit of the wind farm over its lifetime. A typical objective function for this is the internal rate of return (IRR). The revenue is calculated by taking into account time variations in electricity prices. The equation for this objective is given in equation 3.3.

$$0 = \sum_{t=1}^T \frac{REV_t - OPEX_t}{(1+IRR)^t} - CAPEX \quad (3.3)$$

The chosen objective function has a big impact on the found optimal layout as it gives value to certain aspect of the layout, and can exclude other aspects. To illustrate what impact the choice of the objective function can have on the layout a comparison can be made between taking AEP and LCoE. By using AEP, the influence of water depth variation on the cost of the support structures is ignored, while it could be considered when using LCoE. Therefore, layouts optimised for the latter objective function may deviate from the layout with maximum AEP to trade some yield for a reduction in costs.

#### *design variables*

The typical design variables consist of the continuous  $x$ , and  $y$  coordinates of each wind turbine. However, variations to this design vector exist. When a wind farm developer wants a regular layout, the  $x, y$  coordinates are limited to only having design variables that build a regular layout. A heavy computational optimisation can be prevented by limiting the design space. This can be achieved by discretization of the continuous design variables or by giving turbines a fixed location.

If an economic objective function is used, other design variables need to be introduced. Such as support structure dimensions and cable topology. These variables will then be co-optimised for each iteration.

#### *constraints*

Before starting an optimisation, the constraints need to be specified. Two constraints are considered for OWFLO. Area and turbine spacing constraints. It is essential that the constraints are well defined so the final optimised layout is feasible.

A safe distance between turbines ensures there are no collisions. Additionally, wind turbines are required to comply with their design codes. In these design codes, a maximum allowable loading is given. It is possible to model the turbulence and set the turbine spacing constraints with maximum allowable turbulence or institute a wind sector management strategy which means curtailing turbine operations for some turbines for a range of wind speeds and directions [19]. When fulfilling the requirements of the design codes, there is still a lot of room to 'play' with, and different choices can be made by the wind farm developer. For instance, having a smaller spacing between wind turbines and increasing the thickness of the tower or having larger spacing and therefore less fatigue. When the minimum spacing is set small compared to the available area, turbines are freer to move around. In contrast, having a larger minimum spacing results in the constraint becoming active more often. Constraints become active more often when optimising for a dense wind farm or when turbines are pushed towards the boundary of the area.

There are several ways to implement constraints, which is dependent on the optimisation algorithm. One example is the penalty function, which imposes a penalty to the objective function if a turbine is placed in an invalid spot.

### **3.2.2. Analysis**

#### *Reality*

Analysing a layout to calculate its expected performance is complex, both in terms of the physics and economics surrounding the placements of the turbines. To calculate the energy yield, the wind conditions at each turbine, over the farm's lifetime, need to be known. Forecasting the wind conditions over a longer period comes with uncertainty as the wind conditions vary each year. The effect of turbines on the wind conditions also needs to be taken into account when they affect the wind conditions for other turbines. High-fidelity models can accurately capture these effects. However, optimisation requires many evaluations presenting a limitation on the computational time for each evaluation. This means that these accurate models, which have high computational time, are prohibited in OWFLO.

The costs of components of the farm and various activities depend on many factors, such as mate-

rial use, labour intensity and market dynamics. These factors make it difficult to assess the impact of the layout on the costs accurately.

#### *Practical implementation*

From the possible objectives described in section 3.2.1 two models emerge: one model that can calculate the AEP of a wind farm and one model that can calculate the costs of a wind farm. First the model for AEP is discussed.

#### *AEP calculation*

The energy that can be extracted from the wind is dependent on several factors, where the wind speed and type of turbine have the biggest impact. The relationship between output power and wind speed is approximated by the power curve. The power curve comes from the specifications of the manufacturer and is usually coupled with the free-stream wind speed at hub-height. Although in reality the wind speeds over the rotor area can fluctuate and impact the power output, the wind speed at hub-height is often used in practice to limit computational time. The wind speeds also fluctuate in time. However, to calculate the power for each time step is to computational heavy for OWFLO, therefore they use averages and statistics to capture the wind speeds at a specific location over a longer period of time. In practice the long-term character of the wind conditions is usually captured by the Weibull distribution, and the wind rose.

In Pywake, the *PropagateDownwind* model is selected for calculating AEP. The *PropagateDownwind* model is fast to run as it performs a minimum of deficit calculations. The effective wind speed at a current wind turbine is taken as the free-stream wind speed minus the sum of the deficits from upstream sources. With this effective wind speed, the deficit caused by the current turbine is calculated on all downstream turbines.

The main part of calculating the AEP is knowing the wind speed at each turbine. The wind speed model consists of several sub-models:

- wake model
- turbulence model
- superposition model
- rotor average model

#### *wake model*

When a rotating wind turbine extracts energy from the wind, it perturbs the wind flow downstream. By perturbing the wind flow it reduces the mean wind velocity and increases turbulence intensity. The reduction in mean wind speed will give a reduction in power output from a wind turbine that is placed downstream. At the same time, the increased turbulence intensity gives increased fatigue for a downstream wind turbine.

The wake models that are used in OWFLO are engineering models, which ensure simplicity and computational speed. Many engineering models exist. Some are implemented in multiple OWFLO tools, and others are less prominent. These are some examples: N.O.Jensen [11], Eddy-Viscosity (Ainslie) [7], Bastankhah(Porté-Agel)[10], Frandsen [9],(GCL) Larsen [8], Xie and Archer, FUGA [21], NiayifarGaussianDeficit [22]. The main parameters that are used within these models are wind speed, hub height, rotor diameter, thrust coefficient, downstream distance, and wake expansion factor.

A thrust coefficient curve of the wind turbine is used to get the thrust coefficient at the different wind speeds. The wake expansion factor can be fixed, dependent on the ambient turbulence conditions or on the local turbulence conditions. When the wake expansion factor is dependent on the local turbulence conditions a turbulence model is required for calculating the wake.

#### *turbulence model*

Wake induced turbulence is turbulence generated by wind turbines. Various ways of modeling wake-induced turbulence have been developed. One of the more famous ones is the Frandsen model that is included in the IEC61400-1-standard for wind turbine safety [23]. A turbulence model can be used for calculating loads on downstream turbines and for calculating the wake expansion factor.

#### *superposition model*

In a wind farm with multiple turbines wakes can overlap and therefore interact with each other. The interactions between wakes are approximated with superposition models. Wake interactions have an effect on the total wind speed deficit and wake-induced turbulence. In practice different superposition models are used in OWFLO. The five frequently used superposition models are geometric sum, linear summation, energy balance, quadratic summation, and maximum deficit.

#### *rotor average model*

The wind speed across a rotor varies, both in the horizontal and vertical direction. Therefore an average wind speed is needed. In general, a number of points covering the rotor are used to calculate the weighted mean of the wind speed. The computational cost and accuracy increase with the number of points. However, the way the distribution of points is set also has an impact on the rotor's average wind speed. The rotor's average wind speed is used in the calculation of the wake and the power output.

#### *Cost calculation*

Three models to calculate the costs of a wind farm are distinguished:

- Capital expenditure (CAPEX)
- Revenues
- Operational expenditure (OPEX)

#### *CAPEX*

The CAPEX consist of the wind turbine, foundation, electrical equipment, installation, and development costs. Two cost models are usually considered in OWFLO. The first one is the *electrical collection model*. As the layout changes, cable lengths, cable types, and the cable layout can change. These design changes influence the costs. The second model is the *support structures model*, which is influenced by water depth and turbulence intensity. Often, the change in mass is used as a proxy for the change in cost.

The influence of the CAPEX models on the response surface is dependent on the site conditions. Within a large area the electrical collection cost will influence the turbines that are pushed to the edges of the wind farm as the costs will be higher for larger distances. If the water depth changes drastically within the area, some turbines may be pushed away from deep water to trade some support structure cost for energy yield.

#### *Revenues*

The revenue is calculated by taking into account time variations in electricity prices. Defining future electricity prices together with time variations presents a complex model, which brings uncertainty. The revenues model directly signifies the value of the energy that is produced.

Suppose the wind farm is set to trade on the market with high wind power capacity. Installing large turbines may not be optimal as the energy price will drop when the wind blows. Therefore, producing additional MW's by installing large and expensive turbines may not give the best business case.

#### *OPEX*

The OPEX is dependent on the operation and maintenance (O&M) costs. Except for routine maintenance checks, maintenance costs come with high uncertainties. This is due to the lack of experience

with the new wind turbines. A general assumption can be made that higher turbulence increases fatigue and therefore increases the OPEX costs. One model that captures this is the *wake turbulence-induced fatigue degradation model* [24]. Another influencing factor that can be taken in the OPEX cost is the travel time for maintenance crews and vessels. However, they have minimal influence.

### 3.2.3. Optimiser

#### *Reality*

In reality, some layouts meet the designer's wishes less when the layout is subjected to minor deviations. This suggests that a designer might have found an optimal layout and can therefore end their search. However, layouts can differ greatly in turbine placements while satisfying the designer's wishes even better or to a similar extent. On the one hand, this complicates the search, as the designer may think they have found the best layout when this is not the case. On the other hand, this may not be detrimental since it may not matter that much when the found layout doesn't differ much from the actual best layout. However, before changing the layout, the designer doesn't know whether this will lead to meet his wishes even more or meet his wishes less. Together with the endless possibilities of placing the turbines, this presents a problem for deciding when to stop the search.

#### *Practical implementation*

Two methods are distinguished for optimisation algorithms, a gradient-based method and a gradient-free method.

#### *Gradient-based methods*

The gradient-based methods use the gradient of the objective function to determine the search directions. Gradient-based methods are not widely used for OWFLO problems. This is because by using gradient information, these methods are highly vulnerable to local optima [25]. They are therefore not well suited for problems that contain significant non-convexity. Despite this weakness, they have been shown to find good solutions to OWFLO problems [26]. The final converged solution depends heavily on the initial starting point in the design space. That is why a multi-start approach reduces the sensitivity of gradient-based optimisation to local optima. The difficulty of the OWFLO problem is due to the large number of variables and constraints and the multi-modal nature of the problem's design space [1]. The number of variables gives a high-dimensional problem for which gradient-based optimisation methods are well suited. Due to their low computational cost and their ability to handle many variables and constraints, they are gaining interest.

#### *Gradient-free methods*

The gradient-free optimisation methods do not use the gradient of the objective function to determine the search directions. The main elements of the gradient-free optimisation method are diversification and intensification. These optimizers typically use nature-inspired algorithms to search the design space on a more global level. They can include some elements of randomness as well. Although these optimisation algorithms try to alleviate the problem of exact algorithms finding local optima, they are also known to find local optima in OWFLO. This can be identified by the different resulting layouts that almost have the same AEP or LCoE [16]. With a more comprehensive exploration of the search space comes a computationally heavier optimisation, which converges slower to an optimal solution.

A hybrid method can also be used in OWFLO. This method uses a gradient-free and a gradient-based algorithm. By using the gradient-free method, the design space is first searched globally, while the gradient-based method then optimizes further to find the local optimal point.

## 3.3. Known phenomenons that are not implemented

All models can be seen as an abstract representation of reality. Within the abstraction process of reality some parts are left out in their practical implementations. There can be several reasons for not including these parts:

- They may not be of interest as they are not considered to influence the outcome of the created model.
- The reality is not yet fully understood.
- Some wishes cannot be put into a figure of merit.
- The computational time is too heavy for a multi-iterative optimisation.

The last reason is something which is a strong consideration when performing OWFLO. As the layouts need to be evaluated for each iteration.

Several effects that are not taken into account do impact the wake, and therefore the wake losses. The list below gives some examples of phenomena that are often not implemented in practice:

- atmospheric stability and wind farm wakes
- deep array effect
- wake meandering
- atmospheric gravity waves
- wind-farm-scale blockage

#### *atmospheric stability and wind farm wakes*

Atmospheric stability is not regularly implemented in OWFLO. However, it is found to have a significant impact on the wake. From the results of remote sensing observations, numerical and analytical studies, the wind speed deficits downwind of offshore wind farms tend to be larger in stable than in unstable conditions, and the lengths of wakes are longer [27]. Under stable atmospheric conditions, wind-farm wakes may extend up to 70 km downwind [28]. Traditional engineering models assume neutral conditions, and these are therefore found to underestimate the overall wake losses. Before implementing this phenomenon some questions need to be answered. For instance, how often do unstable, stable, and neutral conditions occur, and are stable conditions coupled to certain wind directions? Further analysis for different atmospheric conditions needs to be made to provide a clearer quantitative relationship between wind speed, turbulence intensity, atmospheric stability, and wake length [27]. Without this quantitative relationship implemented in the models, the models fall short in accurately capturing the conditions while atmospheric stability plays a major role in the evolution of wakes.

#### *deep array effect*

The deep array effect is an additional reduction in wind speeds around and within a wind farm, which is not captured by traditional engineering wake models. Theory and experiments show that for larger arrays, this effect occurs. They show that the wind profile outside the zone of direct wake effect is also changed and reduces the overall wind energy available within and around the wind farms arrays. All traditional models ignore the two-way interactions between the atmosphere and the wind farm. Specifically, the wind upstream and outside the zone of typical wake models is taken to be unaffected. These assumptions have been found to be the cause of underestimations of wake losses in large wind farms. New engineering models are made that are able to implement this effect, like the Openwind Deep Array Wake Model [29]. However, there is not yet a full consensus on the existence of a 'deep array effect' [30]. Also, the impact of an irregular layout and the turbine density is not yet fully understood.

#### *wake meandering*

Wake meandering refers to the fluctuating movement of the whole wake in the horizontal and vertical directions, illustrated in Figure 3.3. As the wake is being displaced the power output of a downstream turbine increases. In full-scale measurement studies by Baker and Walker [31], and Taylor [32], this phenomenon was observed. Wake meandering is a well-known but less understood phenomenon. Models have been proposed by Larsen et al. [33], and Braunbehrens and Segalini [34]. However, these models have generally not yet been implemented in OWFLO. The wake models used in practice

do not explicitly account for wake meandering.

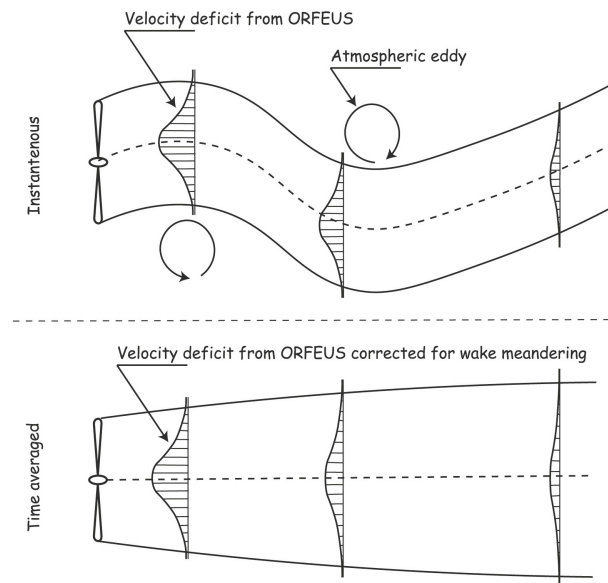


Figure 3.3: Schematic representation of wake meandering [34]

#### *atmospheric gravity waves*

Atmospheric gravity waves are buoyancy oscillations that can occur in a stable atmosphere. They can be triggered by:

- Topography (hills, ridges, mountains)
- Frontal passage
- Thunder storms
- Turbulence

Atmospheric gravity waves are frequently observed above the sea. This happens often when the wind is perturbed vertically by a terrain feature like a coastal ridge together with a strong temperature inversion. The AEP of a wind farm is decreased by atmospheric gravity waves. Wind farms can also create so-called self-induced gravity waves, which can affect both their upstream flow blockage and their wind farm wakes. The impact on the wind farm wakes is dependant on the stratification. If the stratification is weak a turbine downstream would see a decrease in power production. For stronger stratification the decrease is rapidly reduced. Self-induced gravity waves are difficult to simulate correctly, and require further research and validation.

#### *wind-farm-scale blockage*

Wind farm scale blockage loss is the difference between the power produced by a turbine in isolation and by the same turbine in an upstream position in a wind farm, illustrated in Figure 3.4. This loss is neglected by engineering wake models. Single turbines are considered to modify the flow around them, downstream by their wake, and upstream by their induction zone. With an array of turbines the air flow is also diverted to the side and above the wind farm. The wind farm produces an internal boundary layer deflecting air parcels upwards. The work that is required to displace the air parcels gives energy loss which is not available for the wind farm. The main drivers for blockage are the turbine density, and atmospheric stability.

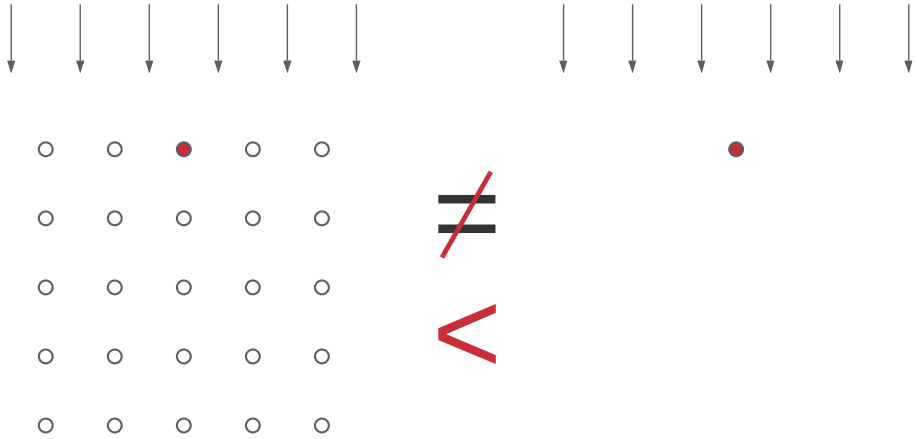
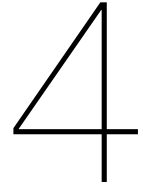


Figure 3.4: Visualisation of the difference in power between a turbine in a wind farm(left) and in isolation(right)



# Description and analysis of the referent

This chapter gives a description and analysis of the referent. First, a description of the referent is given. Secondly, three cases are introduced. Thirdly, the characteristics of the OWFLO problem are analysed by optimising the cases a hundred times and analysing the results. Fourthly, a special form of the response surface is explored. Finally, the insights obtained in this chapter are discussed.

## 4.1. Description of the referent

This section describes the referent, which is used for finding and understanding the characteristics of the OWFLO problem in section 4.3 and 4.4.

### 4.1.1. Overview and purpose

The referents problem formulation, analysis, and optimiser choices are illustrated in Figure 4.1. Each selection is further elaborated on in the subsequent sections. The selected site conditions, which contain essential parameters for the analysis, are also shown in Figure 4.1. They will be further elaborated in section 4.2.

The idea of the referent proposed by Roza [18] is that it represents a best-practice model. However, there are no clear best-practice models that can perform multi-iterative optimisation. Therefore, the choices for the referent are considered to have a general consensus within the OWFLO community and to be a good representation of reality. The computational time constraint dominantly limits the reality within the referent. Without this constraint, better models could be selected. However, the purpose of the referent is not to use it as the ground truth. For the coming sections, the referent models need to be used for optimisation. The purpose of the referent in chapter 5 is to compare the deviations and spread between alternative models and the referent and not to validate or benchmark those models.

### 4.1.2. Problem formulation

Section 3.2.1 gave several examples of the most commonly used objective functions, design variables and constraints for OWFLO. Here a selection is made of these examples for the referent.

#### *Objective function*

Maximizing AEP has been selected as the objective function for the referent. This is considered the most straightforward objective function, which can show the OWFLO problem's characteristics. Including cost into the optimisation will further complicate the OWFLO problem and increase computational time. With respect to the time of this thesis, it was decided not to include cost models. The characteristics found with this objective function are assumed to be also valid for other objective functions as the impact of the AEP on the economic objective functions is dominant.

#### *Design variables*

The x and y coordinates of each wind turbine are taken as continuous design variables.

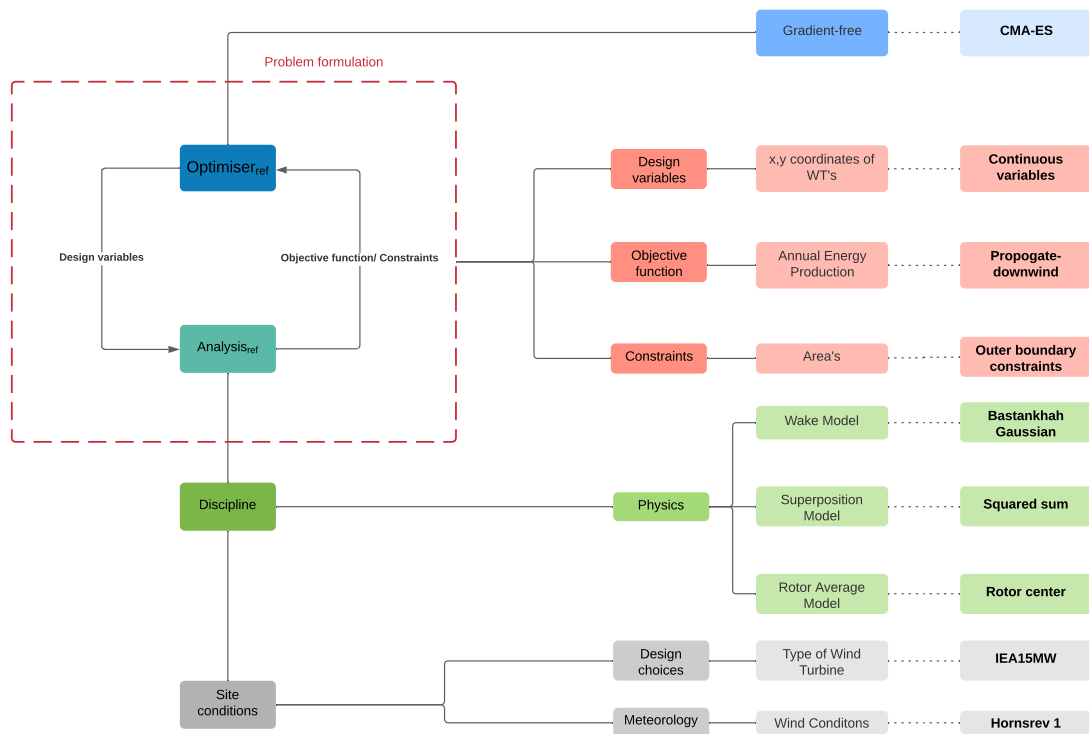


Figure 4.1: Referent overview

### Constraints

The outer boundaries of the wind farm are considered to be the only constraint. Therefore, no minimum spacing between turbines, maximum loading on turbines, or added area constraints are implemented in the referent.

### 4.1.3. Analysis

Section 3.2.2 gave several examples of the most commonly used models for calculating wind speed. Here a selection is made for the referent. The wind speed is converted to wind power by the *PropagateDownwind* model specified in section 3.2.2 .

### Wake model

The Bastankhah Gaussian(BG) model is selected as the wake model. The implementation is done according to Bastankhah M and Porté-Agel F [10]. The BG model is chosen because it is derived by applying conservation of mass and momentum, and it assumes a Gaussian distribution for the velocity deficit in the wake. Wind-tunnel measurements, numerical simulations, and data of operating wind farms observe this Gaussian shape of the velocity deficit in turbine wakes [10]. Therefore, considering a top-hat shape for the velocity deficit of NOJensen [11] is regarded as a less accurate assumption. The difference between the shapes is illustrated in Figure 4.2.

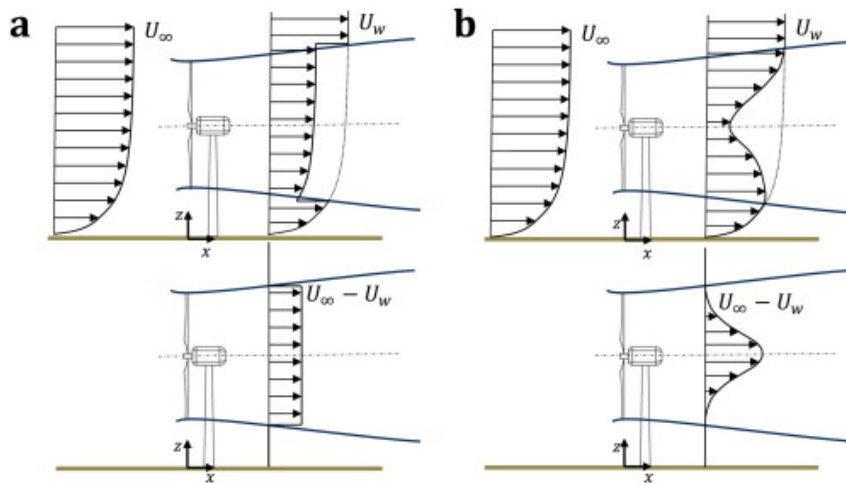


**Figure 4.2:** Schematic of the vertical profiles of the mean velocity (top) and velocity deficit (bottom) downwind of a wind turbine obtained by assuming: (a) a top-hat and (b) a Gaussian distribution for the velocity deficit in the wake. [10]

#### *Superposition model*

The selected superposition model is the squared summation model. This is a simple and widely used summation technique. It is obtained by taking the square root of the sum of the upstream single wake deficits.

#### *Rotor average model*

The rotor centre model is used in the referent. Although the rotor-average wind speed is not well-defined by the wind speed at the rotor centre, computational time didn't allow the calculation of a set of points.

### 4.1.4. Optimiser

The optimiser that is used for the referent is a gradient-free optimiser called the Covariance Matrix Adaptation Evolution Strategy (CMA-ES) [35]. CMA-ES is a stochastic numerical optimisation algorithm for non-convex optimisation problems that have continuous search spaces. Finding different layouts with similar performances, which is expected to be a characteristic of the OWFLO problem, requires a non-deterministic optimiser. This can be achieved in two ways, either by using a gradient-based optimiser together with a multi-start approach or by having a gradient-free optimiser. A gradient-free optimiser is selected here.

After optimising with the CMA-ES, a test is done for several cases to see whether the optimiser is able to really find a local optimum. The test consists of running a sequential gradient-based optimisation and seeing if this changes the layout and performance. The gradient-based optimisation that is used is the sequential least-squares quadratic programming (SLSQP) taken from Topfarm [24]. The SLSQP found a slight improvement by a minute change of the layout. This was considered neglectable as the change in AEP was less than 0,001 %. This test confirmed that the CMA-ES optimiser is able to find local optima.

## 4.2. The three cases

Three cases have been defined to find and understand the characteristics of the OWFLO problem. The differences between the cases are the number of wind turbines and the size of the outer boundary constraints. All three have a square outer boundary constraint and no area constraints within the boundaries. The number of wind turbines is 9, 25, and 64, with a boundary constraint of 14D x 14D, 28D x 28D, 49D x 49D, respectively. The boundary constraints and their corresponding number of turbines are illustrated in Figure 4.3, where D is the turbine diameter. The size of the area is made to fit a regular layout with a spacing of 7D. The typical wind turbine spacing that is used in actual wind farms nowadays is 6 to 10D [36], making 7D a reasonable spacing. This is done to have an appropriate

turbine density.

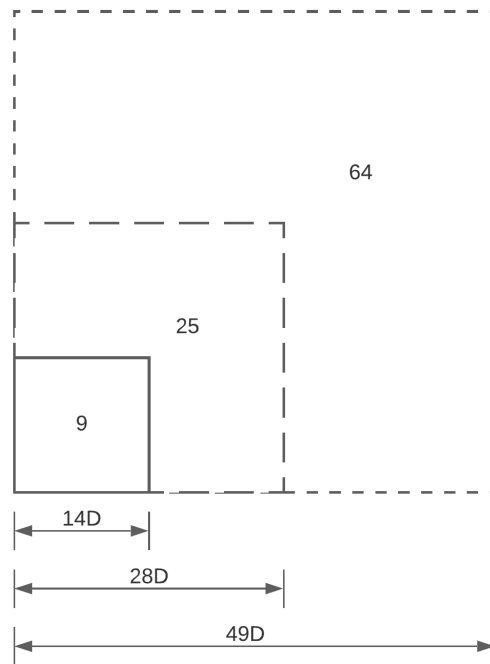


**Figure 4.3:** Visualisation of the number of turbines and the boundary constraints

#### *Wind turbine*

For all three cases, the same wind turbine is selected. As wind turbines are still developing at a rapid pace, selecting a state-of-the-art wind turbine was required to make the research relevant now and in the coming years. However, the turbine data from the leading wind turbine manufacturers are not publicly available. Therefore, a reference wind turbine called the IEA15MW is used, which was specifically made to give open benchmarks for studies exploring new design methodologies. The IEA15MW is a 15-megawatt (MW) offshore wind turbine with a fixed-bottom monopile support structure [37]. It is a Class IB direct-drive machine, with a rotor diameter of 240 meters (m) and a hub-height of 150 m [37]. The rotor diameter, hub height, thrust curve and power curve were used. The thrust coefficient curve and power curve are illustrated in Figure 4.4.

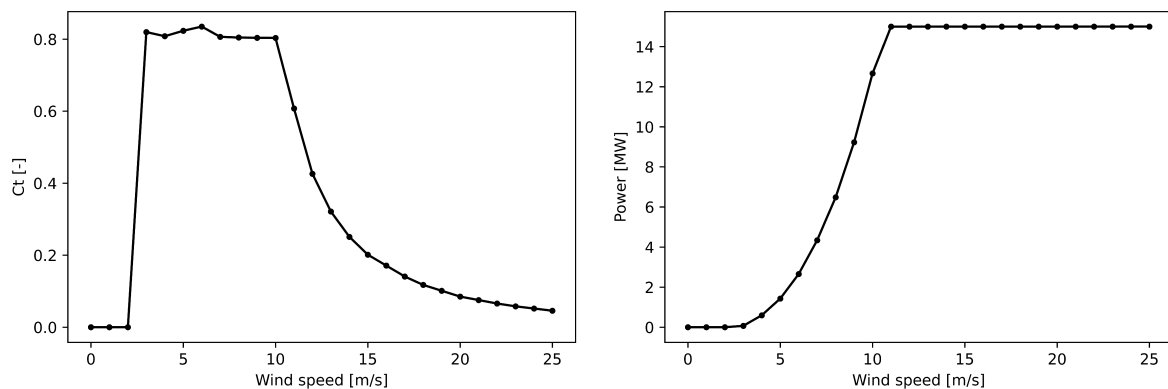


**Figure 4.4:** Thrust coefficient curve and power curve of the IEA15MW

### Wind conditions

For all three cases, the same wind conditions are used. The wind conditions have been taken from Hornsrev 1 and are illustrated in Figure 4.5. The parameters for the Weibull curves have been further detailed in Table 4.1. These wind conditions were already available within PyWake. An alteration needed to be made as these conditions were set at the height of 70 meters. Therefore the power-law with an exponent of 0.11 was used to adjust the wind speed data to the hub height of the IEA15MW. This exponent was taken from literature and was determined under near-neutral stability conditions at sea [38].

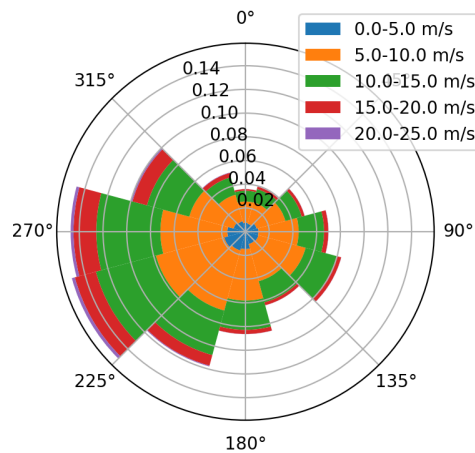


Figure 4.5: Hornsrev 1 wind rose

Direction (°)	Frequency (%)	Scale (a)	Shape(k)
0	3.60	9.18	2.39
30	3.95	9.78	2.45
60	5.17	9.53	2.41
90	7.00	9.91	2.59
120	8.36	10.04	2.76
150	6.43	9.59	2.60
180	8.64	9.58	2.58
210	11.77	10.51	2.55
240	15.16	11.40	2.47
270	14.78	11.69	2.61
300	10.01	11.64	2.63
330	5.17	10.09	2.33

Table 4.1: Hornsrev 1 wind rose table

## 4.3. Identifying the characteristics of the OWFLO problem

The previously defined cases will be used to identify the characteristics of the OWFLO problem. All three use cases have been optimised one hundred times. This gave a hundred different layouts and a hundred different performances for the use cases with 25 and 64 turbines. For the use case with 9 turbines, 35 different layouts were found. This means that 65 layouts were nearly identical to a layout found in an earlier optimisation, which corresponded to the same local optimum. The different found optimal layouts already show that many local optima exist in the cases.

The characteristics of the OWFLO problem are further examined by making a histogram of the performances and a heat map and scatterplot of the turbines positions. The heatmap which is used here is a graphical representation of all turbines positions. It uses colour to show where turbines have been placed within the wind farm. The number of times turbines are placed within the same box, which has a size of  $0.5 D \times 0.5 D$ , is counted and represented by a colour from the color map. The scatterplot shows

the positions of all the turbines resulting from the optimised layouts. On the top and on the right-hand side edge, a histogram indicates the times a turbine is placed within that bin.

#### 9 turbines

First, the results are shown of the wind farm with 9 wind turbines. Figure 4.6 shows the histogram of the performances from the 35 optimised layouts. Although the layouts differ greatly, which will be addressed later, the performances of all layouts are very close to each other. The gap between the highest and lowest found AEP is 0.21 %.

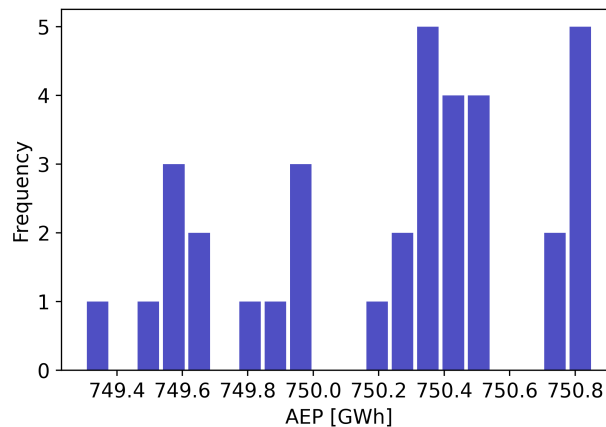


Figure 4.6: AEP histogram for 35 optimized layouts

In Figure 4.7 the heatmap of the 35 layouts is shown. The top left and lower right corners are dark red, indicating that a turbine is placed there for every optimised layout. For the other corners, which are light red, this is true for the majority of the layouts. Placing the turbines in the corners maximises the distance between them. Maximising the distance minimises the wake losses, which is why the optimiser places the turbines in the corner. The shape of the wind rose together with the favourable edge positions can explain other hot spots. The dominant wind direction comes from the west(left), see Figure 4.5. Therefore it is better to place more turbines with larger distances in the direction west to east(left to right) than in the direction from north to south(top to bottom). Which means that putting more turbines on the right and the left edge is more optimal than putting more turbines on the upper and lower edge. In the heatmap a wider spread on the left and right edge can be identified. For the lower and upper edge, one turbine is placed there around the middle. A gap where no turbines are placed is visible between the turbines in the corner and those positioned on the edge. With the turbine density within this case, there is enough room for the turbines to be pushed a certain distance without having the negative effects of another turbine. In the centre of the wind farm, no clear pattern could be identified. The placement of the turbines in the centre is dependent on the placement of the turbines on the edge. As the placement on the edges differs per layout, the local optima within the farm also differ. An indication of a gap between the centre turbines and those on the edge is visible.

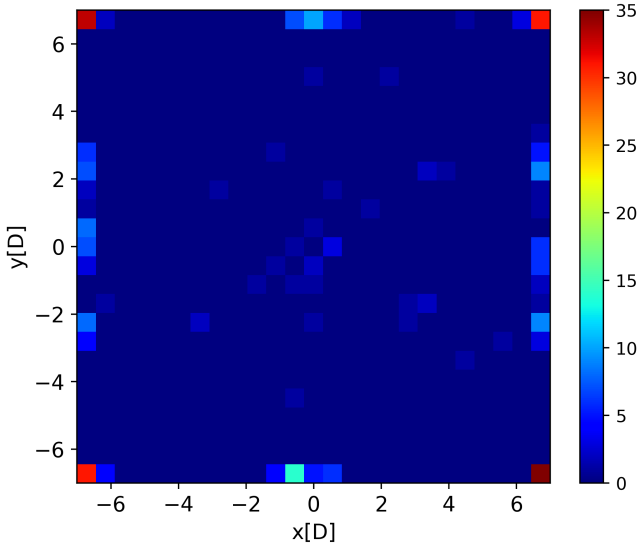


Figure 4.7: Heatmap of wind turbines positions

The scatterplot is illustrated in Figure 4.8. The difference between the height of the histogram on top of the scatterplot and of the histogram on the side confirms the conclusion that more turbines are placed on the edges of the direction of the dominant wind. Besides the conclusions found in the heatmap, there is one other interesting placement found in the scatterplot. At the left and right sides, turbines are placed a small distance from the edge. This 'second row' is found favourable over putting the turbine on the edge of the wind farm by the optimiser. The second-row effect will be assessed in more detail in section 4.4.2

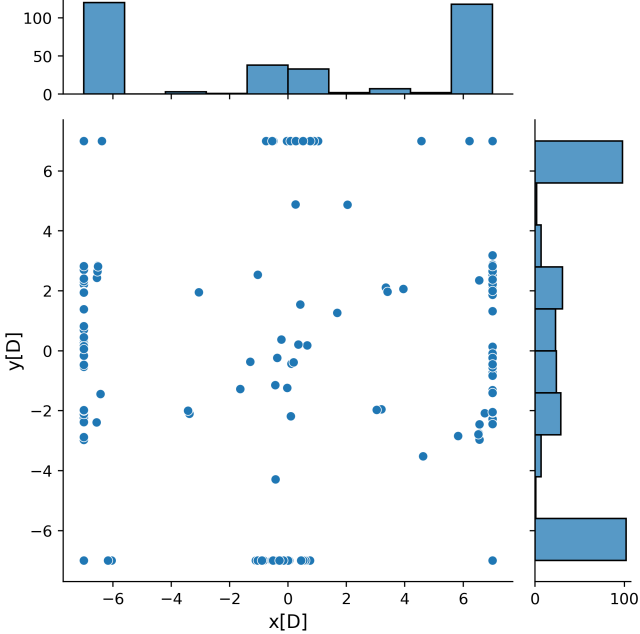
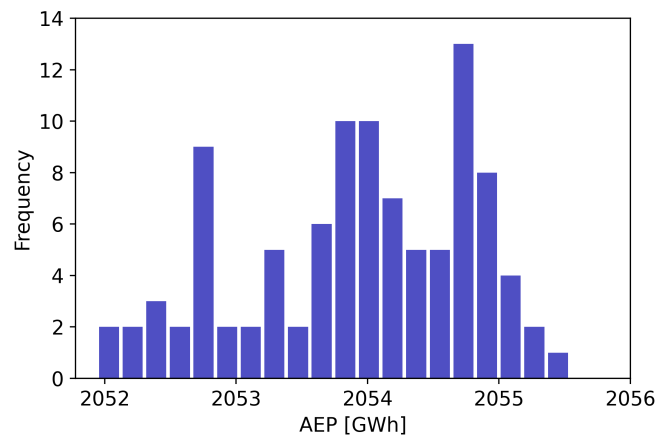


Figure 4.8: Scatterplot of all wind turbines positions

*25 turbines*

Second, the results are shown of the wind farm with 25 wind turbines. Figure 4.9 shows the histogram of the performances from the 100 optimised layouts.



**Figure 4.9:** AEP histogram for 100 optimized layouts

The difference between the highest and lowest AEP is 3.6 GWh, which in percentage is 0.17 %. The frequency drops off at the edge of the higher AEP, suggesting less local optima exist at the higher end. The majority of the performances lie around 2054 GWh.

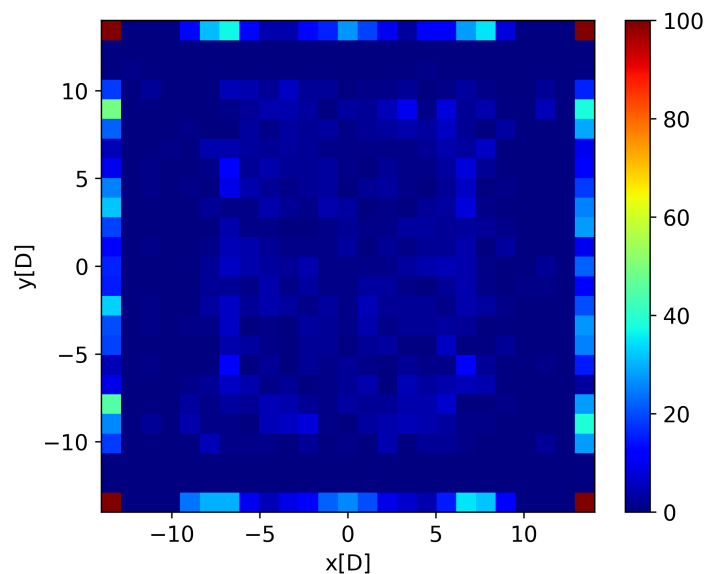


**Figure 4.10:** Heatmap of wind turbines positions

In Figure 4.10 the heatmap of the 100 layouts is shown. The dark red corners indicate that all 100 optimised layouts have a turbine in all corners. Similar to what was seen in Figure 4.7. From the corners, a gap is again visible on the edges where no turbines are placed. From the edge to the centre of the wind farm, a clearer gap is visible than for the 9-turbine case in Figure 4.7. In the middle of the wind farm, no clear pattern can be found.

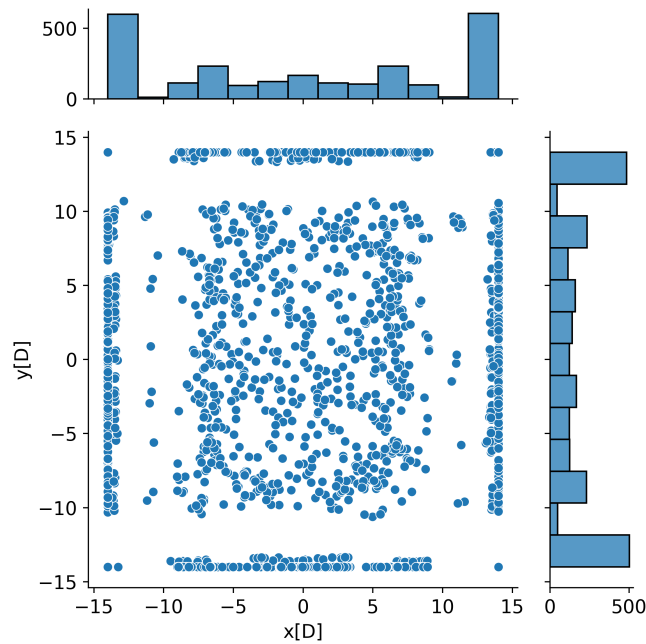


**Figure 4.11:** Scatterplot of all wind turbines positions

The scatterplot is illustrated in Figure 4.11. With 25 turbines, the 'second row' on the edges is more evident and is seen on all edges. This recurring placement is further investigated in section 4.4.2. The histograms of the scatterplot show that turbines are more often placed on the left and right edges than on the upper and lower edges, again indicating that more turbines are placed in the direction of the dominant wind. No significant distinction was found between the number of times turbines were placed on the left or right edge. This is interesting since the wind rose deviates strongly in frequency between easterly and westerly winds. The benefit from placing more turbines on the upstream edge to avoid wake effects from the centre turbines doesn't seem to outweigh the benefit from having the same amount of turbines on the downstream edge.

#### 64 turbines

Lastly, the results from the wind farm with 64 wind turbines are shown. Figure 4.12 shows the histogram of the performances from the 100 optimised layouts.

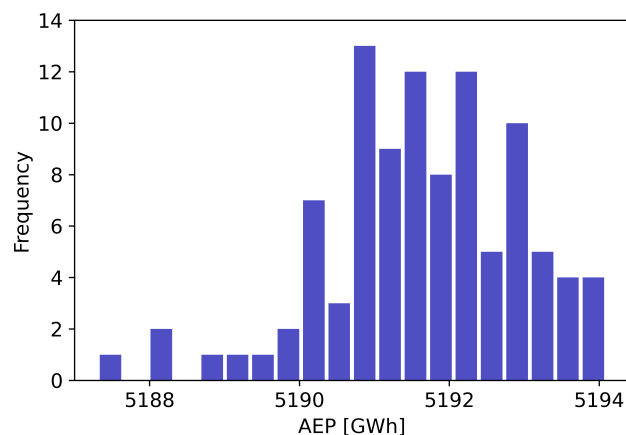


**Figure 4.12:** AEP histogram for 100 optimized layouts

The difference between the highest and lowest AEP is 6.8 GWh, which in percentage is 0.13%. The

histogram shows that the frequency of the relatively low performances is less than those with higher performances. The majority of the performances lie around 5192 GWh.

In Figure 4.13 the heatmap of the 100 layouts is shown. Again the dark red corners indicate that all 100 optimised layouts have a turbine in each corner. Four orange blocks indicate that turbines are placed at a certain distance from the left and right edge corner for most of the layouts. Similar behaviour could already be observed for the 25-turbine case in Figure 4.10, but this was insufficiently clear to make a firm statement about it. The turbines in the corner and the dominant wind direction can explain the specific placement inside the four orange blocks. The area surrounding the four orange blocks is relatively constant when compared to other areas in the wind farm. The deviations from turbines around the orange block are a small duo to the gap to the centre and the gap to the turbine on the edge. The influence of these deviations is also lowered as the influence from the dominant wind is higher. On the upper and lower edge, the yellow-green blocks indicate a similar but less specific spot. This comes from the weaker wind directions, which makes the influence from surrounding turbines relatively higher.

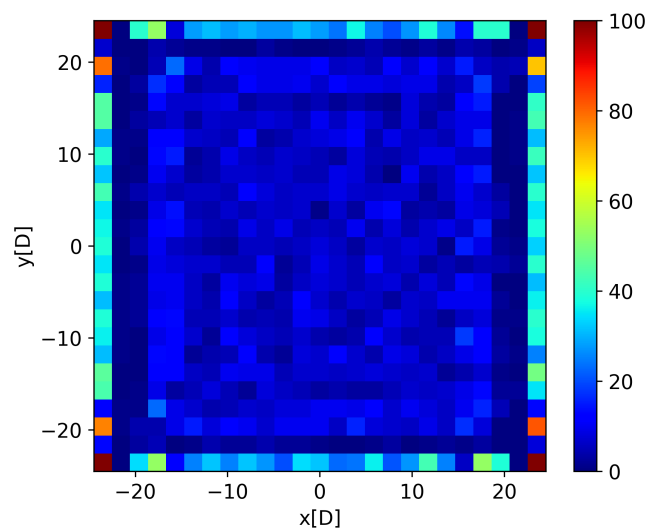


**Figure 4.13:** Heatmap of wind turbines positions

The gap from the edges of the wind farm to the middle of the wind farm, which is again visible, is larger in the direction of the dominant wind than in the less dominant wind direction. This shows that the optimiser is able to consequently put the turbines further away in the dominant wind direction. In the middle of the wind farm, no clear pattern can be found.

The scatterplot is illustrated in Figure 4.14. The 'second row' is visible again on all four edges. The histograms of the scatterplot show that turbines are again placed more often in the direction of the dominant wind. Again no significant distinction was found between the number of times turbines that were placed on the left or right edge.

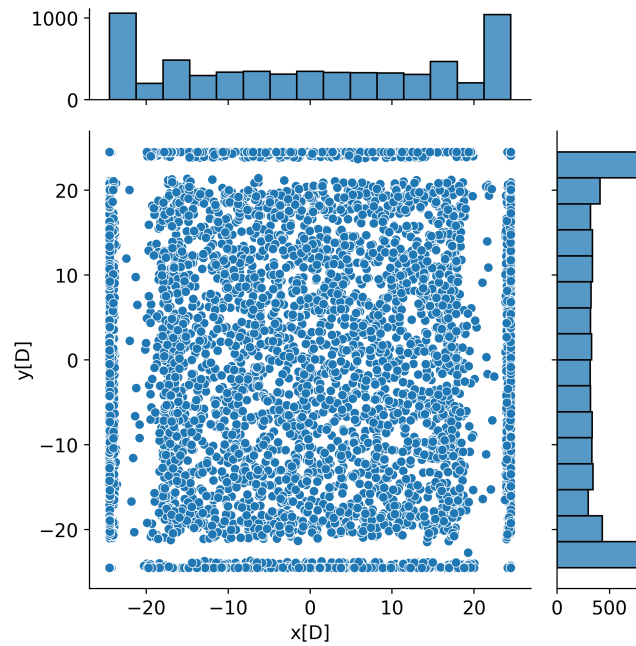


Figure 4.14: Scatterplot of all wind turbines positions

#### Normalized boxplot of the performances

Boxplots give insight into the distribution properties of data and are useful for comparing distributions between many datasets. However, for the unfamiliar reader, they can be challenging to interpret. Therefore, the boxplot and its settings used within this paper are explained here. Figure 4.15 illustrates the different visual features of the box plot and indicates its settings. The orange line shows the median, which is the middle value of the dataset or 50th percentile. The box extends from the lower to upper quartile values of the data. The lower quartile is denoted as  $Q_1$  and is the median of the lower half of the dataset. The third quartile is denoted as  $Q_3$  and is the median of the upper half of the dataset. The interquartile range is used to make the whiskers of the boxplot. The interquartile range is the distance between the upper and lower quartiles,  $IQR = Q_3 - Q_1$ . The whiskers extend from the box to the largest or lowest observed point from the dataset that falls within 1.5 times the IQR. Outlier points are those past the end of the whiskers.

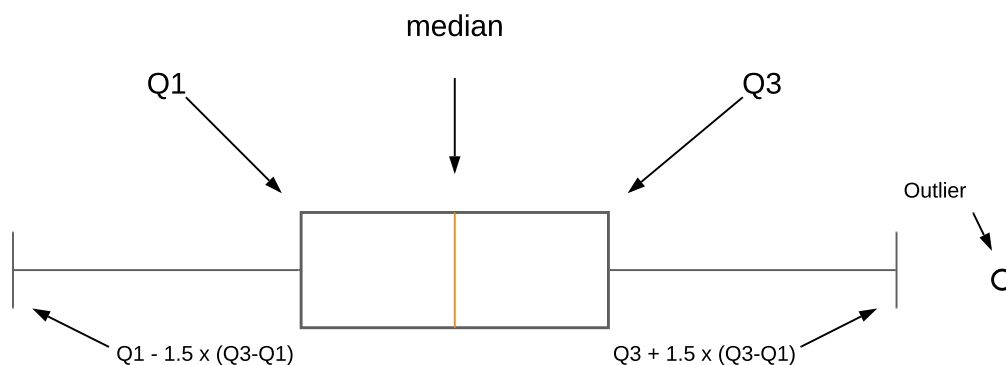


Figure 4.15: Boxplot settings

A decrease in the percentage of the spread of the highest and lowest found AEP was observed from the resulting performances. A normalised boxplot of the use cases is shown in Figure 4.16 to illustrate

this decrease better.

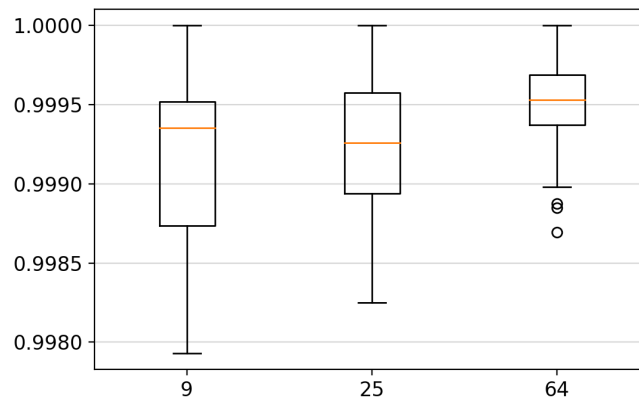


Figure 4.16: Normalized boxplots for the use cases

For a higher number of turbines, the spread decreases, suggesting that the difference in percentage between the highest and lowest found performance will further decrease if more turbines are added.

## 4.4. Response surfaces

This section analyses the case's final found layouts by looking at a special form of the response surface which only has two variables. The placements of turbines on the second row is also further analysed.

### 4.4.1. Optimised layouts

The previous section showed that the response surface of an OWFLO problem is complex and contains many local optima. To better understand the response surface and how these local optima are formed, visualisations are made. A visualisation of an OWFLO problem with multiple design variables is not possible. Therefore, visualisations are made with only two design variables—a turbine's x and y coordinate. All other turbine locations are fixed. An illustration of how the response surface is visualised is given in Figure 4.17.

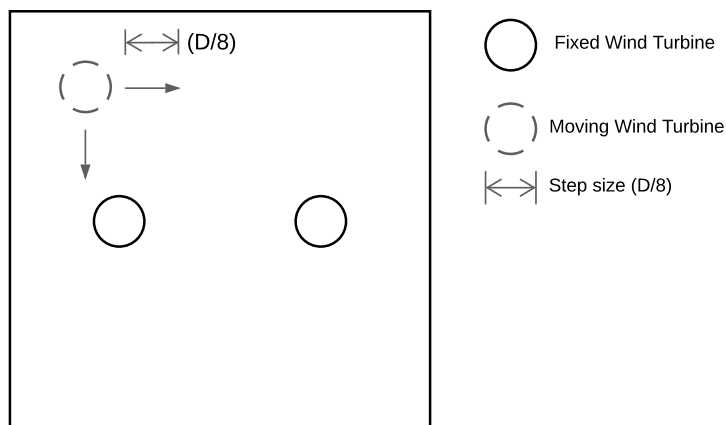


Figure 4.17: Visualisation of how the response surface is made

A turbine is moved across a wind farm with a step size of 30 meters ( $D/8$ ), and for each step, the total wind farm's AEP is calculated with the referent settings. For Figure 4.17 this amounts to the total AEP of three wind turbines. In this way, the wake losses on all wind turbines are taken into account.

By moving one turbine across a wind farm, local optima created by the turbine wakes can be identified. This method is applied for the configuration shown in Figure 4.17 and for some of the optimised layouts of the three cases.

### 3 turbines

The response surface of Figure 4.17 is illustrated in Figure 4.18. A 2D colour plot is used to show the performance in AEP. Green highlights have been added to the colour bar to indicate the best performing places. The two turbines that are fixed are at a distance of 7D and their locations are indicated by a red circle with the size of the rotor diameter. A cross-section is made to further detail the response surface, which is illustrated in Figure 4.19.

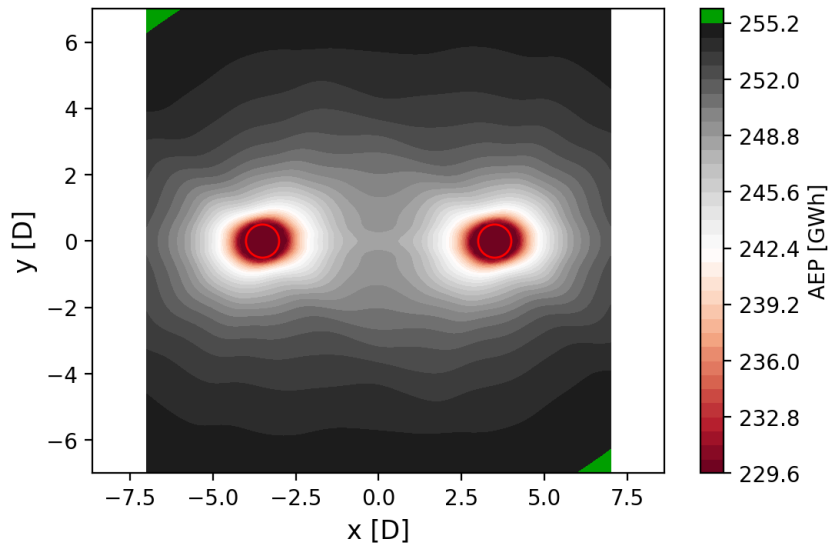


Figure 4.18: Response surface

From the illustrations, it can be concluded that the further away the turbine is placed, the higher the wind farm's AEP. Figure 4.18 illustrates this by the increasingly darker tints towards the edges and in Figure 4.19, by the rising lines from the origin.

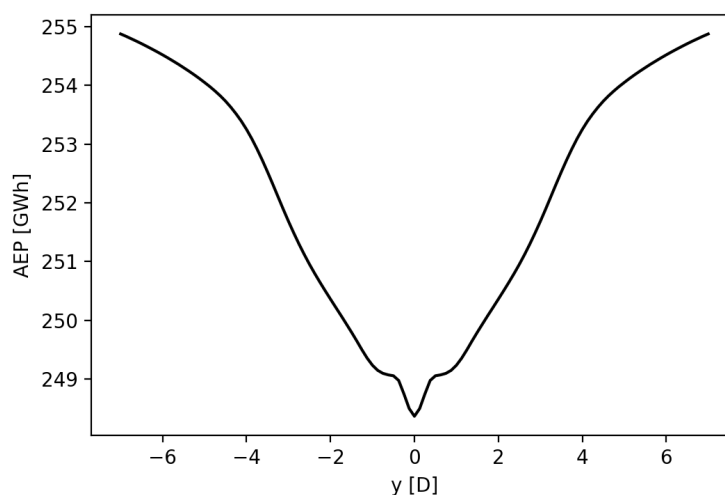


Figure 4.19: A cross section of the response surface at  $x = 0$

An increase in performance with an increase in the distance between turbines is not surprising as

the wake losses reduce when the distance between turbines is increased. Without area restrictions optimising two wind turbines for maximum AEP would be placing them as far away as possible until there is no effect of the wake of the turbines. The two green spots on the top left and bottom right indicate the best-performing configurations and can be explained by the dominant wind directions from the west and south-west. In both spots, the wake losses for these directions are minimised.

The shape of the cross-section around the origin in Figure 4.19 is interesting. At a distance around  $0.5D$ , the gradient of the line becomes almost zero. This indicates that there is another influence around the origin, which counters the benefit from an increasing distance between turbines. This particular shape near the origin will be analysed in more detail in section 4.4.2.

#### 9 turbines

From the results shown in section 4.3, two layouts have been taken from the 9 turbine cases to make two response surfaces. The best and worst-performing layouts of the 35 have been selected. Per layout, one turbine is removed. For the best-performing layout, a turbine placed at the second row was picked to give insight into the response surface around that area. For the worst-performing layout, a turbine placed in the centre of the wind farm was picked to give insight into the expected local optima created by the other turbines. After removing one turbine, a turbine is moved across the wind farm as shown in Figure 4.17.

The resulting response surfaces of the best and worst-performing layouts are illustrated in Figure 4.20 and 4.21, respectively. The blue circle indicates the removed turbine's original placement found by the optimiser. The red circles indicate the eight fixed turbines. Multiple green highlights have been added to the colour bar to see the locations for the best configurations better.

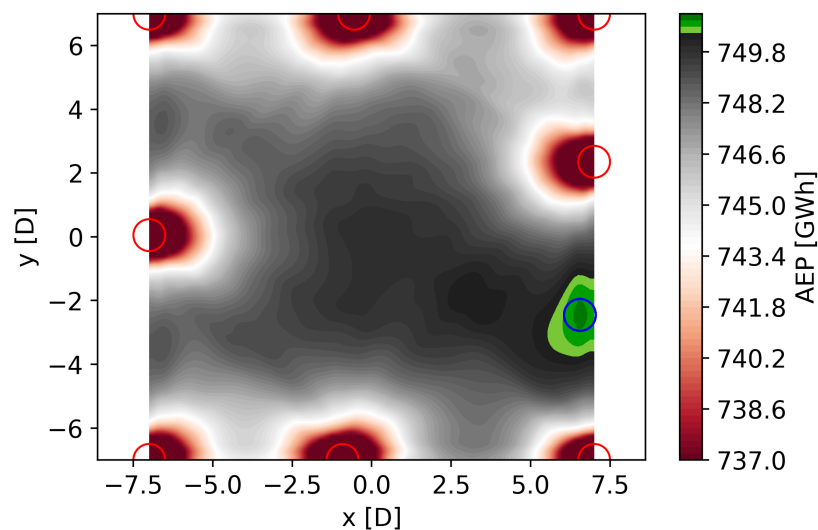


**Figure 4.20:** Response surface resulting from the best-performing layout for case 9 (750.86[GWh])

Figure 4.20 shows that the removed turbine was at the best location for this configuration, which is just off the edge at the second row. The dark green island shows that a higher performance can be achieved just off the edge than on the edge. Why this higher performance is located there will be explained in section 4.4.2. The best-performing layout has all its turbines on the edge (or just off the edge), while the worst-performing layout has two turbines in the centre of the wind farm. Additionally, Figure 4.21 shows that the worst-performing layout's removed turbine was not placed at the best-performing location. The blue turbine is placed on a light-black island, indicating a local optimum, while on the edge a higher performance could be obtained, shown in dark green. The performances of these optima are 749.30 [GWh] and 750.58 [GWh], respectively. This gives a difference of 1.28 [GWh]. If the turbine had been placed at the green island the performance would be close to that of the best-performing layout. Both response surfaces show multiple local optima, which can be identified by darker scaled islands

and the darker green island. The local optima differ both in size and height. These local optima are created by the wakes of multiple turbines and create a challenge for optimisers.

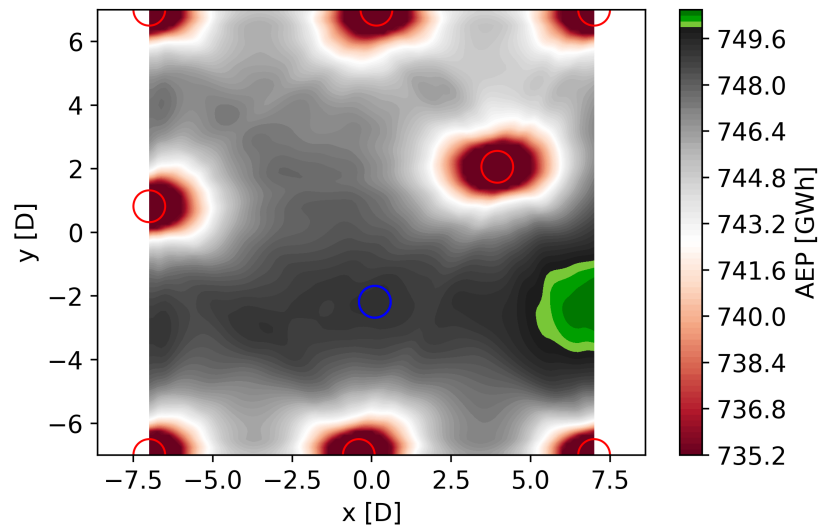


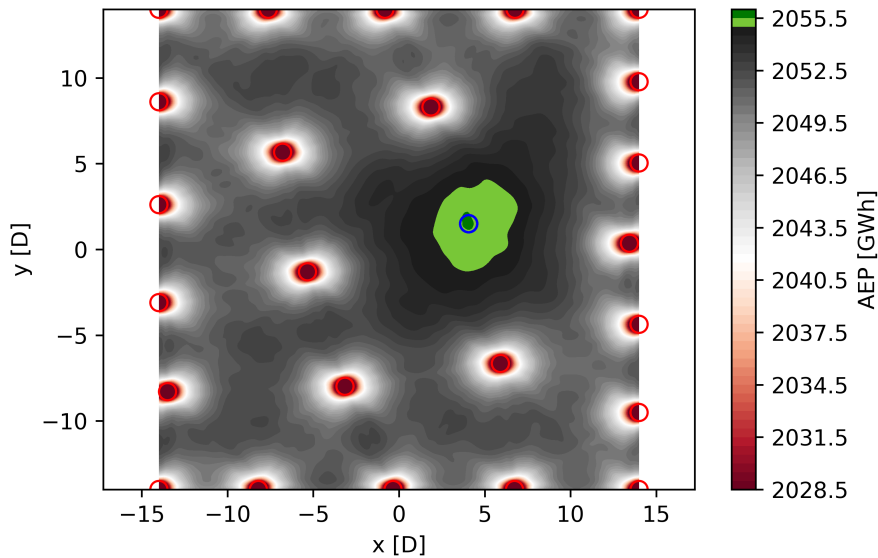
**Figure 4.21:** Response surface resulting from the worst-performing layout for case 9 (749.30[GWh])

The term global optimum is not used for the green islands to prevent confusion with the global optimum of the three cases, which have multiple design variables. As the visualisations made in this section show a special form of the OWFLO problem, with just two design variables, the best-performing location could be called the global optimum. However, as there is no clear indication if the global optimum is found with the three cases, the term global optimum is not used for the best-performing locations. The term local optimum is used for the best-performing locations in the response surfaces as the total configuration of the turbines' locations is considered to be in a local optimum.

#### *25 turbines*

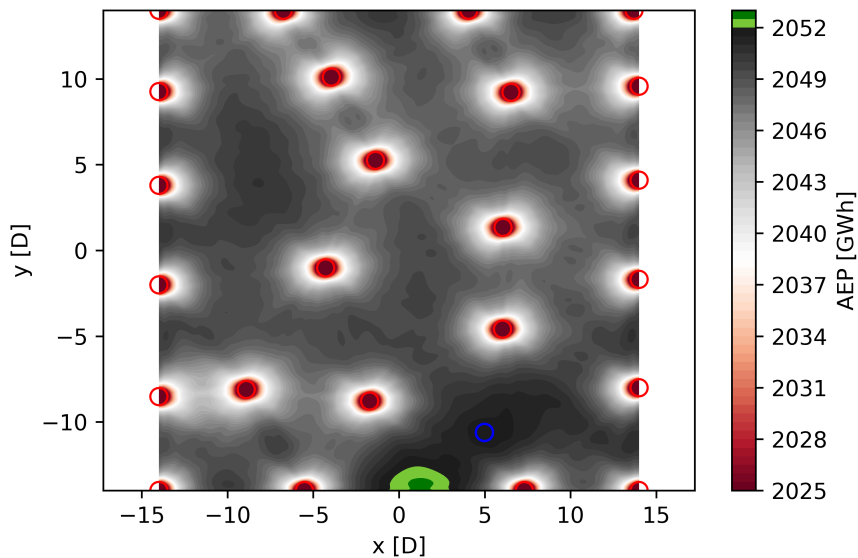
For the 25 turbine case, the same is done as in the previous section. From the 100 resulting layouts of the 25 cases, the best and worst-performing layouts have been selected and per layout, one turbine is removed. For both layouts, a turbine in the middle of the wind farm is removed. After removing one turbine, a turbine is moved across the wind farm as shown in Figure 4.17. The response surfaces are shown in Figure 4.22 and 4.23, representing the layout from the best and worst, respectively.

Figure 4.22 shows that the removed turbine (blue turbine) is placed at the best-performing location for this configuration, namely, on the dark green island. With an increase in turbines, the response surface becomes more complex. The contour lines show more complex shapes and more local optima than there were for the 9 turbine cases. The increase in the number of local optima can be explained by the increase in the number of turbines and the area size, which present more wakes and more areas between turbines.



**Figure 4.22:** Response surface resulting from the best-performing layout for case 25 (2055.54 [GWh])

Figure 4.23 shows that the removed turbine (blue turbine) is not placed at the best-performing location for this configuration. The best-performing location is found on the edge of the wind farm. The difference between the local optima where the turbine is placed and the local optima on the edge is 1.1 [GWh]. The difference between the two local optima is similar to the difference which was found between the two local optima for the worst-performing 9 turbine case in Figure 4.21. While the absolute difference is almost the same, the relative difference has decreased as the total AEP has significantly increased from 750 [GWh] to 2055 [GWh]. The decrease in the relative difference explains the difference in the spread between the 9, 25 and 64 turbines shown in Figure 4.16.



**Figure 4.23:** Response surface resulting from the worst-performing layout for case 25 (2051.94 [GWh])

#### 64 turbines

Only the best-performing layout has been selected for the case with 64 turbines. Regarding the computational time, the step size is changed to 60 meters ( $D/4$ ). A decrease in the step size results in a less accurate response surface. However, for the analysis here, the accuracy with a step size of 60 meters was found sufficient.

Figure 4.24 shows the resulting response surface. The removed turbine was placed at the best-performing location for this configuration. As the area size and the number of turbines increase, so does the number of local optima and the complexity of the response surface. The size of the local optima (islands) differs enormously within the wind farm. Some local optima take up larger spaces between turbines, while others can be found as small dots. The difference between the height of the highest local optima and the second best was found to be 1.2 [GWh]. This indicates that if an optimiser would find a lower local optimum the absolute difference between local optima would still be around 1.2 [GWh], as was found with the previous cases. The total AEP has increased again, meaning that relative to the total AEP, the difference of the two local optima is decreased with respect to the other cases. This is in line with our analysis made in the previous section and the reason why the relative spread decreases for an increasing number of turbines.

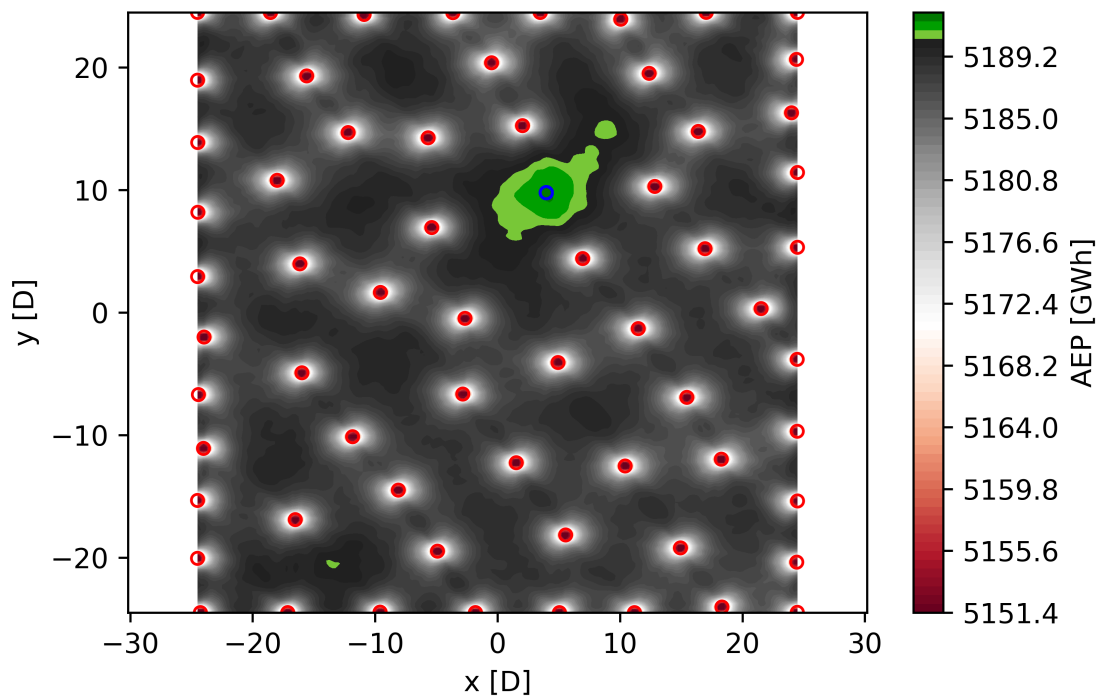


**Figure 4.24:** Response surface resulting from the best-performing layout for case 64 (5194.09 [GWh])

### 4.4.2. Second row

In this section, the second row, which was identified in the scatter plots in section 4.3 and the response surface in section 4.4 is explored.

After visually analysing the resulting layouts, the distance between the two surrounding turbines on the edge when a turbine goes to a second row was around 10 D apart. Therefore, Figure 4.17 is reanalysed by setting the two fixed turbines at a distance of 10 D. Instead of looking at the whole response surface, a response surface line is made perpendicular to the line in which the two fixed turbines lie. The setup is illustrated in Figure 4.25. A more detailed line is made by reducing the step size to 3.75 meters ( $D/64$ ).

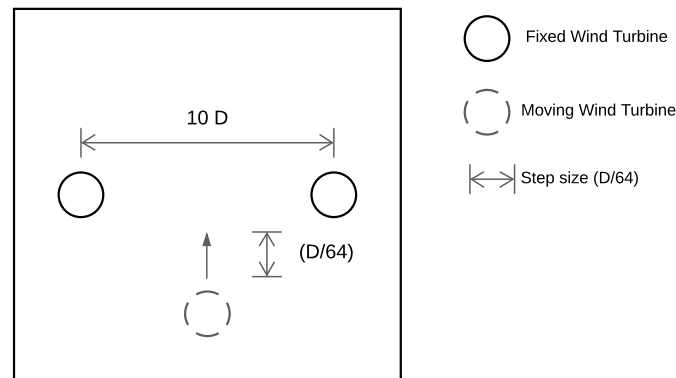


Figure 4.25: Visualisation of how the response surface line is made

The resulting response surface line is illustrated in Figure 4.26. The shape of the response surface line shows two local optima around the origin. The AEP improves when the turbine is moved away from the centre, comparable to a movement from the edge.

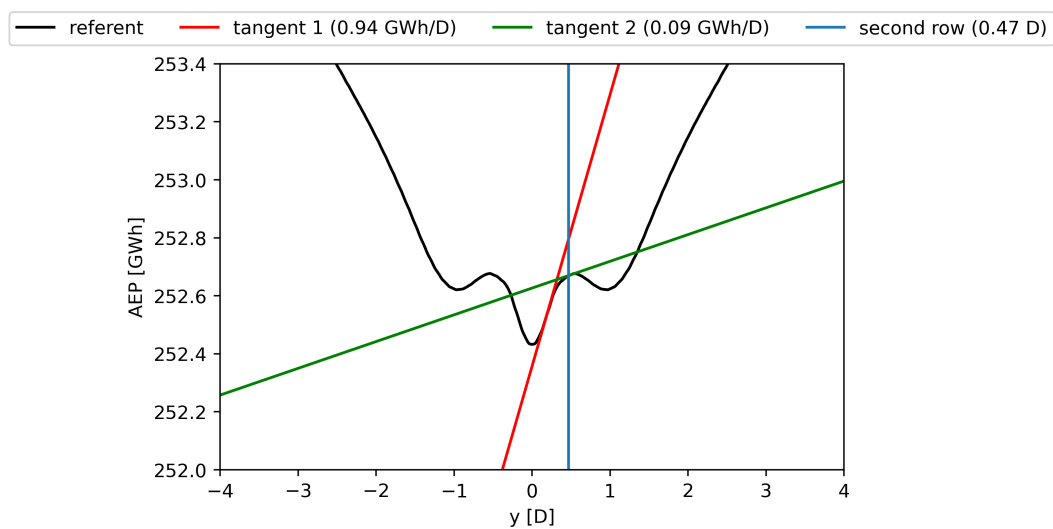


Figure 4.26: Response surface line referent

After a certain distance, the slope decreases and becomes negative before increasing again. The average distance of the second row in the 25 turbine cases is calculated and was found to be at a distance of 0.47 D. This distance is represented in the plot by a blue vertical line. The gradient of this

point on the response surface line is calculated and plotted by the green line. The gradient was found to be 0.09 GWh/D. The gradient is of interest as it is the driving force that pushes the turbine away from the edge. This gradient needs to be larger than the gradient coming from the wakes of the turbines in the middle of the wind farm to be able to push the turbine away from the edge. When the opposing gradient becomes equal to the plotted gradient, they level out, therefore placing the turbine at that location. Both gradients are dependent on the distance between the two turbines on the edge and the distance from the turbines in the centre of the wind farm. That is why not all turbines are placed precisely at the same distance from the edge.

The shape of the response surface line shown in Figure 4.26 can be explained by two factors.

1. The distance between the three turbines
2. The number of wind directions that give mixed wakes

First, when the turbine is moved away from the centre, the distances between the three turbines is increased—increasing the distance results in lower wind speed deficits and, therefore, higher power output. The second factor is a bit more complex and is dependent on the superposition model. The superposition model from the referent models the mixed wake deficits with the root-sum-square(RSS) method. Figure 4.28 and 4.29 shows that if turbine 1 is placed away from the edge, turbine 2 experiences wakes from the other two turbines at two different wind directions. This will twice cause a loss in power in turbine 2 (and for easterly winds, the same would apply to turbine 0). If turbine 1 had been on the edge, as shown in Figure 4.27, turbine 2 would experience the wakes of both turbine 0 and turbine 1 for the same wind direction. However, the loss in power in turbine 2 due to this mixed wake is less than the sum of losses of the two individual wakes of Figure 4.28 and 4.29. The reason for this is that the wind speed deficit in the mixed wake is not the sum of wind speed deficits of the two individual wakes, as can be seen in equation 4.1, which shows the RSS equation. Thus, the separation of mixed wakes into individual wakes that is caused by moving turbine 1 away from the centre leads to an increase of the wake losses, which opposes the benefit of the larger distances that are created for turbine 1.

In equation 4.1  $T_w$  represents the total wake deficit at a location, and  $w_0$  and  $w_1$  represent the separate wake deficits from turbine zero and turbine one.

$$T_w = \sqrt{(w_0^2 + w_1^2)} \quad (4.1)$$

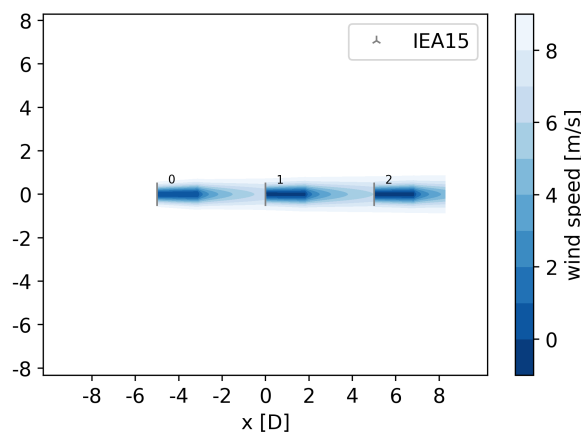


Figure 4.27: Mixed wake turbine 0 and 1 on turbine 2

When the turbine is placed a little bit out of the centre, illustrated in Figure 4.28 and 4.29, the outer turbines experiences almost the same wakes but without mixing. The distance between the turbines

has slightly increased, which reduces the wake from the turbine in the centre. However, this decrease in wake deficit doesn't outweigh the increase in wake deficits coming from the separate wakes. This gives the particular shape around  $0.5D$  found in Figure 4.25.

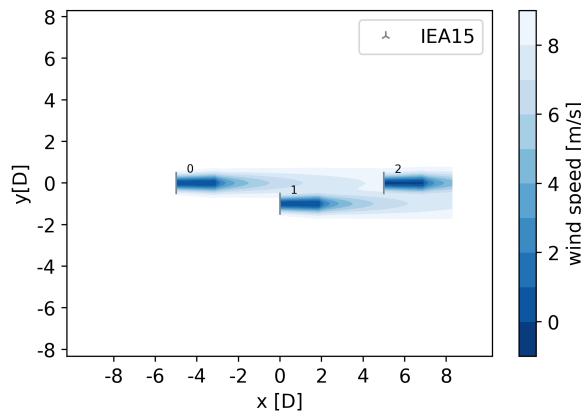


Figure 4.28: Single wake turbine 0 on turbine 2

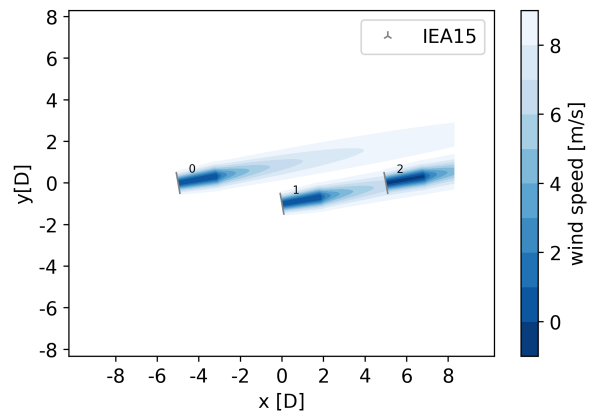


Figure 4.29: Single wake turbine 1 on turbine 2

## 4.5. Insights obtained from the referent cases

The referent and the three cases have been explained and their results have been analysed. The insights that were obtained from the results that contribute towards the research objective are summarized in this section. With respect to the fundamental expectations of OWFLO three main conclusions can be drawn:

- Many local optima exist with similar performances in an OWFLO problem
- The global optimum will not be significantly better than the found local optima
- The spread between the highest and lowest found performance is small and decreases with increasing numbers of turbines

For the 9, 25 and 64 turbine cases, many local optima were found. Respectively, 35, 100 and 100 local optima were found. The optimiser was run a hundred times, meaning that for the latter two cases there is a strong possibility more local optima can be found by running more optimisations. The performances of the local optima were exceptionally close to each other. The spread between the performances were 0,21%, 0,17% and 0,13%, respectively. This shows that the spread between the highest and lowest found performance is small and decreases with increasing numbers of turbines. The spread of the performances suggest that the global optimum will not be significantly better than the best local optimum obtained after a reasonable search.

The visualised response surfaces, with only two design variables, showed that multiple local optima were created by the wakes of the turbines. As the number of turbines increased per case, so did the number of local optima within the visualised response surfaces. When the cases are optimised there are significantly more design variables, which further increases the number of local optima. This explains why for the 9 turbine case, 35 local optima were found, while for the 25 and 64 turbine cases all 100 optimisations lead to a new local optimum. The almost equal absolute difference between two local optima found within the visualised response surface and its effect on the total AEP explains the decrease in the spread of the performances with an increasing number of turbines and area size.

The results also showed interesting characteristics of where turbines were placed within the wind farm. The list below summarises these characteristics:

- The corners of the square wind farms are found to be an optimal placement for the turbines
- The optimiser pushes the turbines to the edges

- 
- Turbines are placed at a 'second row' with a specific distance from the edge
  - There is a lack of pattern in the centre
  - There is a preference for more turbines on the edges both upstream and downstream of the dominant wind direction
  - The number of turbines that were placed on the edge upstream is equivalent to the number of turbines on the edge downstream of the dominant wind direction
  - There is a gap with no turbines between the edge and the centre of the wind farm
  - There is a preference of the placement of a turbine at a certain distance from the corner at the edge

# 5

## The effect of key influencers on optimality

This chapter shows the alternative practical implementation choices of OWFLO and their influence on optimality. First, a logic-based selection is made of the referents key influencers that other practical implementation choices will replace. Secondly, the alternative practical implementation choices are elaborated on. Thirdly, the results of the alternative practical implementation choices are compared. Fourthly, a special form of the response surface is further explored. Finally, the insights obtained in this chapter are discussed.

### 5.1. Selected key influencers

In section 3.2 multiple practical implementation choices have been discussed. From these practical implementation choices, a referent was put together, illustrated in Figure 4.1. In this section, a logic-based selection is made of the implementation choices that are expected to significantly impact the final found layout. These so-called key influencers will be changed to other models, settings or parameters. The problem formulation, which contains the objective function, design variables, and constraints, won't be changed as these resemble the problem presented to the referent. Section 5.3 will further detail how a comparative analysis is conducted to assess the influence of the different practical implementations.

The list of selected key influencers is presented below:

- Wake model
- Super position model
- Wind conditions
- Optimiser

With AEP as the objective function, the wake deficits will logically have a significant impact. Both the wake model and superposition model have a direct effect on the wake deficits. Therefore, they are selected to be compared to other implementation choices. The wake models are expected to have a more significant impact than the superposition model.

In section 4.3 the influence of the wind conditions on the final found layouts was observed. The wind conditions determine which wind directions present dominant wakes and which wind directions don't, therefore influencing the final found layouts. The wind conditions themselves aren't changed, because they are part of the represented problem, but the same wind conditions are known to be implemented in various ways. Furthermore, wind conditions can be misrepresented by using insufficient data.

The previous chapter showed that the response surface of an OWFLO problem contains many local optima. The optimiser will influence which local optima will be found. Therefore, the optimiser is

selected as a key influencer.

## 5.2. Alternative practical implementation choices

For the wake model, three alternative models have been selected. The GC Larsen [8], the NOJensen [11], and the Zong Gaussian [39]. The latter requires a turbulence model to calculate the local turbulence intensity, which influences the wake expansion function. The Steen Frandsen(2017) turbulence model is selected and is implemented according to IEC61400-1, and to Steen Frandsen's thesis [23]. The chosen alternative wake models are illustrated in Figure 5.1.

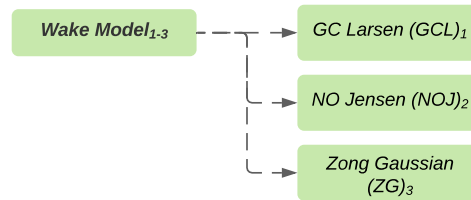


Figure 5.1: Alternative wake models

The shapes of the alternative wake models and referent wake model are shown in two figures. Figure 5.2, illustrates the deficit along the centre line of the turbine per diameter(D) distance. The wind speed that is used is 10 m/s. Especially in the near wake, until  $4/5 D$  distance, the wake models are evidently different. In the far wake region, they start to come closer to each other.

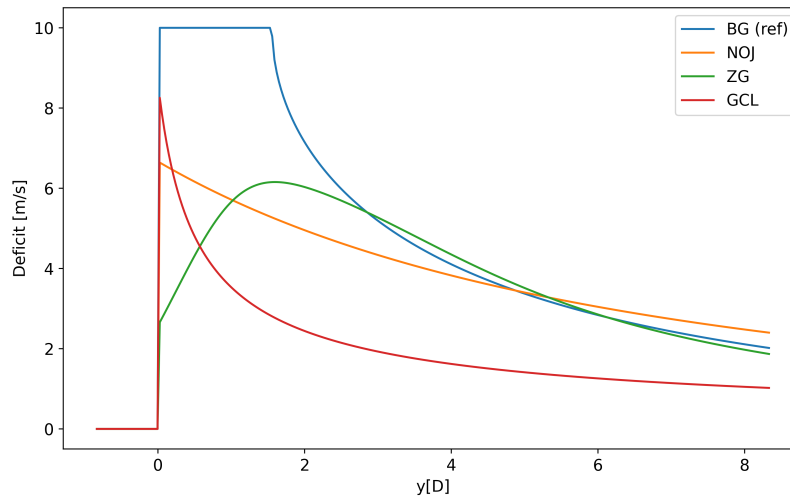


Figure 5.2: Deficit along center line

Figure 5.3, shows the lateral deficit profile at  $2 D$  downstream. The difference between the three gaussian shapes and the top-hat from NOJensen is clearly visible.

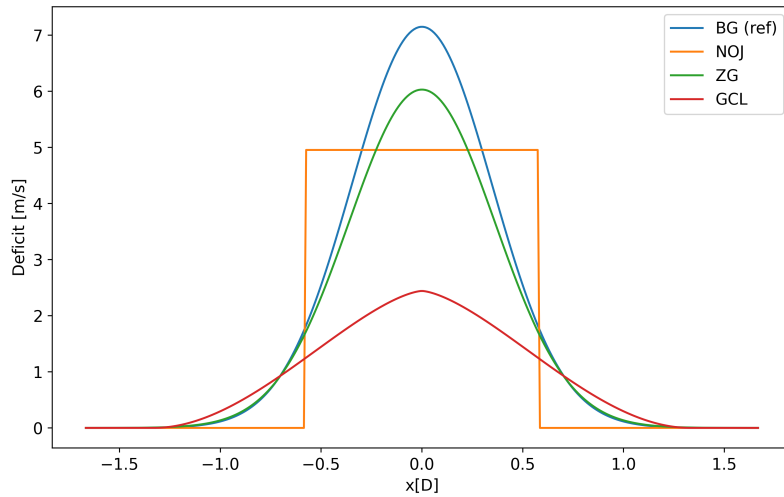


Figure 5.3: Wake deficit at  $y = 2 D$

*Superposition model*

The alternative super position models that are selected are illustrated in Figure 5.4. The linear sum method assumes that the velocity deficits within a wind farm are small. Therefore, it takes the net velocity deficit as the sum of each wake. Instead, the maximum sum method takes into account the maximum deficit found from one wake and neglects all others.

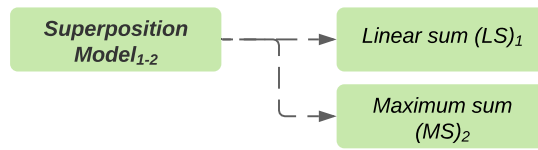


Figure 5.4: Alternative superposition models

*Wind conditions*

The alternative wind conditions are illustrated in Figure 5.5. In section 4.2 the referent model, Hornsrev 1, has been specified. The referent model contained a Weibull distribution per wind rose sector. For the first alternative wind condition, these twelve Weibull distributions have been replaced by one Weibull distribution. The one Weibull distribution is made from the averages of the scale and shape parameters of the Weibull distributions from Hornsrev 1. Various definitions of wind roses use only one Weibull distribution for all wind direction sectors. The computational speed will be the same as with the referent settings.

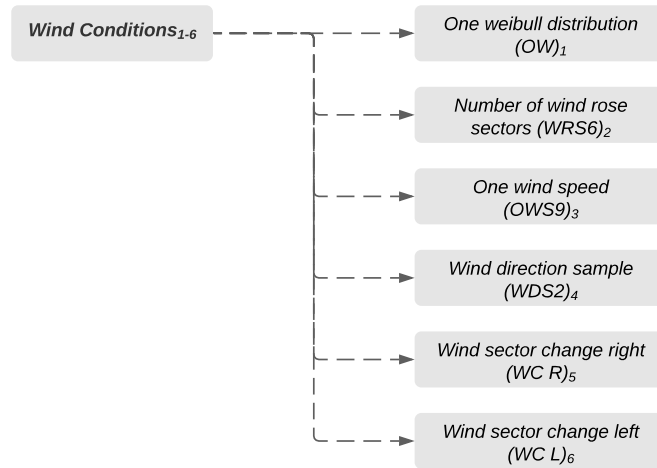


Figure 5.5: Alternative wind conditions

The second alternative wind condition is reducing the number of wind rose sectors. For the referent, the number of wind rose sectors is twelve. Increasing the number of wind rose sectors was not possible as the raw data of Hornsev 1 was not available. Therefore, only a decrease was possible. The number of wind rose sectors is reduced to six. In practice, the wind rose sector sizes vary. Having a wind rose sector size of six is considered low. The wind rose with sector size 6 is illustrated in Figure 5.6

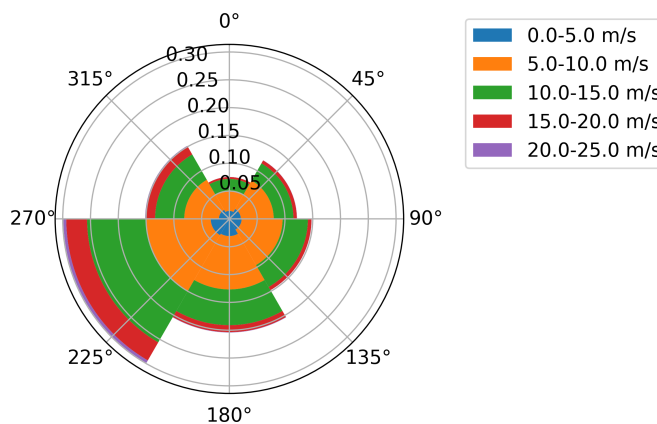
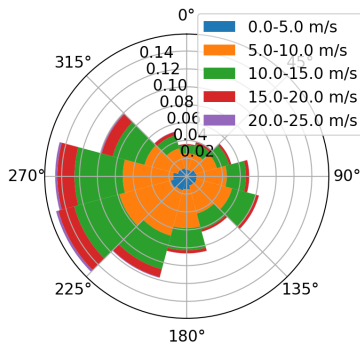


Figure 5.6: The wind rose with 6 sectors

The third and fourth alternative wind conditions are used to increase the computational speed. The first method of increasing computational speed is to simulate only one wind speed. This simplification of the representation of wind conditions is known to be used in industry. When simulating with one wind speed, the selected wind speed needs to be around or lower than the rated wind speed of the turbine. The wind speed needs to be around or lower than the rated wind speed because if a wind speed higher than rated were used, the wakes would not impact the power output of other turbines as they would still produce rated power. If the wakes don't impact the power output of other turbines, then the wakes will not influence the position where a turbine is placed. The rated wind speed for the IEA15MW is 10.59 m/s, and the selected wind speed is 9 m/s. The second method for increasing computational speed is simulating for fewer wind directions. The referent simulated the wind conditions for each degree (0,1,...,359), which gives high accuracy. For the comparative analysis, the wind conditions are simulated with a wind direction step size of 2 degrees (0,2,...,358).

The last two alternative wind conditions look at the sensitivity of the optimal found layouts to a variability in the wind rose. This variability in the wind rose can come from using incorrect input data. The referent's wind farm sectors are given a full sector rotation, which exaggerates the inaccuracy that can normally be expected. The wind rose is given a full sector rotation counterclockwise and clockwise to form two new wind roses. These are called wind sector change left (WC L) and wind sector change right (WC R), and are illustrated in Figure 5.8, and 5.9, next to the wind rose of the referent in Figure 5.7.



**Figure 5.7:** Wind rose of the referent (Hornsrev 1)

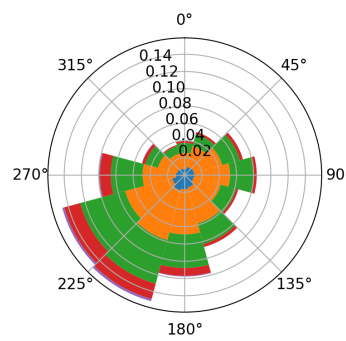


**Figure 5.8:** Wind rose of wind sector change left

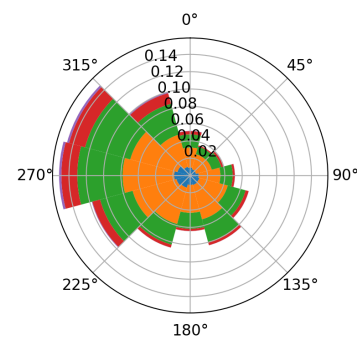


**Figure 5.9:** Wind rose of wind sector change right

### Optimisers

Two alternative optimisers will be used to be compared against the CMA-ES referent optimiser, a gradient-free optimiser, and a gradient-based optimiser. Both are taken from Topfarm [24]. The gradient-free optimiser is a random search algorithm developed at DTU Wind Energy by Ju Feng. The algorithm changes one turbine's location for each iteration using a vector defined by a randomly set angle and amplitude. If the tested solution improves the objective function, the turbine is placed at a newfound location. If it doesn't improve the objective function, the turbine remains at the same location. The maximum allowable distance covered by the vector is set to 10.000 meters. The random search optimiser needs to run for a long time as it changes only one turbine at a time and the position is randomly selected. The time was limited to 4.5 hours per optimisation.

The gradient-based optimiser is the SLSQP optimiser which was also used in section 4.1.4 to test how well the referent optimiser converges to a local optimum. The algorithm was initially developed by Dieter Kraft [40]. The SLSQP optimiser uses the gradients of the objective function to change the design variables efficiently and find an improved design. This searching method is very susceptible to local optima as the global design space is not explored. It is a deterministic algorithm which means that the final solution depends on the initial starting point. Therefore, a random initial starting point is taken before each optimisation.

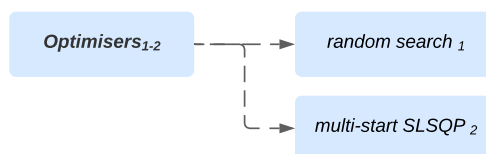


**Figure 5.10:** Alternative optimizers

### 5.3. Comparative analysis

This section explains in detail how the comparative analysis is performed. In section 4.3 three cases were analysed, namely the 9, 25 and 64 turbine cases. The results showed that the number of local optima found was limited for the 9 turbine cases. In comparison, both the 25 and 64 turbine cases found a hundred different local optima. The 64 turbine case was computational heavy. With the prospect of running a substantial number of optimisations, the limited time of this thesis and the ability to find many local optima, the 25 turbine case was selected for the comparative analysis.

Figure 5.11 shows a visualisation of how the comparative analysis is conducted. The steps illustrated in Figure 5.11 show two separate paths, the black path and the orange path, for the analysis alternatives and the optimiser alternatives, respectively. The three steps are explained below:

#### Step 1

**Black path:** One key influencer within the referent analysis( $\text{Analysis}_{\text{ref}}$ ) is changed to an alternative implementation choice. As an example, the wake model is replaced, which means that the referent's BG model is replaced with an alternative implementation choice like the GCL model. All other settings and models within the referent are kept the same. The new analysis is called ' $\text{Analysis}_1$ '

**Orange path:** The optimiser, which is a key influencer, is replaced with an alternative implementation choice. The optimiser doesn't influence the referent analysis. Therefore the orange box represents the replacement of the optimiser with the unchanged analysis from the referent.

#### Step 2

**Black path:** The referent analysis is replaced by the new analysis. As an example,  $\text{Analysis}_1$ , obtained in step 1, replaces  $\text{Analysis}_{\text{ref}}$ . The problem formulation of the case with 25 turbines is used.

**Orange path:** The optimiser in the OWFLO problem from the referent is replaced by an alternative optimiser. The same problem formulation with 25 turbines is used as in the black path.

#### Step 3

**Black path:** The new OWFLO problem is optimised one hundred times. This results in one hundred layouts and one hundred performances( $\text{AEP}_{1-3}$ ). The performances for the example in step 2 are calculated by  $\text{Analysis}_1$  resulting in  $\text{AEP}_1$ . Thus, the index for AEP refers to the used analysis alternative and not to one of the one hundred layouts. The performance of the final found layouts is then recalculated with  $\text{Analysis}_{\text{ref}}$  resulting in  $\text{AEP}_{\text{ref}}$ . The hundred performances from  $\text{AEP}_{\text{ref}}$  are shown in a boxplot to be compared to other implementation choices.

**Orange path:** The new OWFLO problem is optimised one hundred times. This results in one hundred layouts and one hundred performances ( $\text{AEP}_{\text{ref}}$ ). The performances are already calculated by the referent analysis and can therefore be used straight away for making the boxplot.

These steps were performed for each alternative implementation choice from section 5.2. In section 5.4.1, the boxplots are compared to the referent per key influencer. The boxplots are compared to determine the effect of the key influencers on the optimality of the found solutions. In section 5.4.2 the performances of the  $\text{AEP}_{1-3}$  and  $\text{AEP}_{\text{ref}}$  are compared to determine how well the performance that the designer sees with the selected analysis corresponds with the actual performance as represented by the referent analysis.

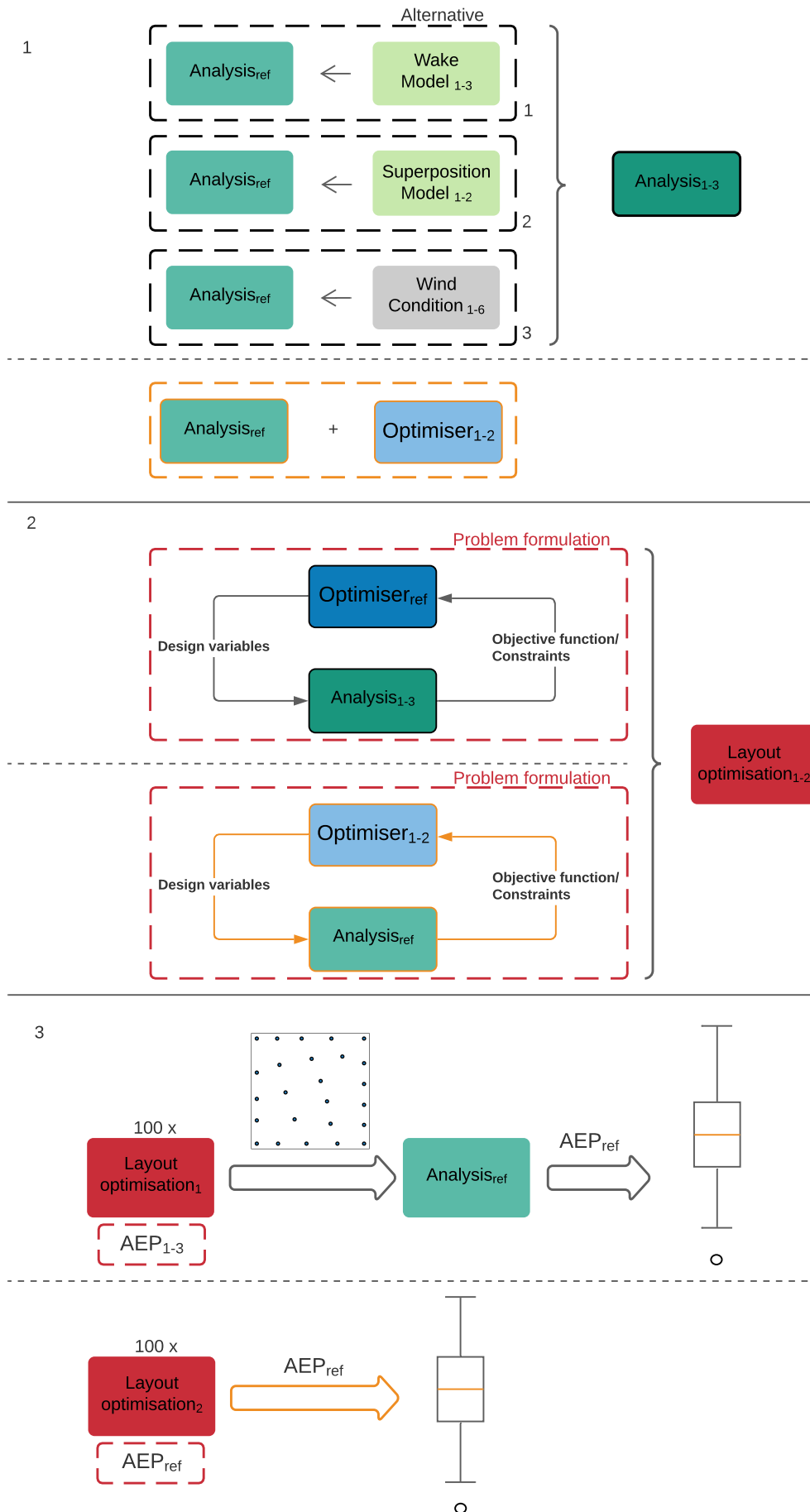


Figure 5.11: Visualisation comparative analysis

## 5.4. Results from the comparative analysis

This section presents the results of the comparative analysis.

### 5.4.1. Influence from the alternative implementation choices

The boxplots shown in this section are made with the same boxplot settings as indicated in section 4.15. With each key influencer, the results from the referent in section 4.3 are added to the overview of boxplots to be compared against the alternative implementation choices.

#### *Wake models*

The boxplots of the different wake models are illustrated in Figure 5.12. At boxplot level, some conclusions can be drawn. The overview shows that for all wake models, the performances median is relatively close to each other. They indicate that the wake model's influence is relatively small on the optimality of the performances.

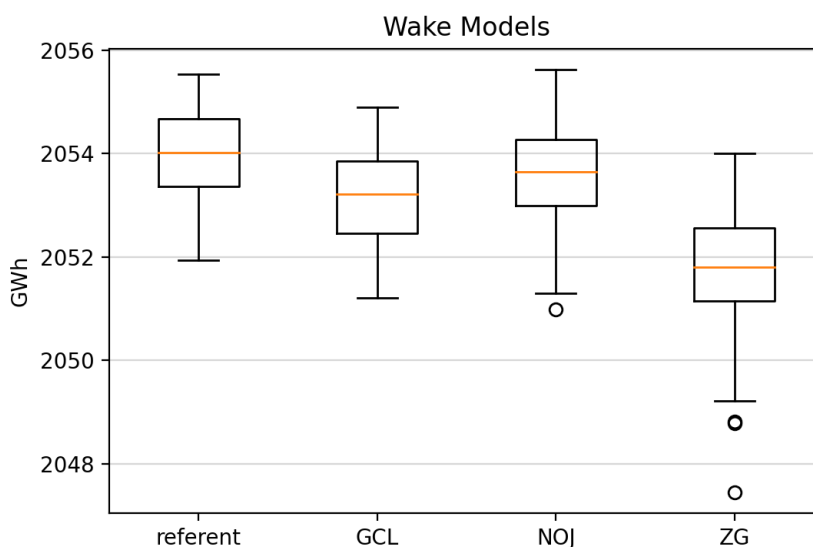


Figure 5.12: Boxplots of  $AEP_{ref}$  from the alternative wake models

The performance resulting from the NOJ model has been influenced the least compared to the performances of the referent, the median is closest, and the spread also covers the higher performances. Overall the NOJ model has only a little more spread than the referent. The NOJ model has even found a higher performance layout than the optimisations of the referent did. Having found a higher performance with the NOJ model is an interesting result, highlighting that it is still uncertain if the global optimum is found for this OWFLO problem. The scatterplot of the referent layouts and the NOJ model layouts are illustrated in Figure 5.13 and Figure 5.14, respectively. Both scatterplots show a distinctive second row and a similar gap between the edges and the centre of the wind farm. The overlap in the boxplots and the similarity in the characteristics of the scatterplots show that the referent's local optima lie closely with those from the NOJ model.

The GCL model shows a robust result with a median less than 1 GWh lower and an almost identical width of the spread as was found with the referent. The GCL model doesn't find the higher end of the performances found by the referent. The scatterplot of the GCL model in Figure 5.15 gives an indication why the higher end of performances is not found as there is no second row visible. In section 5.5.2 the cause of this difference is analysed. The most significant influence comes from the ZG model. The difference between the referent's median and the ZG's is 2.2 GWh. Relative to the median of the referent, the difference of 2.2 GWh is 0,11 %, which shows the little influence the wake model has on the optimality of the performances. The results of the ZG model shows that the local optima for this

model have been influenced the most. This is again indicated by the lack of a second row, illustrated in Figure 5.16.

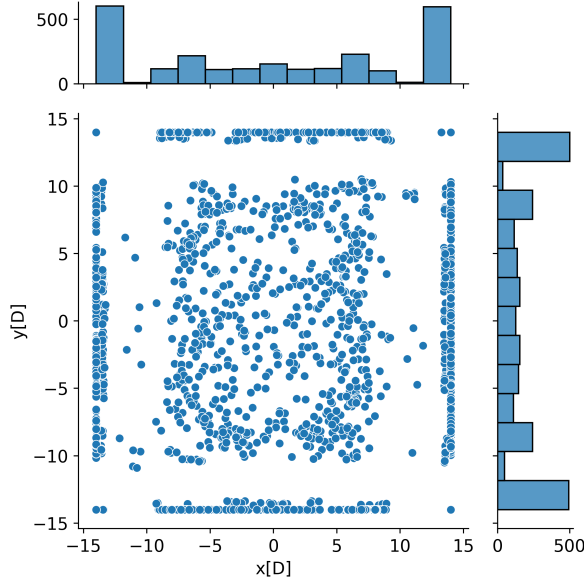


Figure 5.13: Scatterplot of all wind turbines positions from referent

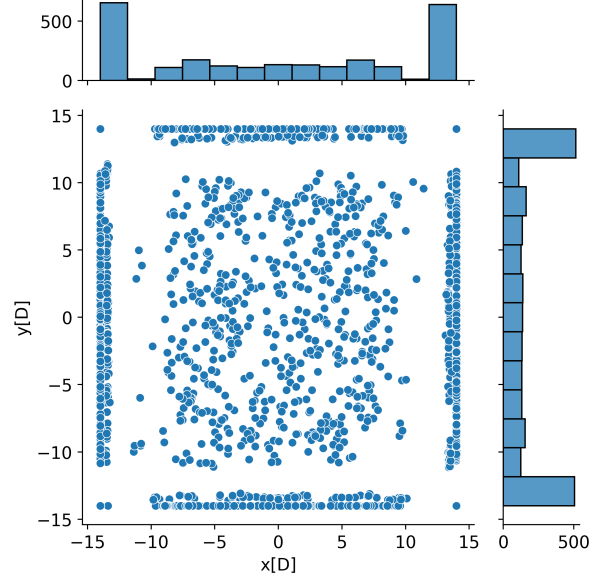


Figure 5.14: Scatterplot of all wind turbines positions from NOJ

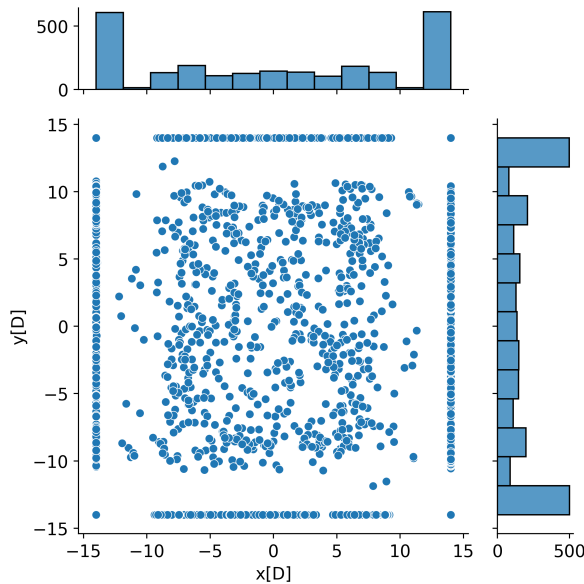


Figure 5.15: Scatterplot of all wind turbines positions from GCL

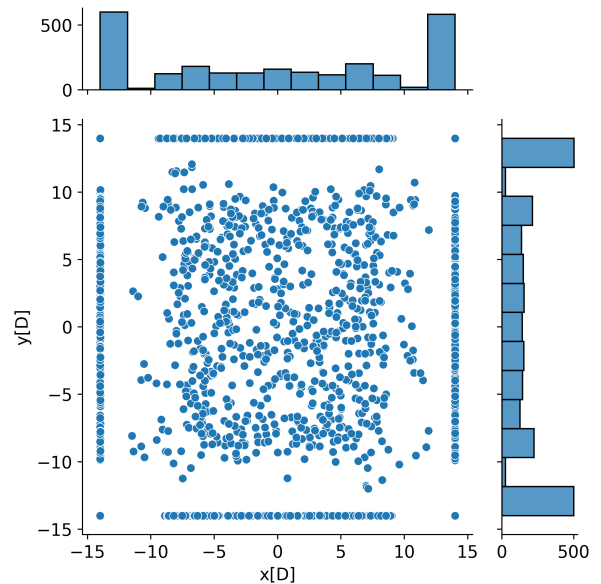
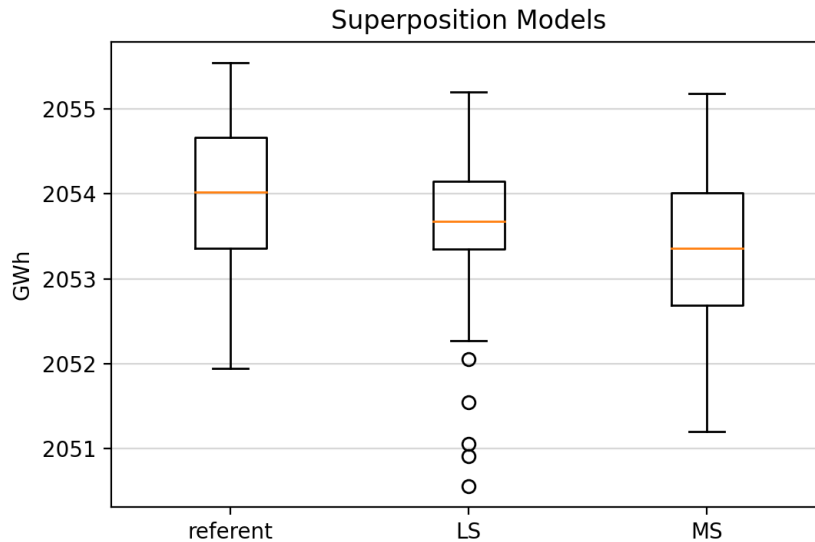


Figure 5.16: Scatterplot of all wind turbines positions from ZG

The main features that the wake models have in common can explain the relatively close performances of the wake models. There are clear differences between the shapes of the wake and the absolute wake deficit, which were illustrated in Figure 5.2 and Figure 5.3. However, when used in optimisation, all models' main feature is creating distance between turbines and pushing the turbines towards the boundaries. Surprisingly the NOJ model was closest to the referent results from the three models, although the shape of the wake is a top-hat. The relative close performances indicate that the selection of wake models has a limited effect on the final found performances. The absence of the second row for the GCL and ZG model shows an effect on the layout of the chosen wake model.

### *Superposition models*

The boxplots of the superposition models are illustrated in Figure 5.17. The LS model shows a slightly lower median with a smaller spread compared to the referent. The LS model has a few outliers on the lower side. Apart from these outliers, the spread is inside that of the referents. The MS model has a lower median than the LS model and a larger spread. Both the LS and MS models do not cover the higher end of the performances.



**Figure 5.17:** Boxplots of  $AEP_{ref}$  from the alternative superposition models

The differences between the superposition models and the referent indicate their little influence on the final found layouts performance. Both the medians are well within 1 GWh difference, which relative to the median of the referent is 0.05%. The scatterplots of the LS model and MS model are illustrated in 5.18 and 5.19, respectively. The second row of the LS model is further away from the edge than for the referent and MS model. In section 5.5.2, the larger distance of the second row for the LS model will be explained. The influence of alternative superposition models on the performances and the layout is small.

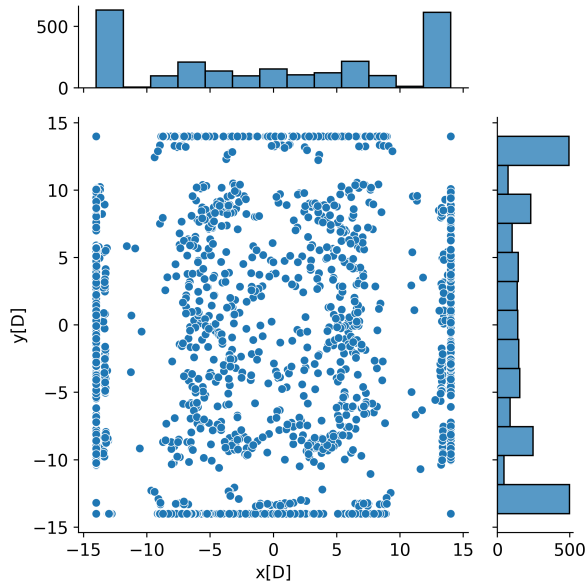


**Figure 5.18:** Scatterplot of all wind turbines positions from LS

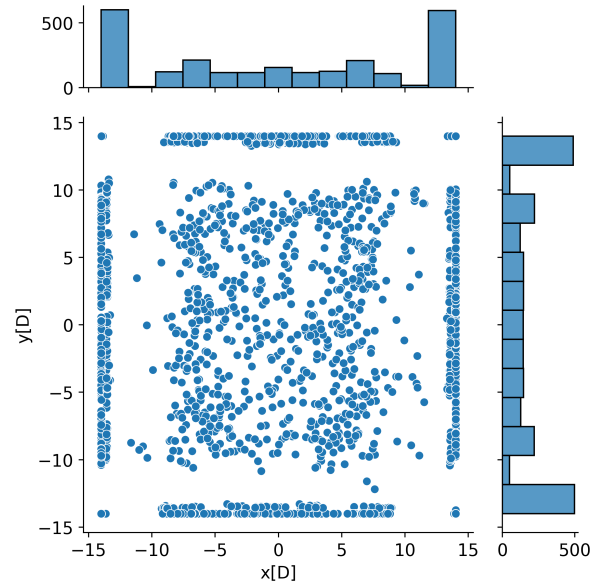


**Figure 5.19:** Scatterplot of all wind turbines positions from MS

#### *Wind conditions*

The boxplots of the different wind conditions are illustrated in Figure 5.20. The influence from some alternative wind conditions show a larger influence on the performances than was found by the wake and superposition models.

The first interesting result is that from the one Weibull distribution. The boxplot from the one Weibull distribution shows a higher median than that of the referent and less spread (apart from the one outlier). The one Weibull distribution seems to aid the optimiser in searching the design space more globally, therefore finding higher performances on average. The smoother response surface resulting from having one Weibull distribution can explain the more robust results than the referent's wind condition gives. As Weibull distributions change per wind rose sector, the response surface will provide small jumps or steps as the wind direction moves from one wind rose sector to another, making the response surface rougher. A rougher response surface presents a bigger challenge for an optimiser, preventing an optimiser from getting out of lower local optima. When there is only one Weibull distribution, these steps are decreased. Even though the one Weibull distribution doesn't represent the referent's wind conditions, a layout equal to the best performing layout of the referent was found with the one Weibull distribution.

The reduction in the number of wind rose sectors to six has a substantial influence on the performance of the found local optima compared to other influences. However, reducing the number of wind rose sectors to six is considered quite a drastic decrease in the accuracy of the wind rose. Despite this, the median is just 2 GWh, or 0,1 %, lower than the median of the referents. By reducing the wind rose sector size, the wind rose loses accuracy of the wind conditions without gaining computational speed.

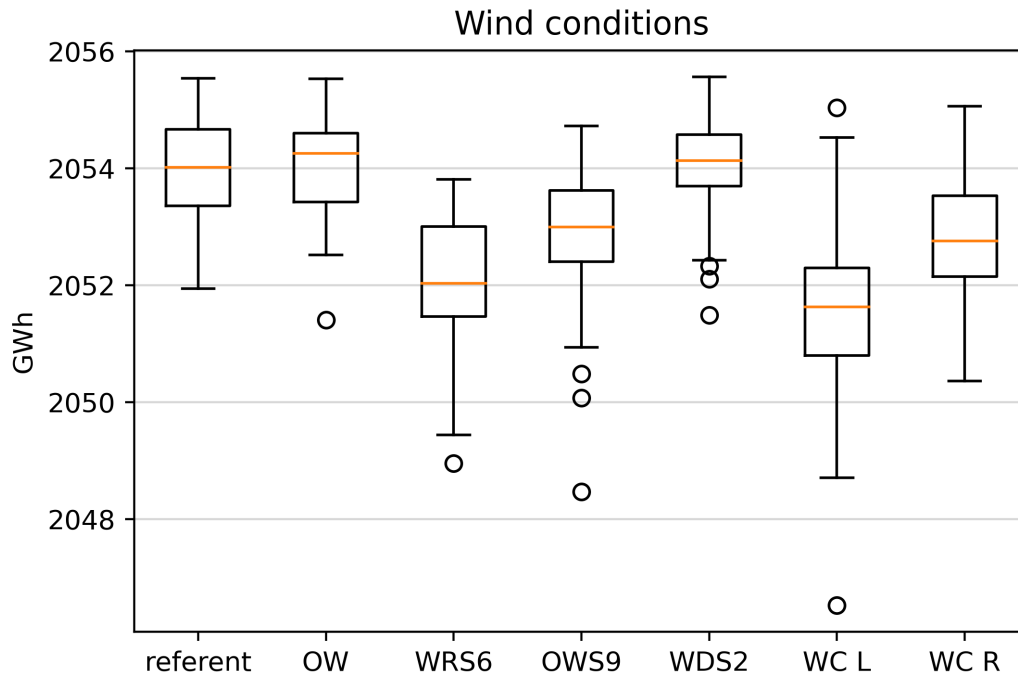


**Figure 5.20:** Boxplots of  $AEP_{ref}$  from the alternative wind conditions

The boxplot of OWS9 shows that the influence on the performance from simulating with one wind speed is small. The boxplot shows some outliers on the lower side, but most of the OWS9 boxplot overlaps with the referent's boxplot. The higher spectrum of the referent's boxplot is not covered by the OWS9 boxplot, and the median of OWS9 is 1 GWh lower. The computational speed was more than two times faster compared to the referent's computational speed. The small influence shown here provides a justification for simulating with one wind speed and demonstrates how little effect imprecise modelling of the wind speed distribution has on layout optimisation. The second method for increasing computational speed was simulating the wind direction with a step size of 2 degrees. The boxplot of WDS2 shows a more robust performance than the referent's boxplot. Except for the outliers, the spread of WDS2 is smaller, and the median is higher when compared to the referent. Similar to the one Weibull distribution, simulating with a step size of 2 degrees seems to help an optimiser to search more globally without losing the accuracy of the referent's conditions. The computational speed is again more than two times faster than that of the referent. These results give an incentive for increasing the simulation step size without losing performance. It is expected that further increase will eventually result in losing too much accuracy, making the performance drop significantly.

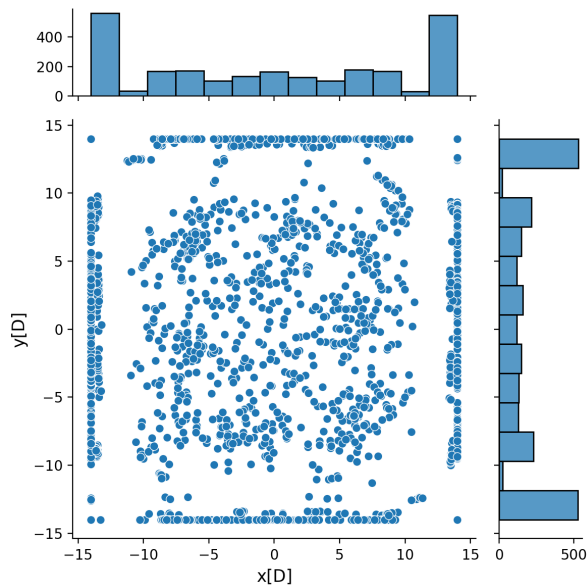


**Figure 5.21:** Scatterplot of all wind turbines positions from WC L

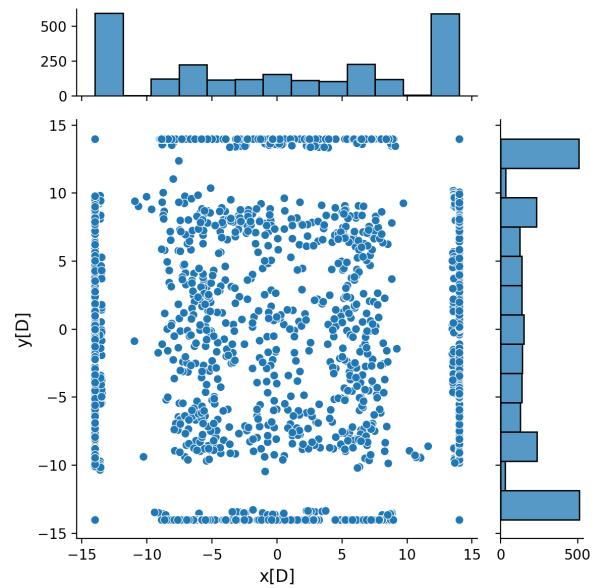


**Figure 5.22:** Scatterplot of all wind turbines positions from WC R

The boxplots of wind sector change left and right show that the influence depends on which direction the change is made. The influence from WC L is larger than from WC R. Both boxplots show a wider spread than the referent, with the WC L conditions having the largest spread. The WC L conditions have a lower median than the WC R conditions, making the influence from WC L higher. The difference in influence can be explained by the dominant wind direction, which for WC L is changed more to the south and for WC R more to the west. The change to the south changes the dominant wind direction towards the corner of the area. A dominant wind direction to the corner of the area gives significantly different layouts, which explains the larger influence from WC L. When looking at the scatterplots of the layout illustrated in Figure 5.21, and 5.22, the difference between the size of the gaps becomes clear. The difference in the size of the gaps shows why wind sector change left has more influence than wind sector change right.

### Optimisers

The boxplots of the multi-start SLSQP and the random search optimiser are illustrated in Figure 5.23. Four outliers, lower than the y axis shown here, were found by the multi-start SLSQP. They are not shown to better illustrate the boxplots at the higher spectrum of the performances found by the optimisers. The boxplot of the multi-start SLSQP shows that this gradient-based optimiser significantly influences the found optimal layouts. The spread has increased considerably with respect to the referent(CMA-ES) optimiser. From all alternative implementation choices, the multi-start SLSQP has the most considerable influence. The difference between the median of the referent and the multi-start SLSQP is 3.2 GWh. The multi-start SLSQP optimiser is not able to find the higher end of the performances, which can be explained by the high susceptibility of this gradient-based optimiser to local optima. More specifically, higher susceptibility to lower performance local optima. Therefore, not searching the design space more globally. The boxplot of the random search optimiser shows a more robust result with a smaller spread and a higher median. The random optimiser found a higher performance layout than the referent optimiser. The improvement was small, 0,1 GWh, and is therefore not visible in Figure 5.23. The random optimiser, a gradient-free algorithm, is not susceptible to lower performance local optima as it keeps searching globally for better placements of the turbines. Therefore, the random optimiser finds a more robust and higher performance.

Both alternative optimisers increase the computational time drastically. The multi-start SLSQP takes one and a half hours for one optimisation, and the random optimiser takes four and a half hours. In comparison, the referent optimiser takes just twenty minutes. The increased robustness found by the random optimiser, therefore, comes at an expensive computational cost.

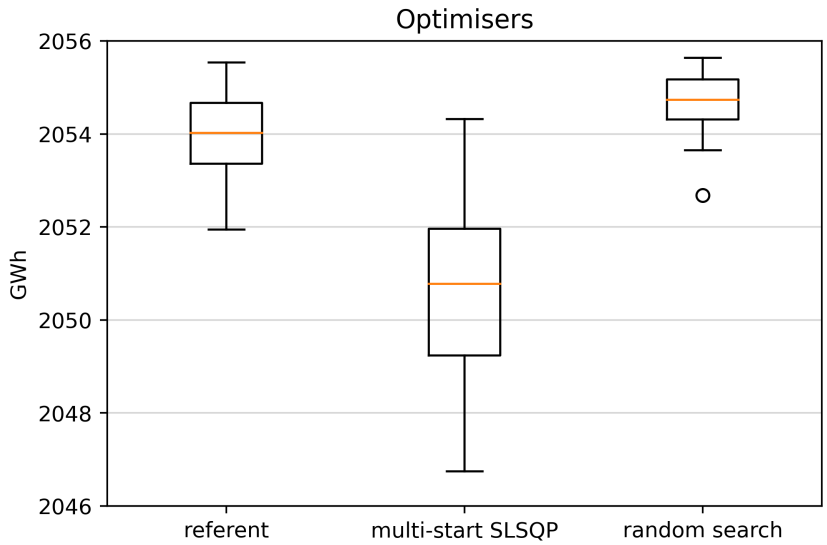


Figure 5.23: Boxplots from the alternative optimisers

The scatterplots of the optimiser’s resulting layouts are shown in Figure 5.24, and 5.25. The multi-start SLSQP’s scatterplot shows that also the lower performance local optima have turbines on the edge. However, the gap between the turbines in the corner and on the edge has disappeared compared to the referent’s scatterplot. The gap between the edge and the centre of the wind farm has also disappeared. This indicates that the lower performance local optima are more spread out over the wind farm area. The scatterplot from the random optimiser shows a distinct pattern both on the edge and in the centre of the wind farm. Gaps where no turbines are placed, are clearly visible both on the edge and in the centre of the wind farm. These patterns indicate that the higher performance local optima are clustered in certain regions of the design space.

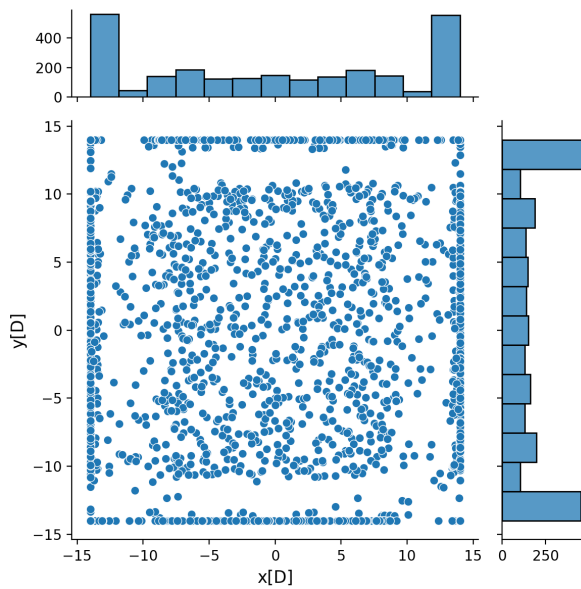


Figure 5.24: Scatterplot of all wind turbine positions from multi-start SLSQP layouts

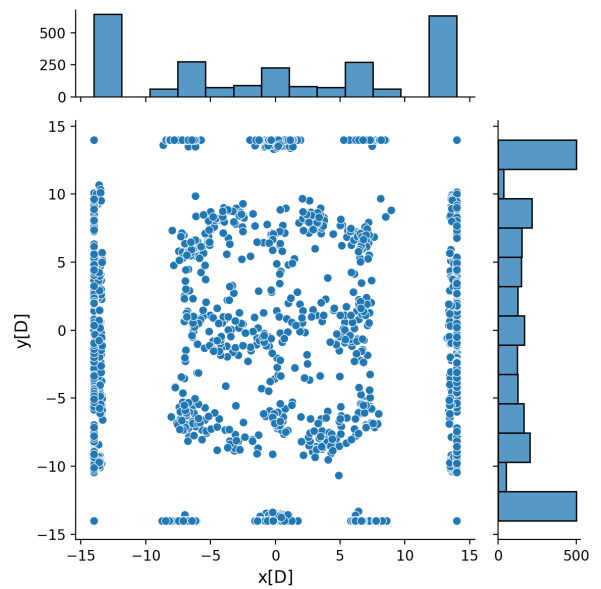


Figure 5.25: Scatterplot of all wind turbine positions from random optimiser layouts

### 5.4.2. Correspondence between the performance of the alternative implementation choices and the referent

In this section, the correspondence between the performance of the alternative implementation choices and the referent's performance is analysed. In Figure 5.11 they are indicated by  $AEP_{1-3}$  and  $AEP_{ref}$ . In practice, a wind farm designer is limited to the information that they obtain from their practical implementation choice. The analysis in this section gives an indication of how wrong or how right their results can be from interpretations of their results with regards to the 'true' optimality. The referent doesn't provide the absolute true optimality, so no absolute statements about validity can be made.

The scatterplots of the performances of wind direction step size 2 (WDS2) and one wind speed 9 (OWS9) are illustrated in Figure 5.26 and Figure 5.27, respectively. For both scatterplots, the x-axis consists of the performances calculated by the referent and the y-axis of the performances resulting from the alternative implementation choice. The AEP from WDS2 and the referent AEP are on a straight line, meaning that if AEP goes up according to WDS2, the performance according to the referent also goes up. This is favourable behaviour, since WDS2 may be wrong, but the best performance according to WDS2 still corresponds to the best performance in 'reality'. This is not the case for OWS9, since there are many sets of 2 points where an improvement in performance according to OWS9 corresponds with a decrease in performance in 'reality' (according to the referent). The point in the top-right of the graph show that in this data set the best performing layout according to OWS9 is also the best performing layouts according to the referent, but that seems largely coincidental.

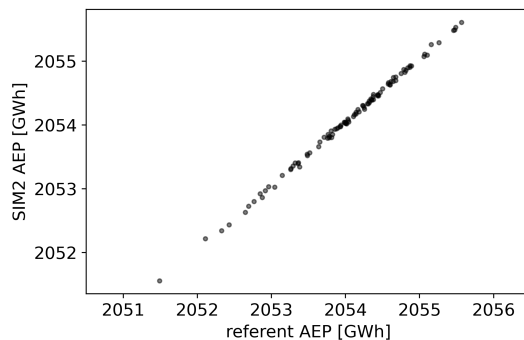


Figure 5.26: scatterplot performances WDS2

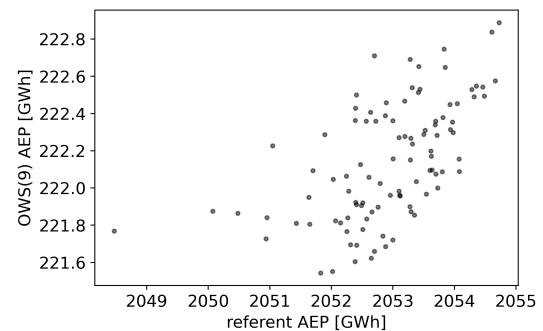
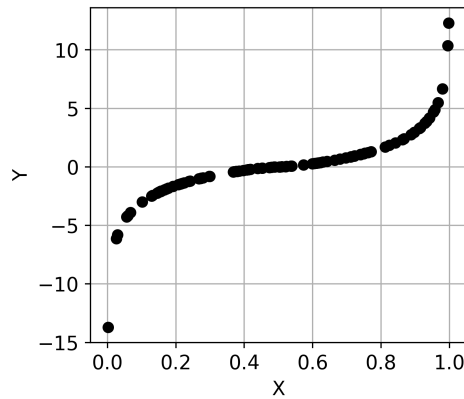


Figure 5.27: scatterplot performances OWS9

Rather than rely on visual inspection, the correspondence can be quantified in a single parameter. Multiple ways of measuring the correspondence between two sets of data exist. Different options have been considered, including a standard deviation, Spearman's rank correlation coefficient, Pearson product-moment correlation coefficient and Kendall's tau rank correlation coefficient. The standard deviation indicates the absolute value of deviations, while the coefficients are normalised. The absolute values are informative, but they are already largely shown in the boxplots. Therefore, two correlation coefficients were selected from the options as they were found most relevant for the analysed data. The Spearman's rank correlation coefficient and the Pearson product-moment correlation coefficient have been selected.

The Spearman correlation assesses how well the relationship between two variables can be described by using a monotonic function. A monotonic function is a function between ranked sets that keeps the given order. A Spearman correlation of +1 or -1 is measured when the variables are perfect monotone functions of each other. An example of a Spearman correlation of 1 is illustrated in Figure 5.28. As can be seen, the monotonous relation doesn't have to be linear and it actually doesn't have to follow any particular form.

The Pearson correlation measures the linear correlation between two sets of data. The covariance of two variables is divided by the product of their standard deviation, which means the result will always have a value between -1 and 1. The Pearson correlation ignores many other types of relationship or correlation. In Figure 5.28 the Pearson correlation is 0,84.



**Figure 5.28:** A plot of data points that have a Spearman correlation of 1 and a Pearson correlation of 0,86

Both Spearman and Pearson coefficients have been chosen for the assessment of the alternative implementation choices. However, Spearman is considered more relevant as the emphasis lies on the monotony of the related performances. Suppose there is a little curvature in the scatter plot, then the Pearson coefficient will deteriorate, while that is not really a problem for the usability of the alternative implementation choice. The Spearman correlation is less sensitive than the Pearson correlation to strong outliers that are in the tails of both samples.

An overview of the Spearman and Pearson correlations between the referent and the alternative implementation choices is given in Table 5.1.

**Table 5.1**

<b>Wake models</b>	Spearman	Pearson
NOJ	0,78	0,78
GCL	0,88	0,88
ZG	0,77	0,78
<b>Superposition models</b>		
LS	0,94	0,95
MS	0,97	0,98
<b>Wind conditions</b>		
OW	0,98	0,99
WRS6	0,69	0,71
OWS9	0,62	0,58
WDS2	1	1
WC L	0,67	0,71
WC R	0,94	0,94

The interpretability of the coefficients is not trivial, especially when deviating from 1. However, some soft conclusions are drawn here when the correlation coefficients deviate substantially from 1 and when they are close to or are 1. The Spearman and Pearson correlation coefficients are almost identical for each alternative implementation choices. These similar correlation coefficients indicate that the correlation is primarily a linear one.

There seems to be a correlation between all wake models and the referent. The GCL model shows the highest correlation. From the boxplots, in Figure 5.12 the NOJ model seemed to be mostly correlated to the referent as the boxplots overlapped the most. However, the correlation coefficients indicate that the GCL model is more correlated to the referent than the NOJ model.

The superposition model's correlation coefficients, which are both close to 1, indicate a strong correlation between the referent and the alternative superposition models. The small influence from alternative superposition models, which was found in Figure 5.17, is confirmed with the high correlation between the referent and the alternative superposition models. The strong correlations could also indicate that wake mixing plays an insignificant role in the AEP calculations of optimal found layouts. The absolute values resulting from the superposition models are different. However, the influence of the superposition model on the AEP for different layouts is minimal. The maximum sum superposition model doesn't mix wakes, as it only uses one wake, namely the maximum wake. The almost perfect correlation with the referent's superposition model indicates that the superposition model has a minimal influence on the AEP calculations for optimal found layouts.

The one Weibull distribution correlation coefficients is almost 1, which confirms that the influence on the performance from the one Weibull distribution is small and is very closely correlated to the referent. In contrast, the low correlation coefficients from the wind rose with six sectors indicates its relatively significant influence.

A large difference is found in the correlation coefficients for the alternative implementation choices that increase computational speed. However, the boxplots in Figure 5.20 showed an overlap with the referent for both OWS9 and WDS2. The correlation coefficients for WDS2 are perfect, while OWS9 is very low. In Figure 5.26 and Figure 5.27, these numerical values of the highest and lowest coefficients are visible. The low correlation of OWS9 indicates that simulating with one wind speed does significantly influence the perceived performance. This, however, did not significantly impact the performance of the optimisation. By simulating with one wind speed, much accuracy is lost for calculating the AEP of a layout, represented by the low correlation with the referent. However, this inaccuracy doesn't seem to be influencing layout optimisation so much, represented by the overlap in boxplots. The main features for layout optimisation, which simulating with one wind speed brings, is creating distance between turbines with consideration of the wind rose and placing turbines outside the wakes of other turbines. The low correlation between AEP comes from, among other things, the non-linear influences resulting from different wake speeds, power curves and Weibull distributions.

There is a significant difference in correlation coefficients from WC L and WC R, which again confirms that the influence from WC L is larger than that from WC R. The full sector rotation introduced rather more imprecision in the representation of inaccuracy of the wind conditions than one would normally expect. The high correlation coefficients for WC R indicate that the direction of the dominant wake with respect to the boundaries of the area plays a crucial role in the significance of the influence from the wind inaccuracy.

## 5.5. Response surface

This section again looks into a special form of the response surface with only two variables, which was also done in section 4.4. In this section, the alternative implementation choices are used to calculate the response surface and response surface line. This is done to see how the response surface changes with respect to the location of the local optima within the wind farm, the number of local optima it presents and the roughness of the response surface. The second row is further analysed in detail to determine why it disappeared for some alternative implementation choices.

### 5.5.1. Optimised layouts

In section 4.4.1 the response surface performance was analysed with the referent analysis. In this section, the response surface is calculated with the alternative implementations choices analysis. To show and go into detail with all alternative implementation choices is too comprehensive. Therefore, the most interesting response surfaces have been picked out, and all others can be found in Appendix B.

The layout that is taken for making the response surfaces is the same optimised layout from Figure 4.22. This was an optimised layout found by the referent and can therefore be compared to see how alternative practical implementation choices influence the optimal position of the removed turbine. Moreover, the response surface gives insight into the created local optima and their shift in location

with respect to the referents response surface. The optimal positions for the alternative implementation models are illustrated by yellow turbines. First, the response surface of the ZG model is illustrated in Figure 5.29. The blue turbine's position, which was found optimal by the referent, is slightly off the optimal position (indicated by the yellow turbine) for the ZG model. The white colours, which are more dominant between the turbines, indicate that within the wind farm, more area's have a lower performance. Within these white colours, darker lines can be identified, coming from the turbines. These darker lines create more local optima between the turbines, creating a rougher and more complex response surface than the referent. The rough response surface present the optimiser with a greater challenge, which explains the longer lower tail in the performances found by the ZG model.

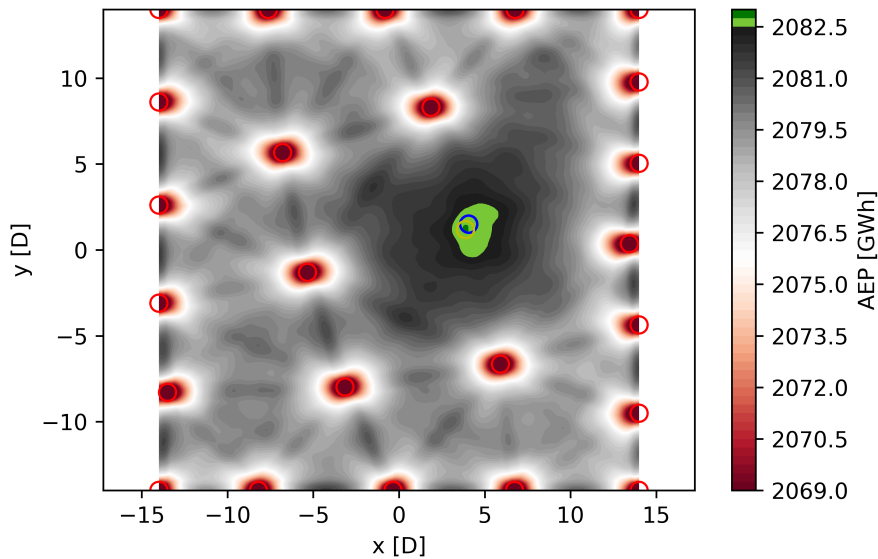


Figure 5.29: Response surface ZG model

The response surface of the GCL model is illustrated in Figure 5.30. The darker shades and the smooth contour lines show that the response surface for the GCL model is smoother than for the referent model. The local optima are more widely stretched, which is indicated by the size of the green and black islands. Moreover, fewer local optima can be identified when compared to the referent's response surface. The yellow turbine is placed almost exactly on top of the blue turbine, which indicates the little difference in location of the local optima. Figure 5.12 showed that the GCL model wasn't able to find the higher end of the performances, and the scatterplot in Figure 5.15 showed no second row. The smooth response surface illustrated in Figure 5.30 and the almost identical location of the local optima indicates that the GCL model does not find the highest end of the performances because of the lack of a second row.

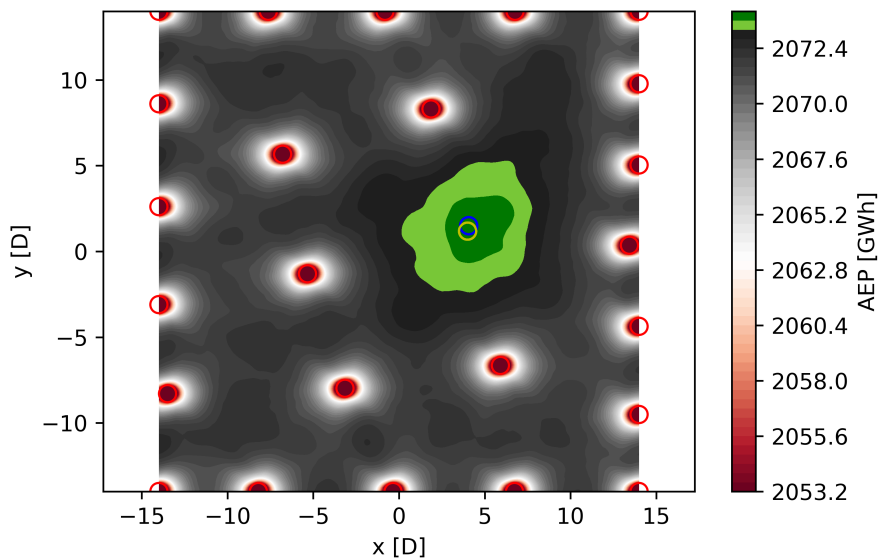


Figure 5.30: Response surface GCL model

Figure 5.31 and 5.32 show the response surfaces from the linear sum model and the maximum sum model, respectively. The response surface from the linear sum is smoother compared to the referent and the maximum sum. The maximum sum presents a rough response surface with more local optima than the referent. The rougher response surface can also be seen by the shape of the green islands and contour lines. The yellow turbine is further away from the blue turbine for the linear sum model than for the maximum sum model, which shows that the location of the local optima has shifted more for the linear sum than for the maximum sum. This indicates that the rougher response surface plays a larger role in the influence on the spread of the performances than the location shift of the local optima, which was illustrated in Figure 5.17.

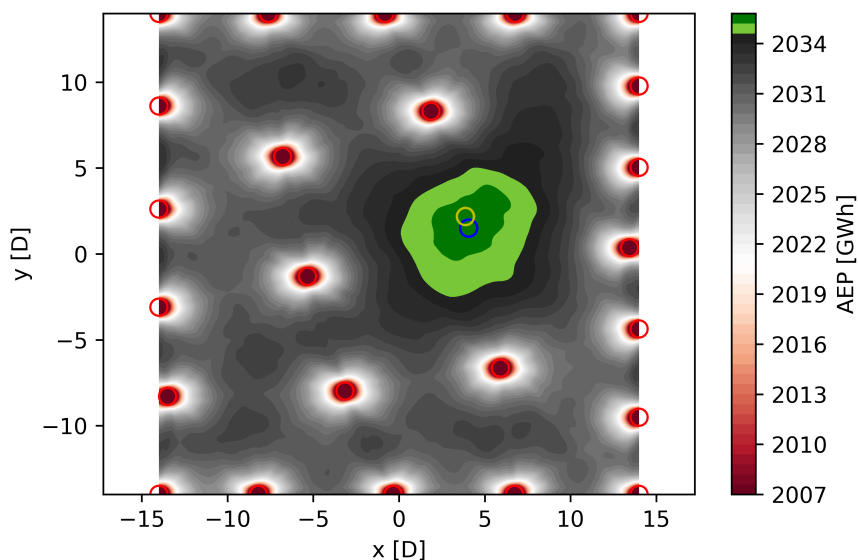


Figure 5.31: Response surface LS model

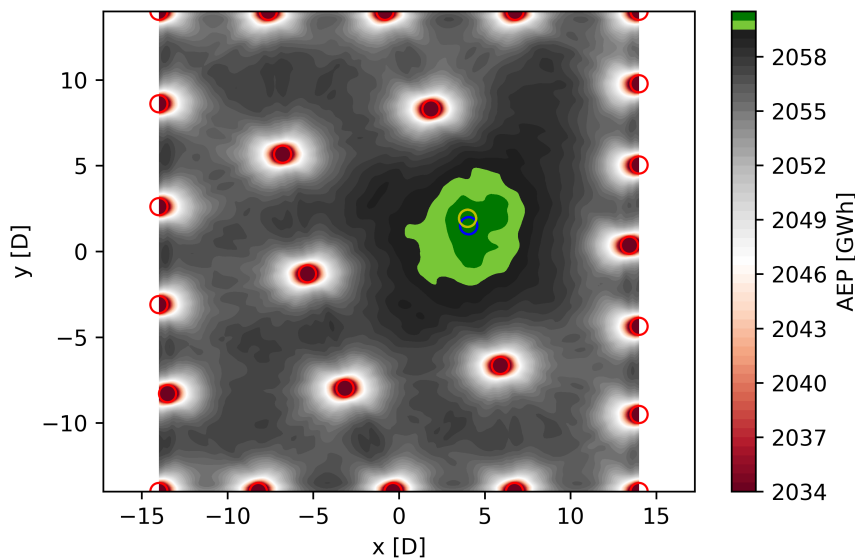


Figure 5.32: Response surface MS model

### 5.5.2. second row

In section 5.4 the scatterplots of some of the alternative implementation choices showed that no second row was created. Therefore, this section will look at the response surface line in the same way which was done in section 4.4.2. However, in this section, the response surface line is calculated with the alternative implementation choices.

All resulting scatter plots of the alternative implementation choices have been analysed to see if they show a second row. This resulted in two lists, namely which did have a second row and which didn't. The lists are given below:

#### Second row:

- referent
- Linear Sum
- Maximum Sum
- NOJensen
- One Weibull distribution
- Wind sector change left
- Wind sector change right
- Simulation sample size 2
- Wind sector size 6

#### No second row:

- GCL
- ZG
- One wind speed (9)

These lists indicate that the second row depends on the selected wake model and the number of simulated wind speeds. For the referent, which has the BG wake model, all other implementation settings give a second row except for having one wind speed. The NOJensen wake model also gives a second row, which explains why the NOJ model was able to find the higher end of the performances.

The response surface line of the Maximum Sum superposition model is illustrated in Figure 5.33. The blue line plots the average distance from the edge. The tangent with the highest gradient is shown in red and the tangent at the blue line is shown in green. The shape of the Maximum Sum response surface line clearly shows the distinct two local optima also found by the referent's response surface line in Figure 4.26. The shape is amplified, showing a deeper valley after the local optima. The amplified shape of the local optima shows why the response surface in Figure 5.32 also shows more local optima.

The average distance from the edge is smaller than was found by the referent. The highest gradient, which is 0.9 GWh/D, is close to that of the referents. The turbines are placed on average when the gradient has significantly decreased from 0.9 GWh/D to 0.57 GWh/D.

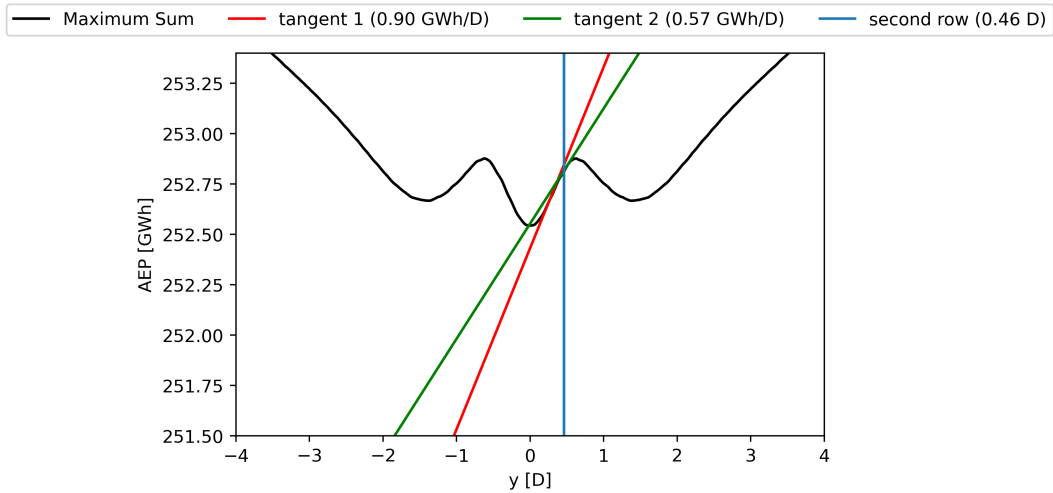


Figure 5.33: Response surface line Maximum Sum

The Maximum Sum superposition model can explain the amplified shape. If wakes are mixed, the Maximum Sum superposition model takes one wake deficit, the maximum wake deficit. By disregarding other wakes, the Maximum Sum will always have less velocity deficit when wakes are mixed compared to the RSS or Linear Sum superposition models. Therefore having two wind directions with a single wake is much worse than having one wind direction with a mixed wake. This can be seen as an amplification of factor 2 from section 4.4.2.

The response surface line of the Linear Sum superposition model is illustrated in Figure 5.34. The shape of the Linear Sum response surface line doesn't show the distinct two local optima found by the response surface line of the referent in Figure 4.26. The highest gradient is 1 GWh/D, which is similar to 0.94 GWh/D, the highest gradient of the referent. A slight decrease in the gradient is visible at around 0.5D from the origin. The second row is placed just after this slight gradient change at a distance of 0.68D. The average distance of the second row is larger when compared to that of the referent.

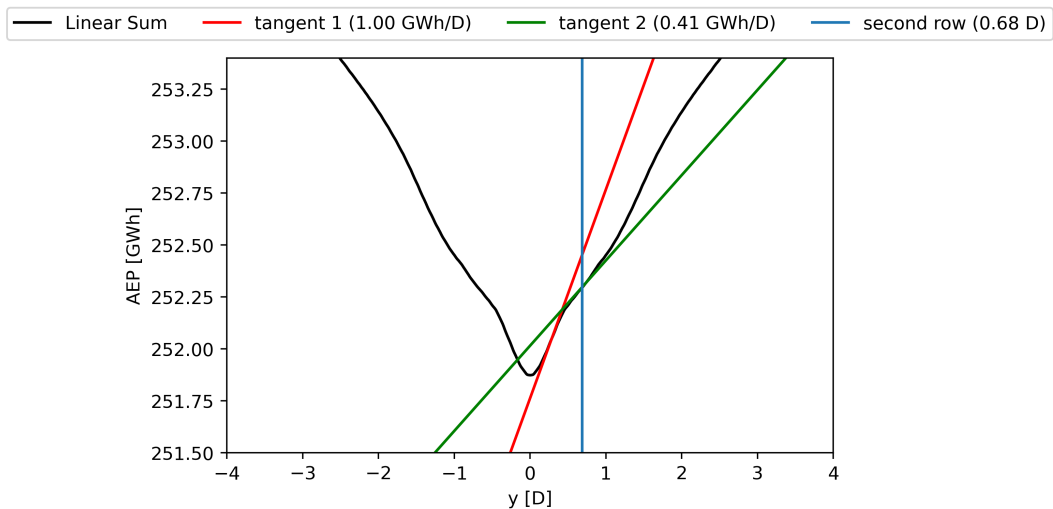


Figure 5.34: Response surface line Linear Sum

The lack of two local optima in the response surface around the origin is because the linear sum adds the wake deficits of multiple wakes. There is no difference between having two separate wake deficits or having two similar but mixed wake deficits by adding the wake deficits. Factor 2 from section 4.4.2 therefore doesn't influence the response surface line when the Linear Sum superposition model is used. The decrease in the gradient shows other factors besides the two presented in section 4.4.2 exist. Even though the response surface line doesn't show any local optima, there is still a second row as the gradient is still positive when moving away from the edge.

The response surface line of OWS9, which didn't show a second row is illustrated in Figure 5.35. The shape of the line around the centre shows a peak at the centre, indicating that moving the turbine away from the centre has a negative effect. The negative gradient explains why no turbines are placed in a second row. The different shape compared to the referent is interesting as they both use the same wake model. To further understand why the number of simulated wind speeds has an effect on the response surface line, another plot is made, illustrated in Figure 5.36. Figure 5.36 shows the normalised response surface lines of wind speeds 9 till 12 m/s and of the cumulative wind speeds 3-25 m/s (All ws) weighed with the Weibull distribution. All ws is the normalized response surface of the referent.

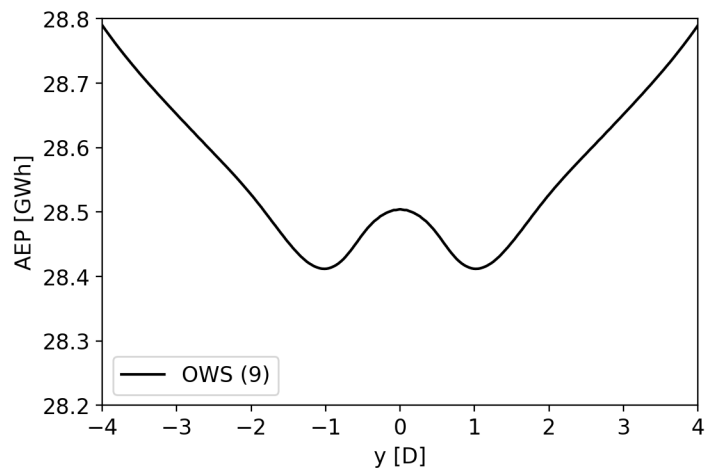


Figure 5.35: Response surface line OWS 9

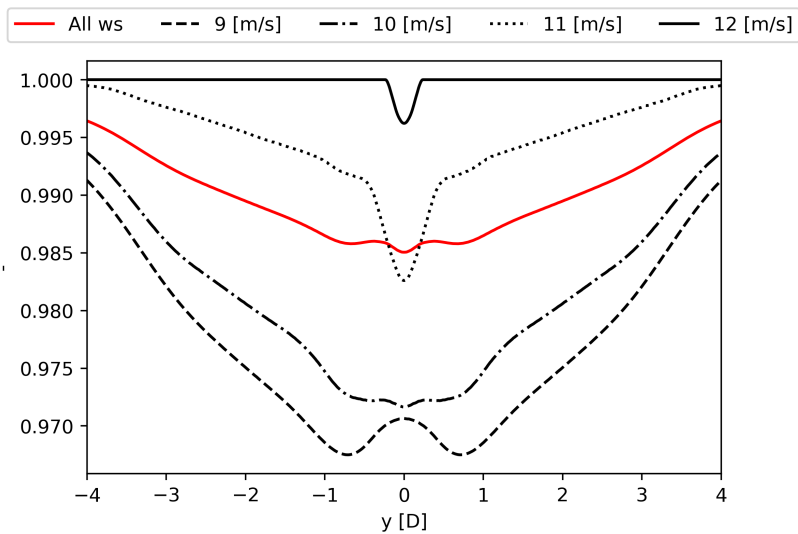


Figure 5.36: Normalized response surface lines

The different shapes of the response surface lines from the wind speeds around the origin stand out. Low wind speeds have a peak and high wind speeds have a dip. The red line shows a dip at the origin, meaning that the impact of the dips in the centre coming from the higher wind speeds prevail over the impact of the peaks coming from the lower wind speeds. The different shapes come from the two factors discussed in section 4.4.2. When there are opposing factors and when these are influenced by complex/non-linear effects, it is difficult to predict which effect will dominate.

The response surface line of the GCL wake model is illustrated in Figure 5.37. The shape of the response surface line is very different from that of the referent. Although a tiny dip is visible, this dip's gradient is not high enough to push the turbine away from the edge, which explains why the GCL wake model doesn't create a second row.

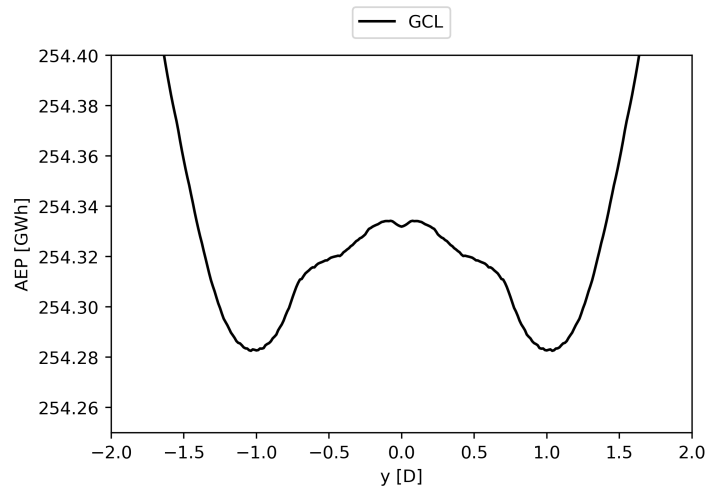


Figure 5.37: Response surface line GCL

The response surface line of the ZG wake model is illustrated in Figure 5.38. The shape is the opposite of that of the referent and looks similar to that of OWS9. A clear performance increase is found on the edge, which explains why also the ZG wake model doesn't create a second row.

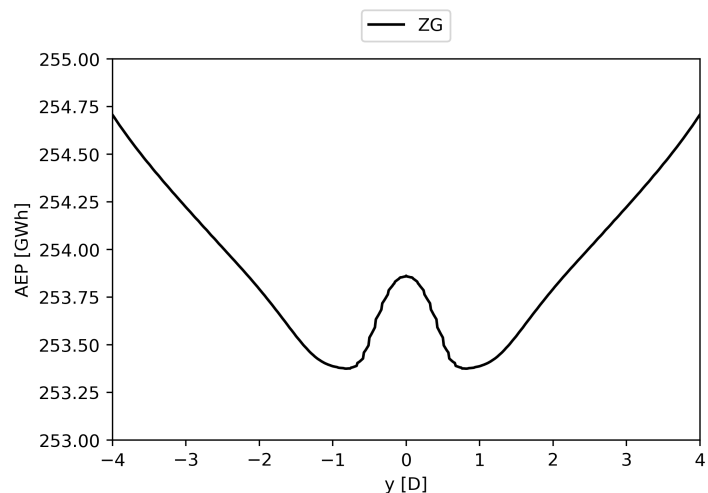


Figure 5.38: Response surface line ZG

## 5.6. Insights obtained from the alternative implementation choices

In this chapter, the effect of key influencers on optimality is presented. The resulting boxplots, scatterplots, response surfaces and response surface lines have been analysed to assess the influence of alternative implementation choices. The influence of alternative implementation choices depends on the slightly different locations of the local optima in the design space and the roughness of the response surface they create. The alternative optimisers showed their influence on the found local optima.

The first effect can be clearly identified by the second row, which some alternative implementation choices have and others don't. As the used referent had a second row, other implementation choices benefited if they also had a second row. A second-row would improve their performances when re-evaluated with  $\text{analysis}_{\text{ref}}$ . Although the local optima in terms of location are slightly different for alternative implementation choices, the influence of these shifts on the performance turned out to be minimal.

The second effect, the roughness of the response surface, indicated that the spread of the boxplots is related to the roughness of the response surface. An increase in the roughness of the response surface means an increase in the spread of the performances. By having more local optima, with larger variation in performance. The increased performance spread comes from the bigger challenge that the rougher response surface presents to the optimiser. The optimiser has more difficulty escaping lower performance local optima.

The difference in performance resulting from the chosen optimiser shows that an unfortunate choice such as a gradient-based optimiser with a random start is a poor choice, that should be avoided. The large spread in performances found by the gradient-based optimiser showed its high susceptibility to local optima. In contrast, the gradient-free random search optimiser showed that a more global search resulted in higher performances and less spread. However, the random search optimiser did not find a significantly better performance than the referents CMA-ES, which indicates that improvements in the optimiser wouldn't necessarily mean improving the performances. This indicates that improvement of a state-of-the-art optimiser is not expected to lead to much better results.

# 6

## Future improvements: an example

This chapter explores the influence of neighbouring wind farms on layout optimisation. This is done to examine if a future improvement of the analysis will also improve results when implemented in layout optimisation. The influence on the power generation of a wind farm from a neighbouring wind farm is a known phenomenon that is often not implemented in Offshore Wind Farm Layout Optimisation. First, the purpose of this chapter is elaborated on. Secondly, the influence from neighbouring wind farms, in reality, is compared to the used model. Thirdly, three cases will be introduced for studying the effect of neighbouring wind farms in layout optimisation. Fourthly, the results and effect on layout optimisation found in the three cases will be discussed. Finally, some preliminary conclusions are drawn.

### 6.1. Future improvements

The previous chapter explored the need to improve models and approaches regarding phenomena that were already considered in common practice. This chapter will explore the need to improve the approach by including a phenomenon that was previously not considered. In section 3.3, multiple phenomena were addressed, which influenced the analysis of a wind farm. From these phenomena, the influence of wind farm wakes on neighbouring wind farms is chosen to be included in the analysis. This chapter is not about coming up with recommendations about how to deal with neighbouring wind farms or which improvements to make within the analysis.

### 6.2. Neighbouring wind farms

The number of offshore wind farms is increasing. Preferred locations with strong and reliable wind conditions and access to transmission lines can become saturated with numerous wind farms. An up-wind wind farm presents wind farm wakes, which reduce the power generation from a downwind wind farm. Some experts consider understanding and accurately modelling the wakes of wind farms to be important for optimising wind farm layouts [27].

An analysis of the effect of wind farm wakes is done by Nygard and Hansen for the wind farms Rødsand II and Nysted [30]. As Rødsand II was built after Nysted, the data before and after the construction of Rødsand II could be compared. In Figure 6.1 the resulting power data for both wind farms is shown for a westerly wind direction. The black line represents the calculated power with the Jensen model. The grey lines indicate the calculated power with the Jensen model when using the original Nysted thrust curve, which contained a mistake and has been changed.

From Figure 6.1 it can be concluded that the Jensen model captures the variation along the curved Rødsand II row and the recovery across the 3.3 km gap between the two wind farms reasonably well [30]. The influence of Rødsand II on Nysted is concentrated around the turbines of Nysted that are closest to the Rødsand II wind farm. After a few turbines, the influence from Rødsand II on the turbine's power generation is decreased. Another interesting consequence found in the measurements by Nygard and Hansen is an increase in the wind speed around the northwest corner of Rødsand II for some wind directions. An increase in the wind speed is not captured by the Jensen model.

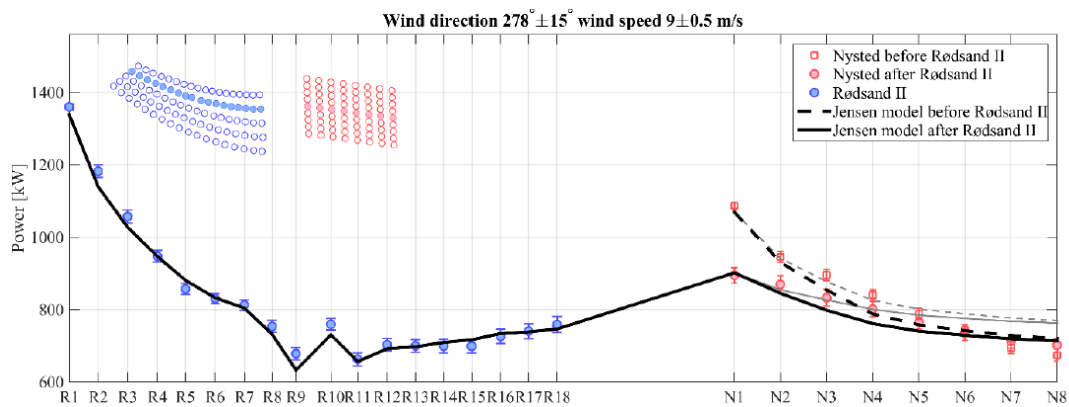


**Figure 6.1:** The power of Rødsand II and Nysted turbines along a row spanning both wind farms. Blue filled circles represent data from Rødsand II turbines, red open squares and filled circles are the observations for the Nysted turbines before and after the construction of Rødsand II, respectively. The error bars represent the 95% confidence interval on the mean value of the observations. Black lines (dashed/solid) are the results of a wake model calculation (before/after Rødsand II). Grey lines indicate the same results when using the original Nysted thrust curve. Inset: the layout of the wind farms with the row of analysed turbines highlighted. Before Rødsand II the inflow wind speed is taken at N1. After the construction of Rødsand II the reference turbine is R1. [30]

The effect of neighbouring wind farms was also discussed in section 3.3, which highlighted the connection between atmospheric stability and wind farm wakes. Wakes are found to extend for significantly longer downstream distances ( $>50$  km) in stable conditions than in neutral and unstable conditions ( $<15$  km) [28]. Therefore, atmospheric stability impacts the effect from a wind farm wake on a surrounding wind farm. As simplified engineering wake models assume neutral atmospheric stability, they underestimate the wake losses from neighbouring wind farms. Nygard and Hansen did not indicate what the atmospheric stability was for the previous showed results.

The results from Nygard and Handsen, and the knowledge of the influence of atmospheric stability present a problem for implementing the influence from neighbouring wind farms in layout optimisation. A quantitative relationship between wind speed, atmospheric stability, and wake length is needed to account for atmospheric stability. Additionally, the measured speed-up is an unknown phenomenon that is not yet implemented in any wake model. Therefore, to test the possible influence from neighbouring wind farms, the influence from atmospheric stability and a possible speed-up is left out in the cases from this chapter. As a simplified engineering model captures the reduction in power generation for the outer turbines quite well, it can be used to explore the influence of this reduction on layout optimisation of the affected wind farm.

### 6.3. Three cases and a reference

Three cases and a reference have been defined to show the influence from neighbouring wind farms on layout optimisation. For the cases, all referent settings from chapter 4 are used. The wind farm, which is optimised and analysed, has 36 turbines and area size of  $35D \times 35D$ , illustrated on the left in Figure 6.2. Three different neighbouring wind farms with 16, 36 and 36 turbines are used, illustrated on the right in Figure 6.2. These three forms of neighbouring wind farms have been chosen as they are expected to significantly influence the power generation of the layout, which is optimised. All three are placed on the same side to see the difference in influence. The layouts of the neighbouring wind farms are further specified in Figure 6.3, Figure 6.4 and Figure 6.5. The distance between the coloured wind farms and the optimised wind farm is set at 4.2 km or  $17.5D$ . The distance between the wind farms is relatively small to have a significant influence on the outer turbines from the neighbouring wind farm. The distance between the farms from section 6.2 was 3.3 km, which in terms of the Rødsand II turbines is  $35D$ , and showed quite an accurate performance for the outer turbines.

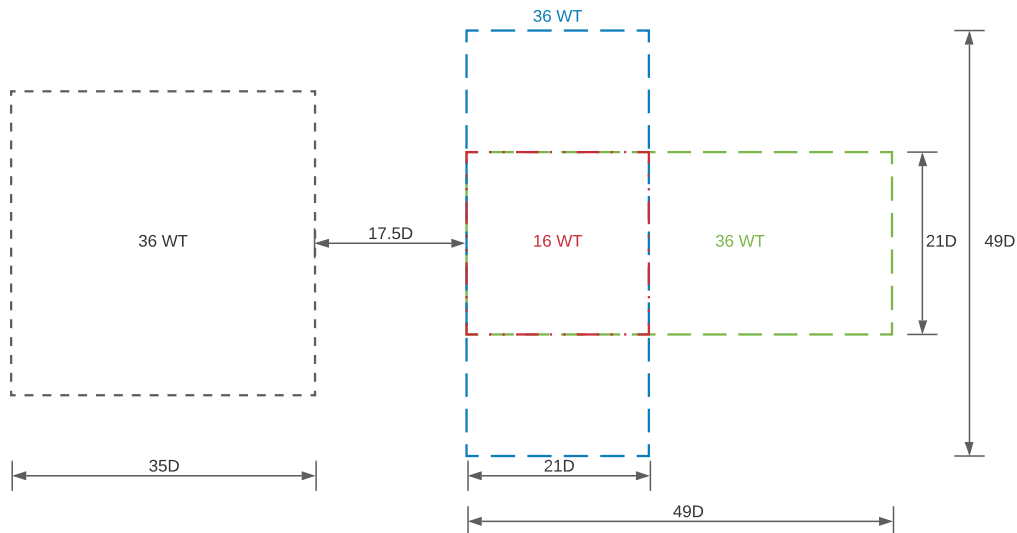


**Figure 6.2:** Visualisation neighbouring wind farm cases

Figure 6.3, 6.4 and 6.5 show the layouts of the neighbouring wind farms. These layouts were made by optimising them one time with the referent. The wind farm, that is optimised, is optimised for three cases and a reference. The wind farm is optimised a hundred times with the blue, red and green neighbouring wind farms and without a neighbouring wind farm (reference), resulting in four times a hundred layouts. The performances of the layouts resulting from optimising without a neighbouring wind farm are recalculated with a neighbouring wind farm and compared to the performances of the layouts which were optimised with the corresponding neighbouring wind farm. Only the performance from the optimised wind farm is considered, not the performance of the neighbouring wind farm.

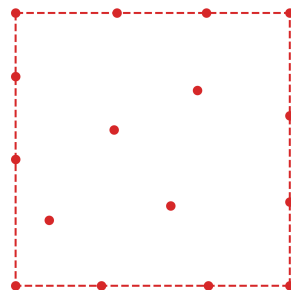


**Figure 6.3:** Layout of red neighbouring wind farm

As an example, consider the case with the red neighbouring wind farm. The performances of the layouts resulting from optimising with the red neighbouring wind farm will be presented in a boxplot. The performances of the resulting layouts from optimising without neighbouring wind farms will be calculated by including the red neighbouring wind farm and will be presented in a boxplot.

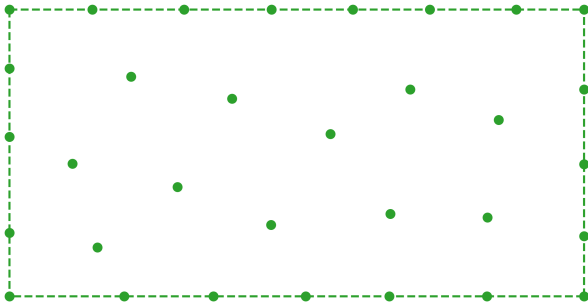


Figure 6.4: Layout of green neighbouring wind farm

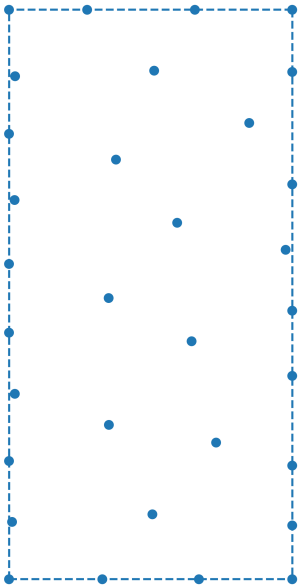
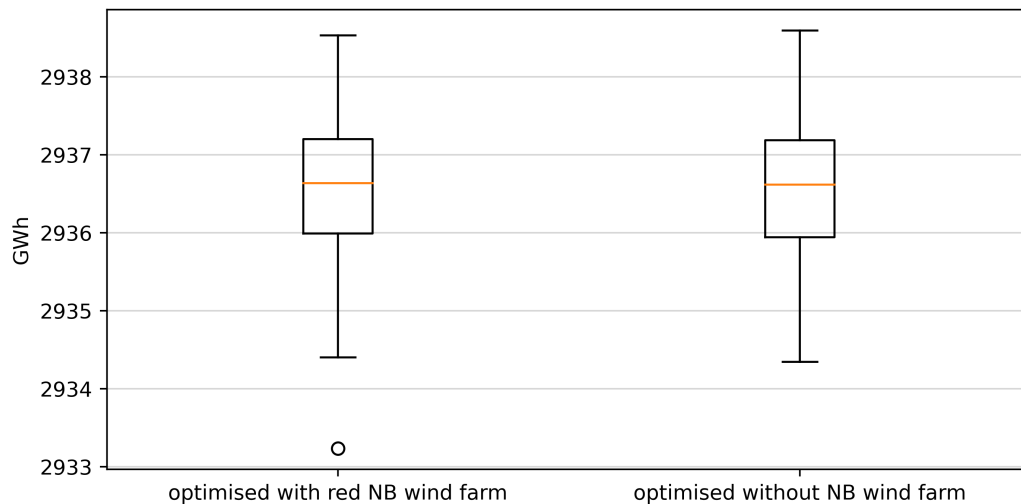


Figure 6.5: Layout of blue neighbouring wind farm

### 6.4. Results from optimising with neighbouring wind farms

First, the boxplots of the performances with the red neighbouring wind farm are presented in Figure 6.6. The difference between the two boxplots is minimal. The highest performance from the layouts optimised without a neighbouring wind farm is slightly higher than that of those optimised with a neighbouring wind farm. The boxplots are almost identical except for the outlier found by the layouts optimised with the neighbouring wind farm. The nearly identical boxplots indicate that the red neighbouring wind farm has only a small influence on the performances of the optimised layouts.



**Figure 6.6:** Boxplot of the performances, evaluated with the red neighbouring wind farm, from layouts optimised with the red neighbouring wind farm and without neighbouring wind farm

Second, the boxplots of the performances from the blue neighbouring wind farm are presented in Figure 6.7. The difference between the two boxplots is more pronounced than in Figure 6.6. The increased influence was expected as the number of wind turbines has increased from 16 turbines for the red neighbouring wind farm to 36 turbines for the blue neighbouring wind farm. The number of wind directions that present wakes has also increased as the orientation of the blue neighbouring wind farm has its long side vertically. The highest performance and median from the optimised layouts without a neighbouring wind farm is higher than those optimised with a neighbouring wind farm. These results are counter intuitive as one would expect that the layout that is optimised with a neighbouring wind farm would perform better as it takes the neighbouring wind farm into account. However, this is not the case. The reason could come from the increased complexity of the response surface.

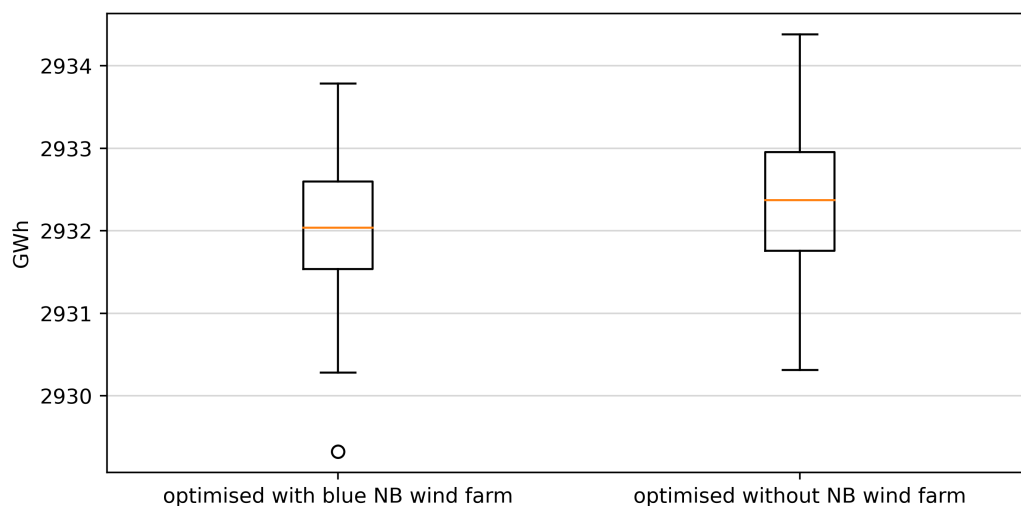


**Figure 6.7:** Boxplot of the performances, evaluated with blue neighbouring wind farm, from layouts optimised with blue neighbouring wind farm and without neighbouring wind farm

Thirdly, the boxplots of the performances from the green neighbouring wind farm are presented in

Figure 6.8. The difference between the two boxplots is again more pronounced than in Figure 6.6. The orientation of the green neighbouring wind farms long side is horizontal, therefore influencing fewer wind directions compared to the blue neighbouring wind farm. As fewer wind directions are influenced, it was expected that the influence on the boxplots would also be less. However, this is not the case. The median, highest performance and lowest performance from the layouts optimised with the green neighbouring wind farm are again worse than those from the layouts optimised without neighbouring wind farms. Again, this can be explained by the more complex response surface created with the analysis that includes the neighbouring wind farm. The increased complexity of the response surface is more difficult for the optimiser. Another indication of this is the two lower outliers, which shows that the optimiser got stuck in significantly lower local optima.

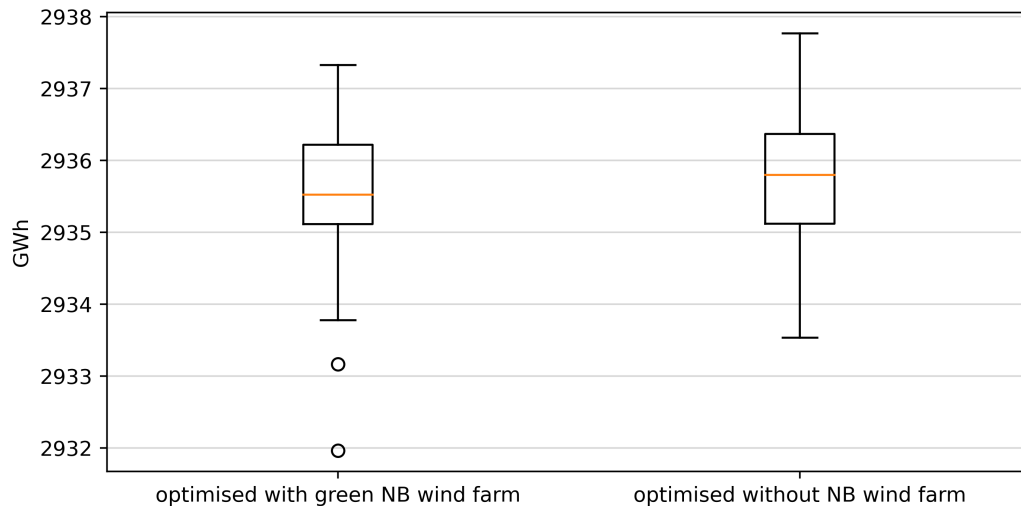


**Figure 6.8:** Boxplot of the performances, evaluated with green neighbouring wind farm, from layouts optimised with green neighbouring wind farm and without neighbouring wind farm

The resulting boxplots showed that for all three cases, the performances of the layouts optimised without a neighbouring wind farm performed better than the layouts optimised with the corresponding neighbouring wind farm. This indicates that adding the neighbouring wind farm to the optimisation lowers the performances of the found layouts. The lower performance is the result from the more complicated response surface resulting from the implemented neighbouring wind farm. The number of wakes for certain wind directions has increased by the turbines from the neighbouring wind farm, thereby increasing the complexity of the response surface.

The neighbouring wind farm influences the placement of the turbines within the wind farm. scatterplots of the resulting turbine placements of the layouts optimised without a neighbouring wind farm and layouts optimised with the red, blue and green neighbouring wind farms are illustrated in Figure 6.9, 6.10, 6.11 and 6.12, respectively.

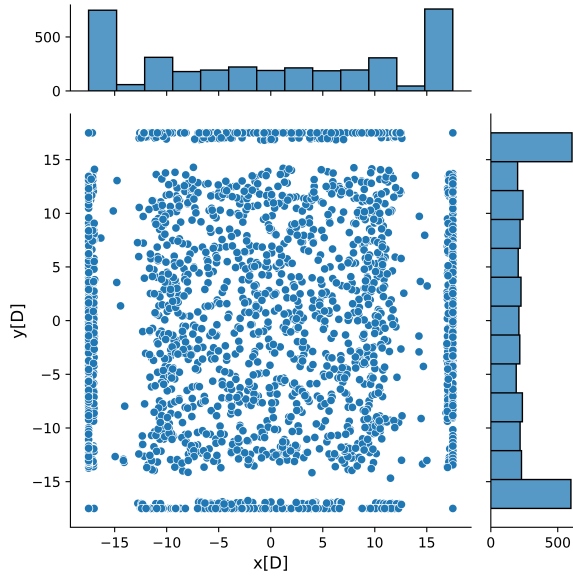


**Figure 6.9:** Scatterplot of all wind turbines positions from optimising without a neighbouring wind farm

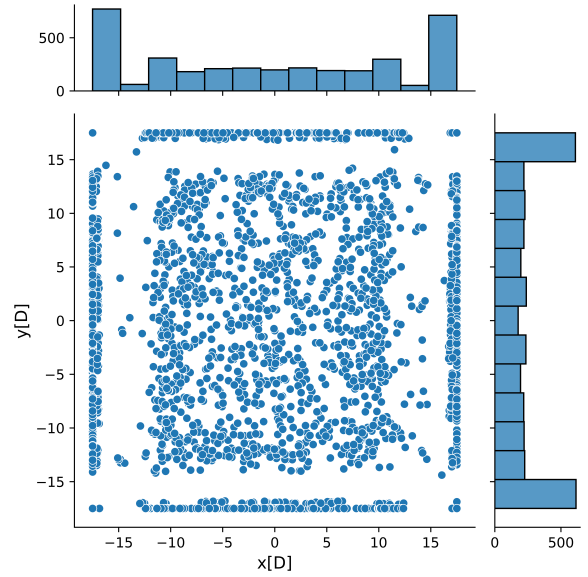


**Figure 6.10:** Scatterplot of all wind turbines from optimising with the red neighbouring wind farm

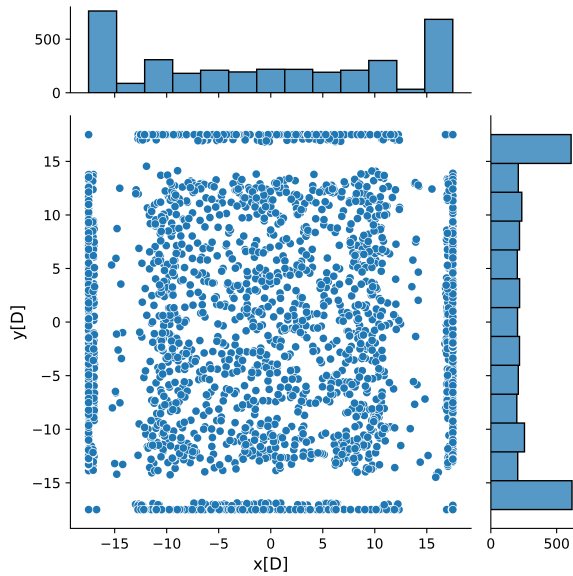


**Figure 6.11:** Scatterplot of all wind turbines from optimising with the blue neighbouring wind farm

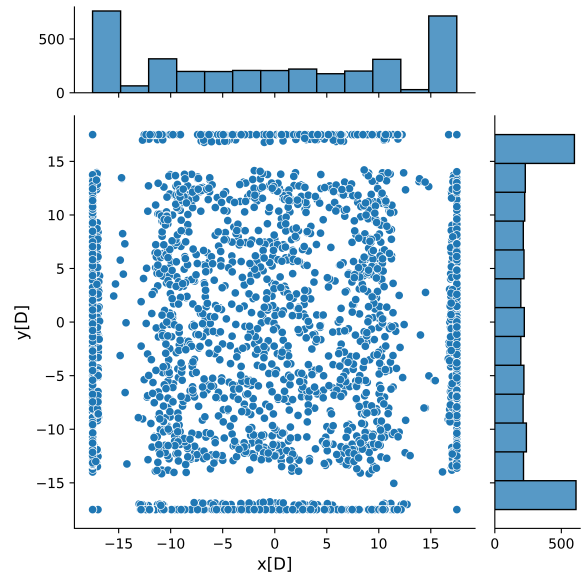


**Figure 6.12:** Scatterplot of all wind turbines from optimising with the green neighbouring wind farm

The scatterplots show that one off the influences from the neighbouring wind farms is on the number of turbines on the edges, as the height of the histograms differ per neighbouring wind farm. To further analyse the influence of neighbouring wind farms on the placement of turbines on the edge of the wind farm, a table shows the number of turbines on each edge. Table 6.1 shows the number of turbines placed on the left, right, upper and lower edge for each case. The number of turbines placed on the right edge has dropped for the cases which have a neighbouring wind farm, and the number of turbines placed on the left edge has increased. This shows that the influence from the neighbouring wind farms is lowering the number of turbines on the edge where the wind farm is located and increasing the number of turbines on the other side. This seems logical as the neighbouring wind farm has its biggest influence on this edge. However, the change of the turbine's locations reduces the performance shown by the boxplots.

**Table 6.1:** Overview of the number of turbines placed on the edges

	left	right	upper	lower	total
no neighbouring wind farm	494	526	467	481	1968
red neighbouring wind farm	548	479	477	450	1954
blue neighbouring wind farm	541	473	440	450	1904
green neighbouring wind farm s	519	491	487	463	1960

For the cases here, the influence from the neighbouring wind farm showed that the turbines are moved away from the edge on the side where the neighbouring wind farm is located. However, the decrease in the performance showed that it is better to have larger distances between turbines within the optimised wind farm, even though this makes the turbines come closer to the edge on the side where the neighbouring wind farm is located. The question rises whether the global optimum to this problem does have more turbines on the left-hand-side edge. Or that there is a strong push to local optima that have less turbines on the right-hand-side edge, while the global optimum has a more equal distribution of turbines on all four edges. The gain from having more turbines on the dominant-wind-sides edges seems higher than the loss coming from the neighbouring wind farm wakes.

Implementing neighbouring wind farms for OWFLO seems logical as the influence from the wakes of neighbouring wind farms on power production has been proven with multiple studies. Adding neighbouring wind farms for accurate energy yield assessments is therefore necessary as the wind farm wake's impact on the energy is clear. Not including neighbouring wind farms would overestimate the energy yield of a wind farm. However, for layout optimisation, the benefit of including neighbouring wind farms is not evident.

The simplified engineering models used here are implemented without atmospheric stability in consideration. Even though the influence of atmospheric stability plays a major role in wind farm wakes, its influence on layout optimisation has not yet been shown. Also, the measured speed-up by Nygard and Handsen, which could present more favourable locations, is not implemented here.

# Conclusion and Recommendations

In this chapter, the main conclusions of this thesis are presented and some recommendations with respect to OWFLO and future research are given.

## 7.1. Conclusion

The research questions of this study are answered below:

*What are the characteristics of the OWFLO problem?*

Optimisation of multiple cases with the referent showed that an OWFLO problem contains many local optima. Although the layouts differed significantly, their performances were exceptionally close to each other. The spread in performances ranged between 0.2% and 0.1% for the smallest and largest farm, respectively. This shows that the spread between the highest and lowest found performance is small and decreases with increasing numbers of turbines. The high number of local optima with similar performances is a strong characteristic of an OWFLO problem. The local optima within the response surface were further explored by assessment of the response surface for a small part of the design space, which showed that the wakes of turbines create the local optima. This exploration also showed that the decrease in the spread with an increasing number of turbines comes from the almost identical absolute difference between two local optima within this small part of the design space. As the AEP of the turbines increased significantly with an increasing number of turbines, the relative spread decreased. With this small spread of the local optima and with the many local optima with similar performance, it is expected that a global optimum will not be significantly better than the highest found local optimum after a reasonable search.

The resulting layouts showed interesting characteristics of where turbines were placed. The corners of the square wind farms are found to be an optimal placement for the turbines, which is logical as this placement results in the largest distance between the turbines. A preference for more turbines on the edges both upstream and downstream of the dominant wind direction was found, with no clear distinction between the number of turbines that were placed on the edge upstream or downstream of the dominant wind direction. Some turbines on the edge are placed at a 'second row' just of the edge. This happened when the two turbines next to the turbine were on the edge and at a distance of around 10 rotor diameters of each other. Assessment of a small part of the referent's design space revealed that this is a consequence of the trade-off between spacing and wake superposition effects. The results are inconclusive as regards whether this characteristic is an artefact of the chosen models or that it is inherent to wake effects in reality.

*With maximizing AEP as objective, what are the influences and uncertainties from the selected key influencers?*

The effect of key influencers on optimality was explored by a comparative analysis between alternative

implementation choices. The influence of alternative implementation choices for the wake analysis was found to be dependent on the slightly different locations of the local optima in the design space and the roughness of the response surface they create. The alternative optimisers showed their influence on the found local optima.

Although the local optima in terms of location are slightly different for alternative implementation choices, the influence of these shifts on the performance turned out to be minimal. The main features for layout optimisation, which all alternative implementation models kept, is creating distance between turbines with consideration of the wind rose and placing turbines as much as possible outside the wakes of other turbines. Without being able to say which models come closer to reality, there is no justification for choosing any model over another.

The spread of the boxplots was found to be related to the roughness of the response surface that alternative implementation choices make. An increase in the roughness of the response surface meant an increase in the spread of the performances. The increased performance spread comes from the bigger challenge that the rougher response surface presents to the optimiser.

Improvement of the state of the art of optimisers used for OWFLO is not expected to lead to much better results. This was demonstrated by a comparison of several good optimisers. Nevertheless, one has to be aware that a poor choice of optimiser can significantly reduce optimality of the layout design, as was shown for a gradient-based optimiser with a random start.

*Is there a need to improve the analysis by adding phenomena currently not considered in OWFLO?*

Improvement of the analysis by adding phenomena currently considered in OWFLO does not necessarily improve OWFLO. This is shown by the performances of the layouts found with the implementation of a neighbouring wind farm in OWFLO, which were lower than the performances of the layouts found without a neighbouring wind farm. A known improvement for accurate energy yield assessments can therefore not always be considered to be an improvement for layout optimisation.

## 7.2. Recommendations

The research questions have been answered and several interesting results have been presented. There are, however, other research approaches that still can be done. Therefore, this section considers some recommendations for future work and advises on possible future improvements.

Within this research, the objective of the OWFLO problem has been maximising AEP. However, optimising for profit or for levelized cost of energy is often used in practice. By including cost models for the electrical collection system and the support structure design, their influence on the characteristics of the OWFLO problem can be explored. The effect of an increase in the cost of cables due to the increase in distance between the turbines as well as the water depth will present local optima to shift or change. The local optima may reduce in numbers, or the spread of performances may lie closer to each other or deviate more. It will be interesting to know what influence these cost models will have on the local optima.

The square area used within this thesis could be changed for different shapes to see their influence on the local optima and placement of the turbines. In reality, wind farm projects have an assigned area that has all kinds of shapes. The influence of the shape of the boundaries and local optima could be further explored.

The placement of turbines found within the cases in this thesis showed that more turbines on the edge increased the AEP. With the knowledge of wind farm scale blockage, this increase may be lower in reality. More research on the effect of wind farm scale blockage could help to know if the placement of more turbines on the edge is actually beneficial in reality.

Possible future improvements for layout optimisation should be done with great care and logical thinking. The implementation with the neighbouring wind farm in this thesis showed that an improvement for accurately calculating the energy yield not necessarily always benefits layout optimisation. Other future improvement should therefore be done with layout optimisation in mind and not with accurately calculating the energy yield.

Within this thesis, the roughness of the response surface showed its influence on the spread of the performances. When performing layout optimisation and deciding for implementation choices, the roughness can therefore be taken into consideration. Some alternative implementation choices and the neighbouring wind farm showed that even with a less accurate representation of reality, they could find better performances.

# Reference

- [1] J J Thomas and A Ning. “A method for reducing multi-modality in the wind farm layout optimization problem”. In: *Journal of Physics: Conference Series* 1037 (June 2018), p. 042012. DOI: 10.1088/1742-6596/1037/4/042012. URL: <https://doi.org/10.1088/1742-6596/1037/4/042012>.
- [2] B. Saavedra-Moreno et al. “Seeding evolutionary algorithms with heuristics for optimal wind turbines positioning in wind farms”. In: *Renewable Energy* 36.11 (2011), pp. 2838–2844. ISSN: 0960-1481. DOI: <https://doi.org/10.1016/j.renene.2011.04.018>. URL: <https://www.sciencedirect.com/science/article/pii/S096014811100190X>.
- [3] Yunus Eroğlu and Serap Ulusam Seçkiner. “Design of wind farm layout using ant colony algorithm”. In: *Renewable Energy* 44 (2012), pp. 53–62. ISSN: 0960-1481. DOI: <https://doi.org/10.1016/j.renene.2011.12.013>. URL: <https://www.sciencedirect.com/science/article/pii/S096014811100694X>.
- [4] K. Chen et al. “Wind turbine positioning optimization of wind farm using greedy algorithm”. In: *Journal of Renewable and Sustainable Energy* 5.2 (2013), p. 023128. DOI: 10.1063/1.4800194. eprint: <https://doi.org/10.1063/1.4800194>. URL: <https://doi.org/10.1063/1.4800194>.
- [5] S. Salcedo-Sanz et al. “Offshore wind farm design with the Coral Reefs Optimization algorithm”. In: *Renewable Energy* 63 (2014), pp. 109–115. ISSN: 0960-1481. DOI: <https://doi.org/10.1016/j.renene.2013.09.004>. URL: <https://www.sciencedirect.com/science/article/pii/S0960148113004710>.
- [6] Sittichoke Pookpant and Weerakorn Ongsakul. “Optimal placement of wind turbines within wind farm using binary particle swarm optimization with time-varying acceleration coefficients”. In: *Renewable Energy* 55 (2013), pp. 266–276. ISSN: 0960-1481. DOI: <https://doi.org/10.1016/j.renene.2012.12.005>. URL: <https://www.sciencedirect.com/science/article/pii/S0960148112007604>.
- [7] J F Ainslie. *Calculating the flowfield in the wake of wind turbines*. Jan. 1988.
- [8] Gunner Chr. Larsen. *A simple stationary semi-analytical wake model*. English. Denmark. Forskningscenter Risoe. Risoe-R 1713(EN). Risø National Laboratory for Sustainable Energy, Technical University of Denmark, 2009.
- [9] Sten Frandsen et al. “Analytical modelling of wind speed deficit in large offshore wind farms”. In: *Wind Energy* 9.1□2 (2006), pp. 39–53. DOI: <https://doi.org/10.1002/we.189>. eprint: <https://onlinelibrary.wiley.com/doi/pdf/10.1002/we.189>. URL: <https://onlinelibrary.wiley.com/doi/abs/10.1002/we.189>.
- [10] Majid Bastankhah and Fernando Porté-Agel. “A new analytical model for wind-turbine wakes”. In: *Renewable Energy* 70 (2014). Special issue on aerodynamics of offshore wind energy systems and wakes, pp. 116–123. ISSN: 0960-1481. DOI: <https://doi.org/10.1016/j.renene.2014.01.002>. URL: <https://www.sciencedirect.com/science/article/pii/S0960148114000317>.
- [11] N.O. Jensen. *A note on wind generator interaction*. English. Risø-M 2411. Risø National Laboratory, 1983. ISBN: 87-550-0971-9.
- [12] Luc Rademakers, H. Braam, and T Obdam. “Estimating costs of operation and maintenance for offshore wind farms”. In: (Jan. 2007).
- [13] R Damiani, Katherine Dykes, and G Scott. “A comparison study of offshore wind support structures with monopiles and jackets for U.S. waters”. In: *Journal of Physics: Conference Series* 753 (Sept. 2016), p. 092003. DOI: 10.1088/1742-6596/753/9/092003.
- [14] Gabriel Bazacliu, George Cristian Lazaroiu, and Virgil Dumbrava. “Design of wind farm layout for maximum wind energy capture”. In: *UPB Scientific Bulletin, Series C: Electrical Engineering* 77 (Jan. 2015).

- [15] Rabia Shakoor et al. "Wake effect modeling: A review of wind farm layout optimization using Jensen's model". In: *Renewable and Sustainable Energy Reviews* 58 (2016), pp. 1048–1059. ISSN: 1364-0321. DOI: <https://doi.org/10.1016/j.rser.2015.12.229>. URL: <https://www.sciencedirect.com/science/article/pii/S1364032115016123>.
- [16] Nicholas Baker et al. "Best Practices for Wake Model and Optimization Algorithm Selection in Wind Farm Layout Optimization". In: Jan. 2019. DOI: 10.2514/6.2019-0540.
- [17] Tuhfe Göçmen et al. "Wind turbine wake models developed at the technical university of Denmark: A review". In: *Renewable and Sustainable Energy Reviews* 60 (2016), pp. 752–769. ISSN: 1364-0321. DOI: <https://doi.org/10.1016/j.rser.2016.01.113>. URL: <https://www.sciencedirect.com/science/article/pii/S136403211600143X>.
- [18] Z.C. Roza. "Simulation Fidelity Theory and Practice". In: (Jan. 2004).
- [19] UL. "OPENWIND USER MANUAL". In: (2020).
- [20] Mads M. Pedersen et al. "DTUWindEnergy/PyWake: PyWake". In: (Feb. 2019). DOI: 10.5281/zenodo.2562662.
- [21] Ott Søren and Nielsen Morten. "Developments of the offshore wind turbine wake model Fuga". In: *DTU Wind Energy* (2014).
- [22] Amin Niayifar and Fernando Porté-Agel. "Analytical Modeling of Wind Farms: A New Approach for Power Prediction". In: *Energies* 9 (Sept. 2016), p. 741. DOI: 10.3390/en9090741.
- [23] Sten Tronæs Frandsen. "Turbulence and turbulence-generated structural loading in wind turbine clusters". English. Risø-R-1188(EN). PhD thesis. 2007. ISBN: 87-550-3458-6.
- [24] Pierre-Elouan Réthoré et al. "TOPFARM: Multi-fidelity optimization of wind farms". In: *Wind Energy* 17.12 (2013), pp. 1797–1816. DOI: 10.1002/we.1667.
- [25] Xin-She Yang. "Metaheuristic Optimization". In: *Scholarpedia* 6 (Jan. 2011), p. 11472. DOI: 10.4249/scholarpedia.11472.
- [26] Luis Rios and Nikolaos Sahinidis. "Derivative-free optimization: A review of algorithms and comparison of software implementations". In: *Journal of Global Optimization* 56 (Nov. 2009). DOI: 10.1007/s10898-012-9951-y.
- [27] Andreas Platis et al. "First in situ evidence of wakes in the far field behind offshore wind farms". In: *Scientific Reports* 8 (Feb. 2018), p. 2163. DOI: 10.1038/s41598-018-20389-y.
- [28] Beatriz Cañadillas et al. "Offshore wind farm wake recovery: Airborne measurements and its representation in engineering models". In: (2019).
- [29] M.C. Brower and N.M. Robinson. "THE OPENWIND DEEP-ARRAY WAKE MODEL Development and Validation". In: (2012).
- [30] Nicolai Gayle Nygaard and Sidse Damgaard Hansen. "Wake effects between two neighbouring wind farms". In: *Journal of Physics: Conference Series* 753 (Sept. 2016), p. 032020. DOI: 10.1088/1742-6596/753/3/032020. URL: <https://doi.org/10.1088/1742-6596/753/3/032020>.
- [31] Robert W. Baker and Stel N. Walker. "Wake measurements behind a large horizontal axis wind turbine generator". In: *Solar Energy* 33.1 (1984), pp. 5–12. ISSN: 0038-092X. DOI: [https://doi.org/10.1016/0038-092X\(84\)90110-5](https://doi.org/10.1016/0038-092X(84)90110-5). URL: <https://www.sciencedirect.com/science/article/pii/0038092X84901105>.
- [32] G J Taylor. "Wake measurements on the Nibe wind turbines in Denmark". In: (Jan. 1990).
- [33] Gunner C. Larsen et al. "Wake meandering: a pragmatic approach". In: *Wind Energy* 11.4 (2008), pp. 377–395. DOI: <https://doi.org/10.1002/we.267>. eprint: <https://onlinelibrary.wiley.com/doi/pdf/10.1002/we.267>. URL: <https://onlinelibrary.wiley.com/doi/abs/10.1002/we.267>.
- [34] Robert Braunbehrens and Antonio Segalini. "A statistical model for wake meandering behind wind turbines". In: *Journal of Wind Engineering and Industrial Aerodynamics* 193 (2019), p. 103954. ISSN: 0167-6105. DOI: <https://doi.org/10.1016/j.jweia.2019.103954>. URL: <https://www.sciencedirect.com/science/article/pii/S0167610519305458>.
- [35] Nikolaus Hansen, Youhei Akimoto, and Petr Baudis. *CMA-ES/pycma on Github*. Feb. 2019. DOI: 10.5281/zenodo.2559634. URL: <https://doi.org/10.5281/zenodo.2559634>.

- [36] Richard J. A. M. Stevens et al. "Combining economic and fluid dynamic models to determine the optimal spacing in very large wind farms". In: *Wind Energy* 20.3 (2017), pp. 465–477. DOI: <https://doi.org/10.1002/we.2016>. eprint: <https://onlinelibrary.wiley.com/doi/pdf/10.1002/we.2016>. URL: <https://onlinelibrary.wiley.com/doi/abs/10.1002/we.2016>.
- [37] Evan Gaertner et al. *Definition of the IEA 15-Megawatt Offshore Reference Wind Turbine*. Tech. rep. International Energy Agency, 2020. URL: <https://www.nrel.gov/docs/fy20osti/75698.pdf>.
- [38] S. A. Hsu, Eric A. Meindl, and David B. Gilhousen. *Determining the Power-Law Wind-Profile Exponent under Near-Neutral Stability Conditions at Sea*. July 1994. DOI: 10.1175/1520-0450(1994)033<0757:dtplwp>2.0.co;2. URL: [https://doi.org/10.1175/1520-0450\(1994\)033%3C0757:dt%20plwp%3E2.0.co;2%7D](https://doi.org/10.1175/1520-0450(1994)033%3C0757:dt%20plwp%3E2.0.co;2%7D).
- [39] Haohua Zong and Fernando Porté-Agel. "A momentum-conserving wake superposition method for wind farm power prediction". In: *Journal of Fluid Mechanics* 889 (Apr. 2020). DOI: 10.1017/jfm.2020.77.
- [40] D. Kraft. *A software package for sequential quadratic programming*. Deutsche Forschungs- und Versuchsanstalt für Luft- und Raumfahrt Köln: Forschungsbericht. Wiss. Berichtswesen d. DFVLR, 1988. URL: <https://books.google.nl/books?id=4rKaGwAACAAJ>.

# Appendices

## A: Heatmaps

The heatmaps resulting from the case with 25 turbines are illustrated below:

### Wake Models

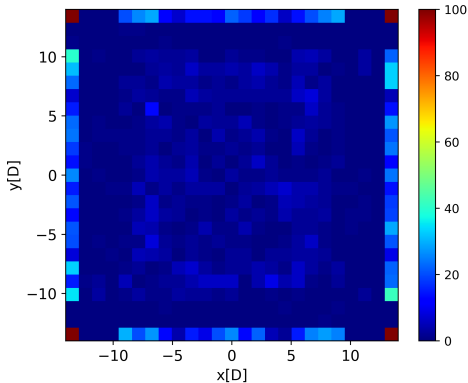


Figure 7.1: Heatmap of wind turbines position from GCL model with case 25 turbines

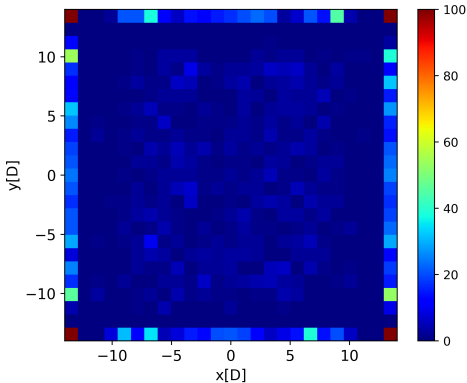


Figure 7.2: Heatmap of wind turbines position from NOJ model with case 25 turbines

### Superposition Models

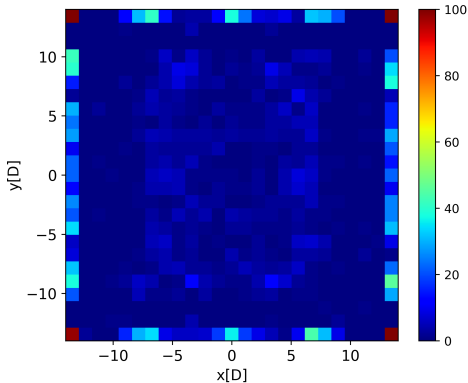


Figure 7.3: Heatmap of wind turbines position from LS model with case 25 turbines

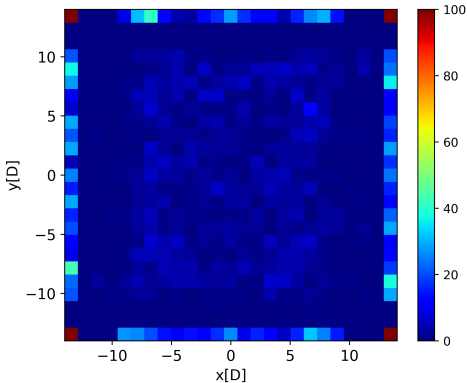
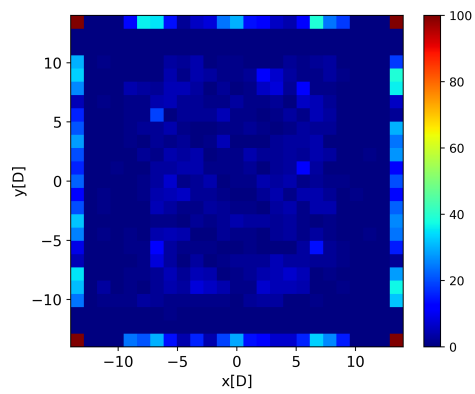
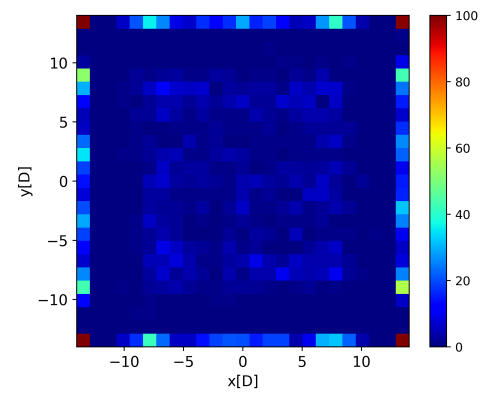


Figure 7.4: Heatmap of wind turbines position from MS model with case 25 turbines

## Wind Conditions



**Figure 7.5:** Heatmap of wind turbines position from One Weibull wind conditions with case 25 turbines



**Figure 7.6:** Heatmap of wind turbines position from sector size six wind conditions with case 25 turbines

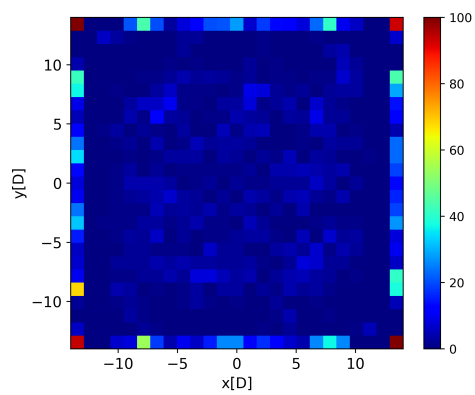


**Figure 7.7:** Heatmap of wind turbines position from wind sector change left wind conditions with case 25 turbines

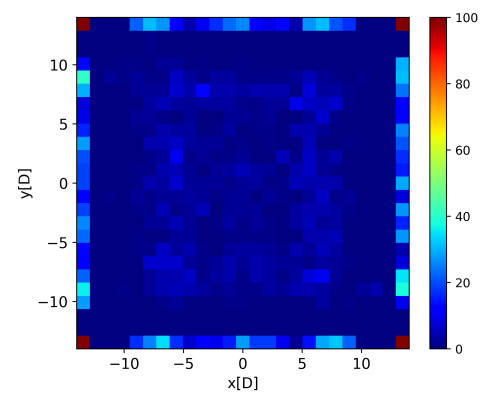


**Figure 7.8:** Heatmap of wind turbines position from wind sector change right wind conditions with case 25 turbines

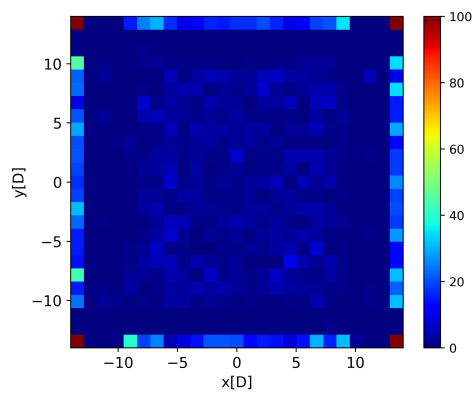


**Figure 7.9:** Heatmap of wind turbines position from one wind speed (9) with case 25 turbines

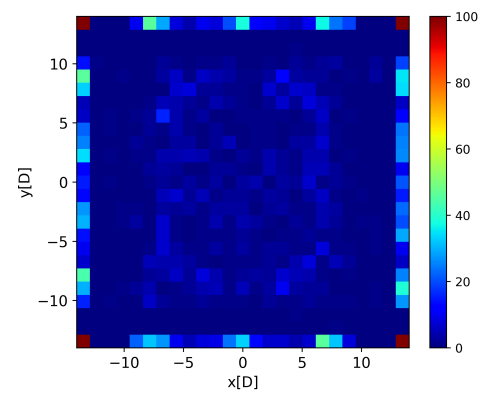


**Figure 7.10:** Heatmap of wind turbines position from simulation sample size 2 with case 25 turbines

Optimisers

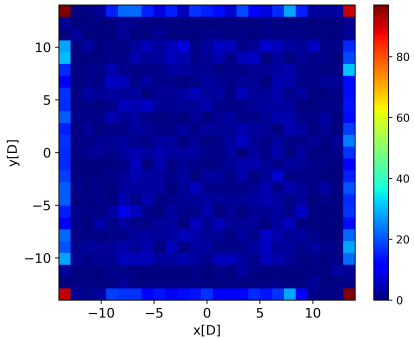


Figure 7.11: Heatmap of wind turbines position from the multi-start SLSQP optimiser with case 25 turbines

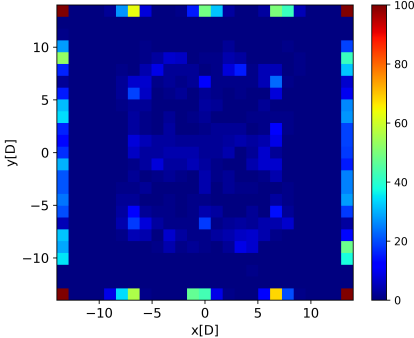


Figure 7.12: Heatmap of wind turbines position from the random optimiser with case 25 turbines

## B: Special form of the response surface

The special form of the response surface for alternative implementation choices that have not been shown in section 5.5.1 are illustrated below:

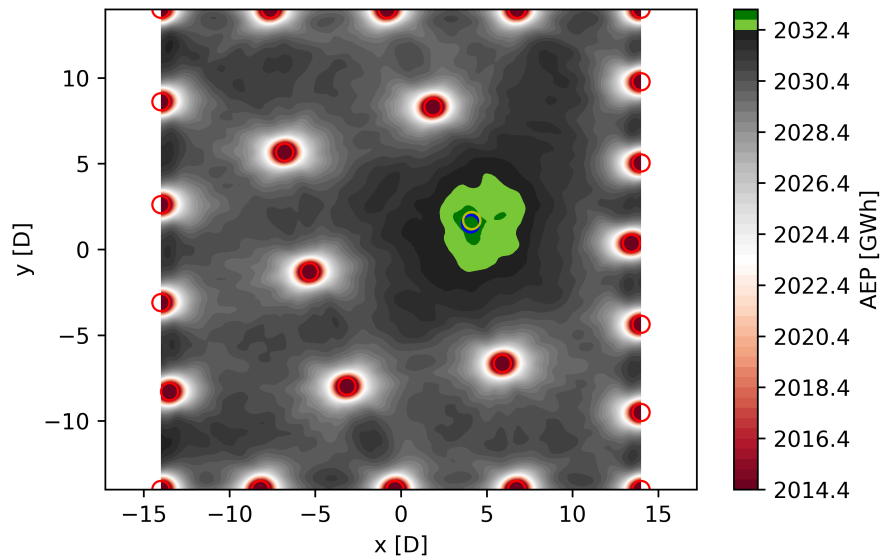


Figure 7.13: Response surface NOJensen

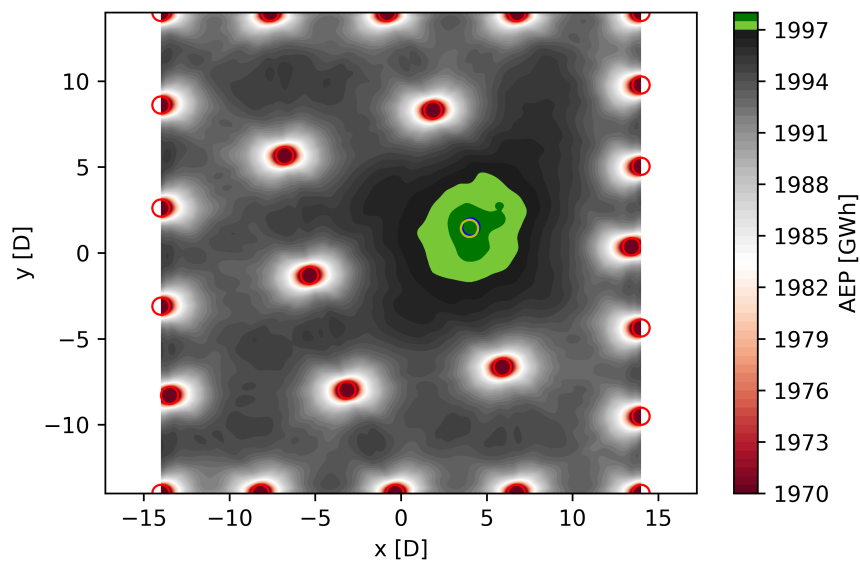


Figure 7.14: Response surface one Weibull

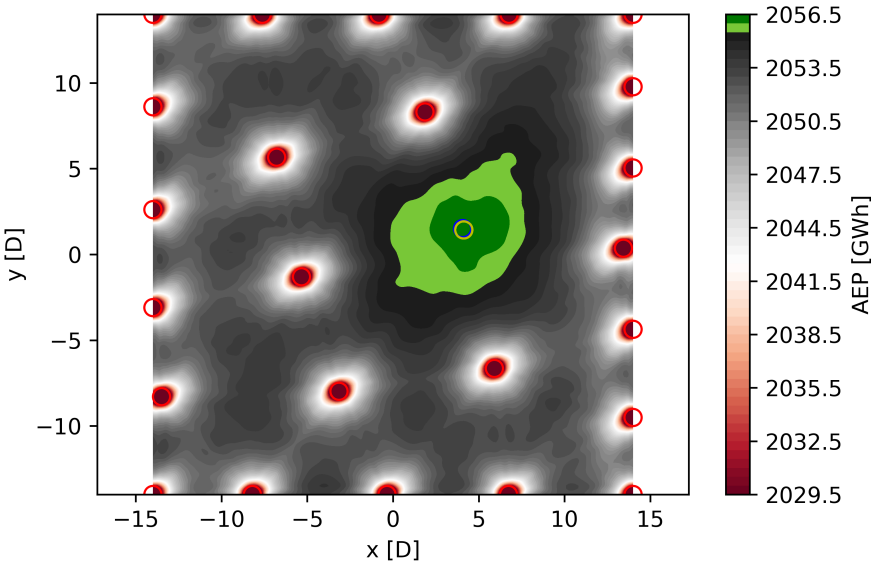


Figure 7.15: Response surface wind rose sector size (6)

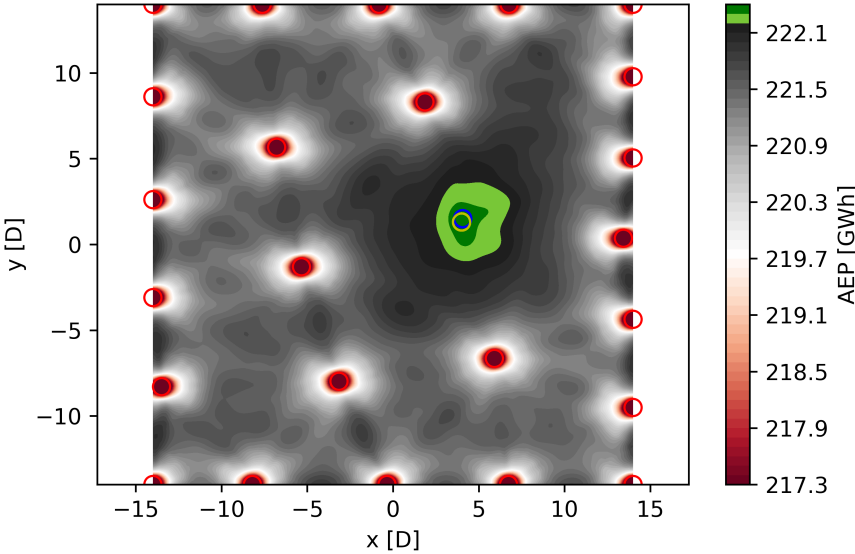


Figure 7.16: Response surface one wind speed

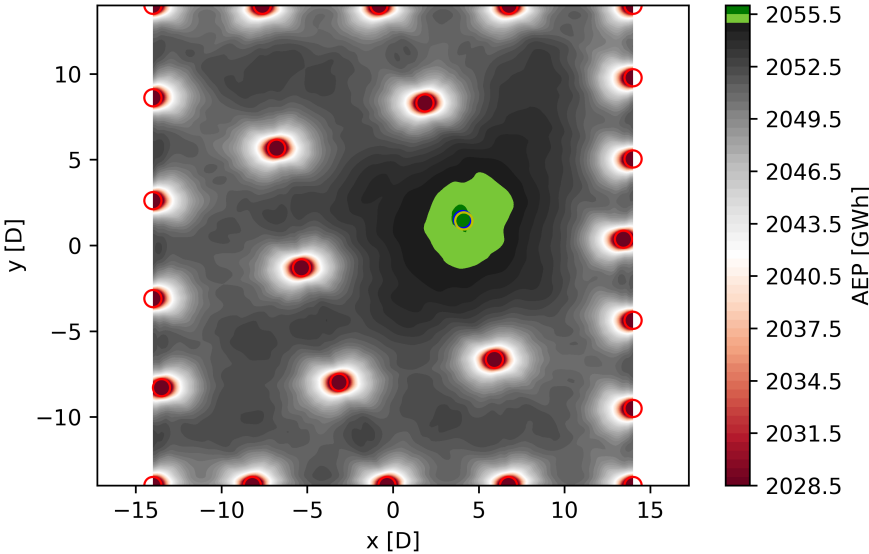


Figure 7.17: Response surface simulation sample size (2)

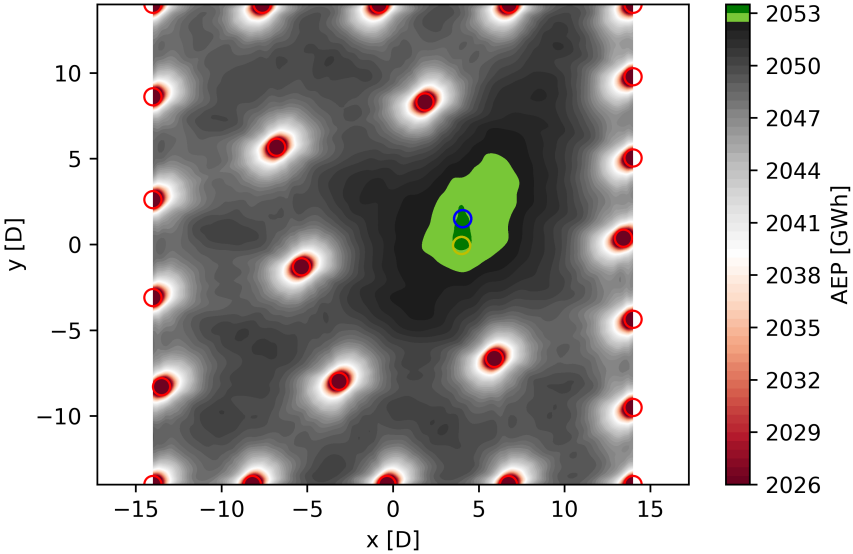


Figure 7.18: Response surface WCL model

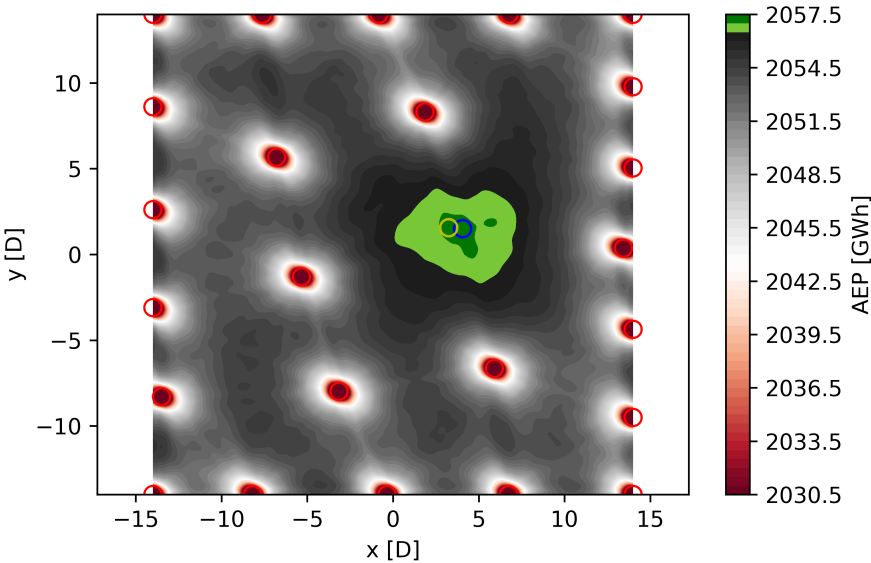


Figure 7.19: Response surface WCR model